



Review

Physical mechanisms in hybrid additive manufacturing: A process design framework



Samantha Webster ^a, Hui Lin ^a, Fred M. Carter III ^{a,b}, Kornel Ehmann ^a, Jian Cao ^{a,*}

^a Department of Mechanical Engineering, Northwestern University, Evanston, IL 60208, USA
^b DMG MORI Advanced Solutions Inc., Hoffman Estates, IL 60192, USA

ARTICLE INFO

Special Editor: Dr. E. Tekkaya

Keywords:

Hybrid additive manufacturing
Metal additive manufacturing
Manufacturing process chains

ABSTRACT

This study defined hybrid additive manufacturing (AM) as “in-situ or series combination of an additive manufacturing process and secondary energy sources in which physical mechanisms are fundamentally altered/controlled to affect the resulting properties of material and/or part.” This definition includes *in-situ* secondary processes as well as process chains, and it is anchored in multi-physical mechanisms such that new hybrid-AM processes can be freely and systematically sought or invented through a systems approach epitomized by the “property – mechanism – energy source – hybrid-AM process (PMEH)” thought process. The sequence of driving forces in this framework are as such: desired material properties determine which mechanism is utilized and, in turn, the energy source to be applied, which ultimately defines the hybrid-AM process. The five unifying physical mechanisms that were identified in this study are: melt pool dynamics, microstructure development, stress state, surface evolution, and thermal gradients. Analysis of properties, mechanisms, energy sources, and processes was conducted on more than 100 papers, and the results ultimately show the effect of mechanisms on material properties. Mechanisms are further classified by energy source, which are in turn broken down by hybrid-AM process. Additionally, each mechanism was defined and reviewed in detail, highlighting the PMEH relationship for metal hybrid-AM materials. Further analysis compares reported mechanical property values for hybrid-AM processes to both AM only and wrought properties for 316 L, Alloy 718, and Titanium Gr 5. Finally, future directions of research as well as clear gaps in knowledge are identified, which includes lack of variety in utilized energy sources, lack of material diversity, process chain integration and improvement, and promising hybrid-AM processes. With the presented analysis and PMEH framework, it is determined that metal AM hybrid processes are well suited to address current problems and show promise in creating superior and versatile materials. Further growth in this field is expected to be exponential, and the developed PMEH framework will aid in framing these innovative processes.

1. Introduction

Innovations in products for their competitive performances and cost in all industrial sectors, ranging from automotive through aerospace and biomedical through communication, demand the smart use of materials. This demand has pushed the limits of the processing abilities of conventional unit manufacturing methods. This trend has, in the last few decades, provided the impetus for the exploration of new process, machine and manufacturing system variants to which the attribute “hybrid” has been attached. However, a search through the technical literature reveals that the attribute “hybrid” assumes an extremely wide range of meanings. To lay a rigorous foundation for the discussions to

follow, we will first review the definitions of “hybrid” followed by the scope of “hybrid” to be reviewed and discussed in this work.

As the field of hybrid manufacturing has become more solidified, hybrid process definitions have become more specific. The most popular, descriptive definitions were probably put forth by the International Academy for Production Engineering (CIRP, College International pour la Recherche en Productique) in 2011, as stated in the review article by Lauwers et al. (2014), where both a narrow and open definition were given. The narrow definition states, “hybrid processes comprise a simultaneous acting of different (chemical, physical, controlled, etc.) processing principles in the same processing zone”. In this definition, the emphasis is put on the relative location and timing of the combined processes. The broad definition was updated in 2014 to reflect

* Corresponding author.

E-mail address: jcao@northwestern.edu (J. Cao).

Nomenclature	
AM	additive manufacturing
AM+	hybrid additive manufacturing
CIRP	the international academy for production engineering
CMT	cold metal transfer
CNC	computer numerical control
CS	cold spray
DED	directed energy deposition
DMLS	direct metal laser sintering
EBSM	electron backscatter diffraction
HIP	hot isostatic pressing
IF	incremental forming
LAM	laser assisted machining
LMD	laser metal deposition
LR	laser remelting
LSP	laser shock peening
MHD	magnetohydrodynamic damping
PBF	laser powder bed fusion
PBF	powder bed fusion
PDZ	plastic deformation zone
PMEH	property-mechanism-energy source-hybrid-AM process
PSPP	process-structure-property-performance
SEM	scanning electron microscope
SLM	selective laser melting
SPIF	single point incremental forming
TEMC	thermoelectric magnetic convection
TEMF	thermoelectric magnetic force
UIP	ultrasonic impact peening
UTS	ultimate tensile strength
WAAM	wire arc additive manufacturing
XRD	X-ray diffraction
YS	yield strength

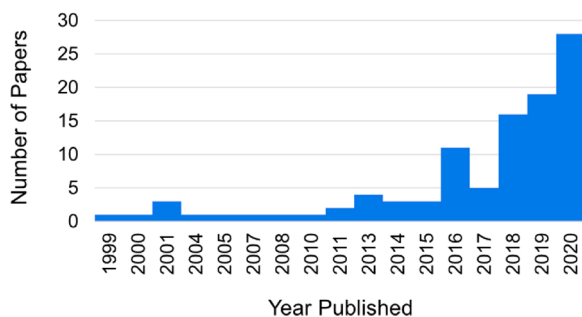


Fig. 1. Number of papers published for each year in metal hybrid-AM that are considered in this study from responses to multiple database searches using ‘metal hybrid manufacturing’, ‘hybrid additive manufacturing’ as keyword(s).

improvement in performance of the manufacturing process through coupling: “hybrid manufacturing processes are based on the simultaneous and controlled interaction of process mechanisms and/or energy sources/tools having a significant effect on process performance.” Note that the emphasis on the simultaneous action at the same location and same time was dropped in the broader definition.

Both of these definitions include hybrid processes of all types and materials; however, the recent popularity of AM processes has led to research and development of a branch of hybrid processes, specifically, hybrid-AM processes. The “popularity” of metal hybrid-AM is clearly shown by the exponential growth in the number of papers over the last twenty years as shown in Fig. 1 (response to searches in Scopus, Web of Knowledge, and Google Scholar using ‘metal hybrid manufacturing’, or ‘hybrid additive manufacturing’ as keyword(s)).

Among the more recent publications, Sealy et al. (2018) defined hybrid-AM as “the use of AM with one or more secondary processes or energy sources that are fully coupled and synergistically affect part quality, functionality, and/or process performance.” This definition re-emphasizes the importance of considering part quality and functionality as in the broader definition discussed above while keeping the nature of “simultaneous” actions used in the narrow definition.

While the merging of hybrid-AM definitions is encouraging, we have not found a systematic analysis/thought process in analyzing and facilitating the further evolution of hybrid-AM processes, and this assertion motivates this work. Furthermore, since rarely only one process (even using different energy sources simultaneously) can meet all the performance requirements of a product, we include process chains into our hybrid-AM definition. Specifically, we consider hybrid-AM as being anchored in multi-physical mechanisms such that new hybrid-AM processes can be freely and systematically sought or invented through a systems approach epitomized by the “property-mechanism-energy source-hybrid-AM process (PMEH)” thought process as shown in Fig. 2, in which the arrows indicate the driving force for the next step. Thus, we define hybrid-AM processes as an *in-situ or series combination of an additive manufacturing process and secondary energy sources in which physical mechanisms are fundamentally altered/controlled to affect the resulting properties of the material and/or part*. This definition will be referred to henceforth as both “hybrid-AM” or “AM + X”, where the latter is the same as hybrid-AM but describes a specific secondary process such as forging, milling, etc.

This work analyzes hybrid-AM processes that fall within the above definition and identifies the five most prominent fundamental physical mechanisms used to influence material and part properties in hybrid-AM. Material properties include two levels, microstructure at the nano- and micro-length scale, and bulk properties at the macro-scale, which has been widely studied for various material systems in the traditional materials science and solid mechanics fields. These two levels are highly inter-related at the fundamental level, defined by the well-known process-structure-property-performance (PSPP) framework that material scientists and engineers use in material design and its corresponding processes that make the material, as in Olson (1997); but this will not be the focus of this paper. The novel aspect that we propose in this paper is the identification of physical mechanisms that are specifically related to metal AM processes, e.g., melt pool dynamics, microstructure development, stress state, surface evolution, and thermal gradients. A definition for each identified mechanism is provided in Section 2 and their corresponding effects on mechanical properties are summarized in Section 3. Section 4 provides a detailed discussion of each mechanism, while mechanisms in process chains are discussed in



Fig. 2. Outline of proposed (PMEH) framework to classify hybrid-AM processes by physical mechanism and energy sources. This shows the relationship of material property to hybrid-AM process and how choice of mechanism and energy source can lead to process innovation.

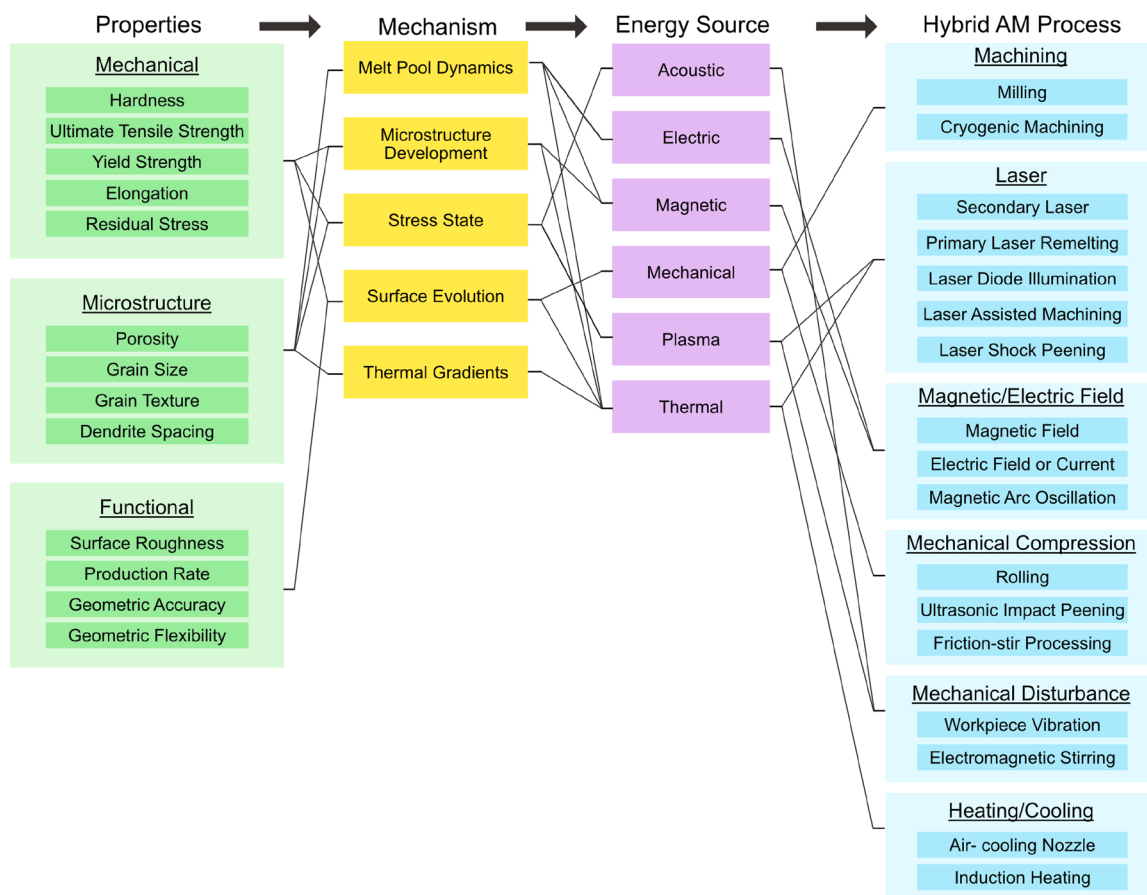


Fig. 3. Property – mechanism – energy source – hybrid-AM process (PMEH) framework for hybrid-AM classified by mechanism and energy source utilization. Black lines indicate major relationships between property, mechanism, energy source, and hybrid-AM process found in the literature search. Mechanism and Energy Source columns are ordered alphabetically, while Properties and hybrid-AM process columns are ordered by most reported to least reported.

Section 5. Finally, a summary of this study and future outlook on the hybrid-AM field is discussed in Section 6.

Depending on the fundamental length-scale, temporal-scale, and energy-level and type needed in driving the physical mechanisms in the framework, various **energy sources** can be identified, such as acoustic, electric, magnetic, mechanical, plasma or thermal, etc. Finally, with a solid footing in the governing physical mechanisms and engineering skills, new **hybrid-AM processes** can be synthesized. The approach, described above and illustrated in Fig. 3, not only expands the scope of processes that are to be considered, but connects processes to the resulting material and part properties through the governing physical mechanisms. It effectively frames hybrid-AM from a materials design perspective and highlights the innovations that can be made from a process perspective to ultimately co-design materials and manufacturing processes.

2. Scope of processes, materials, and mechanisms discussed in this paper

2.1. AM processes

Before further describing the analysis performed in this work utilizing the PMEH framework presented in Figs. 2 and 3, it will be beneficial to the readers to lay out which AM processes will be discussed here as the base for hybrid-AM analysis. AM spans across many materials, from polymers to metals to thin films, and part scales, from nano to micro to macro (Chu et al., 2014). Due to the frequent use and application of metal AM parts in aerospace, automotive, and biomedical industries, this work will focus on hybrid processes that utilize two metal

AM process families as defined by ISO/ASTM52900-15, specifically powder-bed AM processes (family 2), also known as selective laser melting (SLM), or laser powder bed fusion (PBF), or direct metal laser sintering (DMLS), and directed energy deposition (DED, family 7), e.g., powder-blown AM processes, wire arc additive manufacturing (WAAM), and cold spray (CS). Additionally, the secondary or “hybrid” processes considered here include *in-situ* applications, non-traditional processing of AM materials (e.g., forming, rolling, etc.), and combination machines (e.g., DED/PBF + CNC). It is noted that this excludes hot isostatic pressing (HIPing), which is a standard AM post-processing method and requires the material to be transferred to a separate location. HIPing has also been studied extensively among material groups and will not be repeated here (Chen et al., 2018).

Over 100 papers were considered in this study that utilized the aforementioned AM processes. A variety of databases were used for paper searches and keyword(s) during which ‘metal hybrid manufacturing’ and/or ‘hybrid additive manufacturing’ were utilized. A snapshot of the current research landscape generated from the considered literature can be found in Appendix A. Information was manually extracted from collected papers (including mechanism, energy source, process, and properties) and consolidated into a spreadsheet. The collected data was first standardized with respect to materials and properties and then analyzed using a series of python codes in which data categories (mechanism, energy source, material/part property, etc.) could be filtered and connections between categories (such as mechanism and material property) could be realized. Appendix B shows how papers were searched, the information extracted from the papers, and how to analyze this information. Python codes used to filter and analyze the data can be found in the supplementary material.

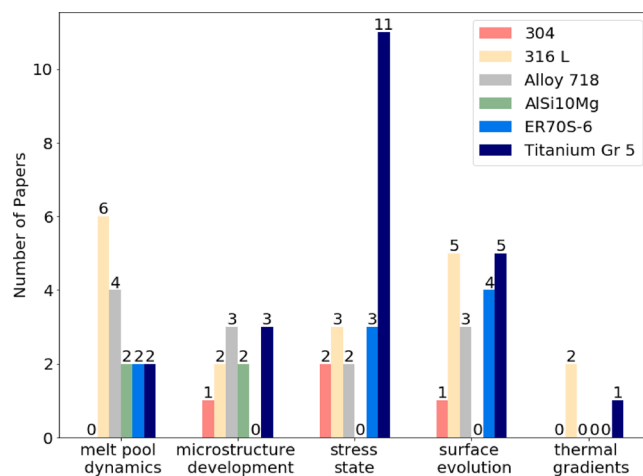


Fig. 4. Material types investigated in each of five physical mechanisms identified in hybrid-AM.

2.2. Considered materials

Metal-based AM is widely accepted to be a very flexible process in both geometry and material, however, in practice there is only a handful of metal alloys that are commonly researched (Debroy et al., 2018). This trend is also seen in metal hybrid-AM, where the six most widely investigated materials are: Titanium Gr 5 (also known as Ti-6Al-4V), 316 L, Alloy 718, ER70S-6, AISI10Mg and 304. The number of papers in this analysis that studied each of the six mentioned materials is shown in Fig. 4 as a function of the five physical mechanisms. The reported materials in this study use AISI naming conventions, for a list of alternate material names please see Appendix C. The three most reported materials are Titanium Gr 5, 316 L, and Alloy 718, which reflects similar trends in AM only processes. For a complete list of reported alloys in

metal hybrid-AM, please refer to Appendix D.

2.3. Physical mechanisms

Hybrid-AM as discussed in Section 1 is defined in both broad and narrow definitions, but is heavily process-oriented. In contrast to this, we synthesized the presented work and selected the five most prominent unifying mechanisms that simultaneous and controlled processes leverage in different ways to ultimately influence, control, or further study the resultant material or parts. These five mechanisms derived from current research are depicted in Fig. 5, as well as the energy sources used to alter them. The mechanisms include melt pool dynamics, microstructure development, stress state, surface evolution, and thermal gradients. Energy sources include acoustic, electric, magnetic, mechanical, plasma, and thermal. It is noted here that acoustic energy includes vibrations, as both solid and gas transmissions are considered. The most utilized mechanism was surface evolution, followed by stress state, melt pool dynamics, microstructure development, and thermal gradients. A definition of each mechanism is provided below and offers insight into the analysis of papers therein. Since the reviewed research focuses on PBF or DED with some additional energy source and/or process “X” (AM + X), the following definitions utilize this format.

Melt Pool Dynamics: In the considered AM families, an energy source from the base AM process is used to establish a melt pool of the respective material which then solidifies and forms the resultant material and part properties. The melt pool in these processes has many associated physics such as heat transfer, fluid dynamics, capillary forces, electro-magnetic forces and others which ultimately drive process outcomes (Kou, 2002). Hybrid-AM processes where the additional process “X” relates to the understanding or control of the melt pool are unified by this mechanism.

Microstructure Development: In metal AM, microstructure development can occur at several stages of the process. In particular, those changes can occur during or after solidification. Research in hybrid-AM that focuses on an additional process “X” with the primary goal of

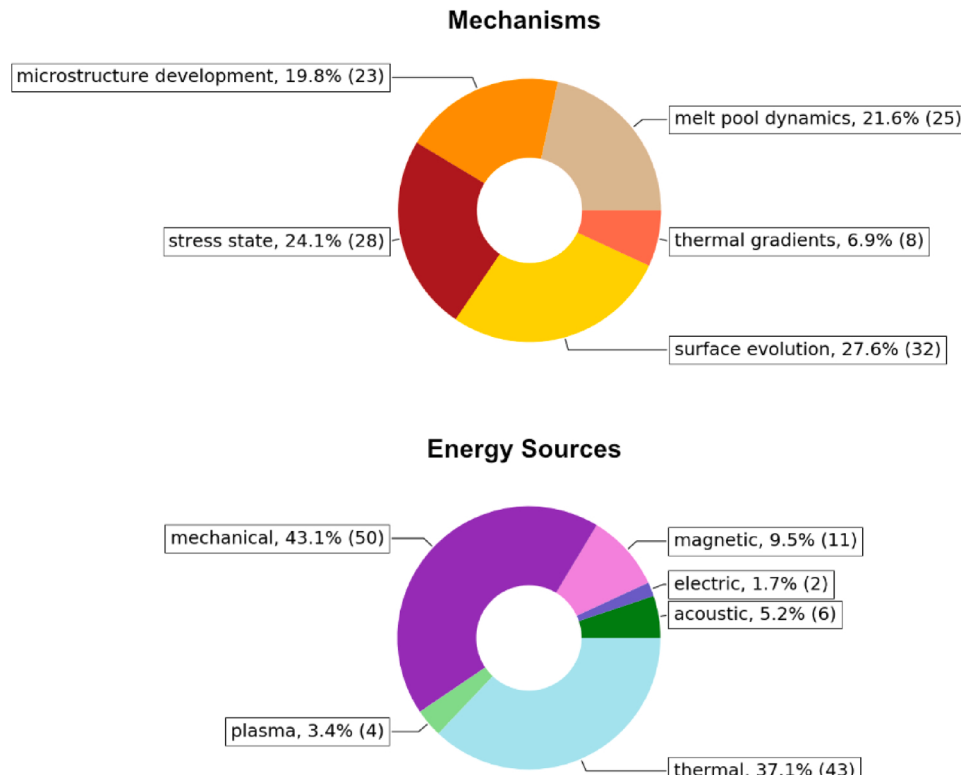
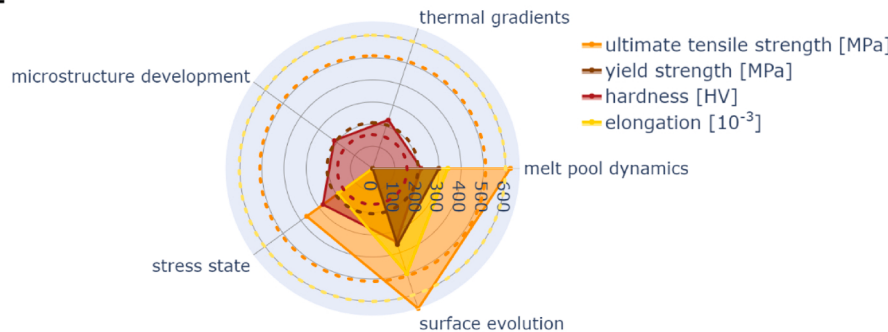
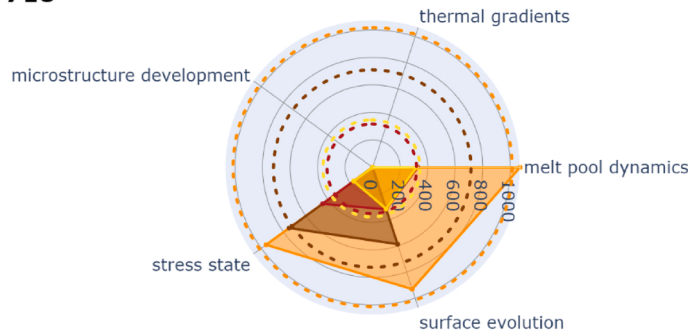


Fig. 5. Breakdown of mechanisms and energy sources in hybrid-AM as percentage(s) and number of papers in parentheses.

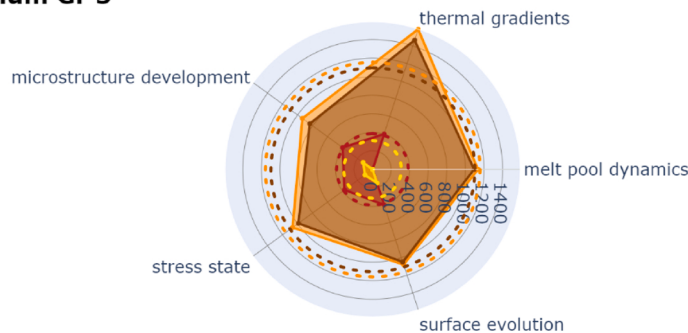
316 L



Alloy 718



Titanium Gr 5



understanding or controlling the microstructure is categorized by this mechanism.

Stress State: Stress state, represented by triaxiality and Lode angle, is known to influence fracture initiation (Xue, 2007), the fracture limit (Cockroft and Latham, 1968), localization (Hill, 1952), and fatigue crack growth rate (Weertman, 1966). PBF and DED metal AM processes inherently generate thermally induced residual stress (Gu et al., 2012), which can be driven by several factors, such as thermal expansion (Safronov et al., 2017), temperature-dependent heat capacity (Xiong et al., 2020), thermal gradient, etc. Hybrid-AM where the additional process "X" focuses primarily on understanding or controlling the stress state is categorized by this mechanism.

Surface Evolution: Metal AM consists of fabricating components using a series of additively-deposited layers. These layers are individually made up of several smaller melting traces commonly called hatch or contour geometry. Different length scales are associated with the process, for instance 0.020–0.100 mm layers are common for PBF and 0.300 – over 1 mm are common for DED (Bennett et al., 2017). Inherently, external surface roughness is commonly in excess of $7 R_a \mu\text{m}$. Surface evolution is the mechanism for hybrid-AM processes where process "X" focuses on understanding or controlling the external structure of additive parts.

Thermal Gradients: While it is true that the mechanisms of Melt Pool Dynamics and Microstructure Development also frequently include consideration of the temperature profiles, these considerations are

Fig. 6. Radar chart of average mechanical properties reported for each mechanism for the three most investigated materials. Averages were calculated for each property if it was reported in more than one paper for any given mechanism. A table of the individual data points for each plot is included in Appendix E for reference. Dashed lines indicate wrought material properties. A value of zero indicates that the property was not reported. There are clear gaps in the investigations reported up to now, specifically seen in 316 L and Alloy 718.

generally focused on a localized level and not directed at the more complete understanding. This mechanism focuses on processes "X" that are primarily concerned with controlling, monitoring, or studying the spatially varying thermal behavior of the additive process at both macro (whole part), and micro (spatially specific) levels. This includes thermal gradients in the melt zone, across multiple layers, or across the complete part.

All analyses were based on the data shown in Appendix D, wherein detailed information of each researched paper is compiled including material type, material/part property, value of property, mechanism, energy source, process, basic information (author, publish year, journal, affiliation, geography), etc.

3. Property-mechanism-energy source-hybrid-AM process (PMEH) framework

Property, mechanism, energy source, and hybrid-AM process data in Appendix D is the basis of the high-level relationships shown in the PMEH framework in Fig. 3. Five fundamental physical mechanisms were found to currently unify hybrid-AM processes, each affecting specific properties in hybrid-AM materials and parts. It is thus evident that if certain properties are desired, it will drive the choice of mechanism and, in turn, the utilized energy source, ultimately determining the hybrid-AM process. This section will give an overview of each relationship in the PMEH framework beginning with the relationship between material

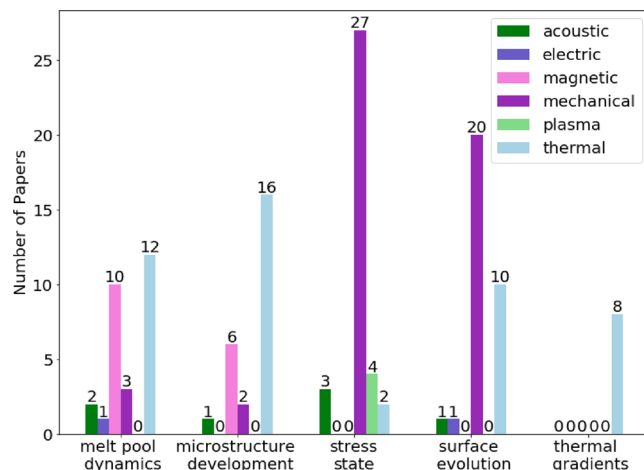


Fig. 7. Energy sources utilized to affect five physical mechanisms in hybrid-AM.

property and mechanism (Section 3.1), followed by energy sources used in each mechanism (Section 3.2) and the respective hybrid-AM processes for each energy source (Section 3.3). While the general framework and the number of papers addressing each mechanism are

presented here, a detailed discussion of various specific PMEH relationships is given in Section 4 within a review of each physical mechanism.

3.1. Material properties and mechanism relationship

Each physical mechanism is directly related to the resulting material structure and, therefore, property, indicating that the choice in mechanism can have a large influence on the resulting material performance. Fig. 6 shows radar plots of the average of reported mechanical properties for 316 L, Alloy 718, and Titanium Gr 5.

In each radar plot, the axis indicates the absolute value of the property and units are shown in the legend. Each data point is the average value of those reported; for example, the data point for [hardness, thermal gradients] for 316 L is the average value of all hardness values reported in papers that utilized the thermal gradients mechanism for 316 L. In this way, the effect of each mechanism on mechanical property, in general, is shown. Further discussions on microstructure evolution, (e.g., grain growth breaking, reduction in residual stresses, and grain refinement), or effects on functional properties, (e.g., surface roughness, production rate, etc.), can be found in Section 4.

The clearest influence of any mechanism is thermal gradients on Titanium Gr 5, where the ultimate tensile strength (UTS) and yield strength (YS) are 400 MPa higher than any other reported average value. This is attributed to grain refinement, reduction of cracks and porosity,

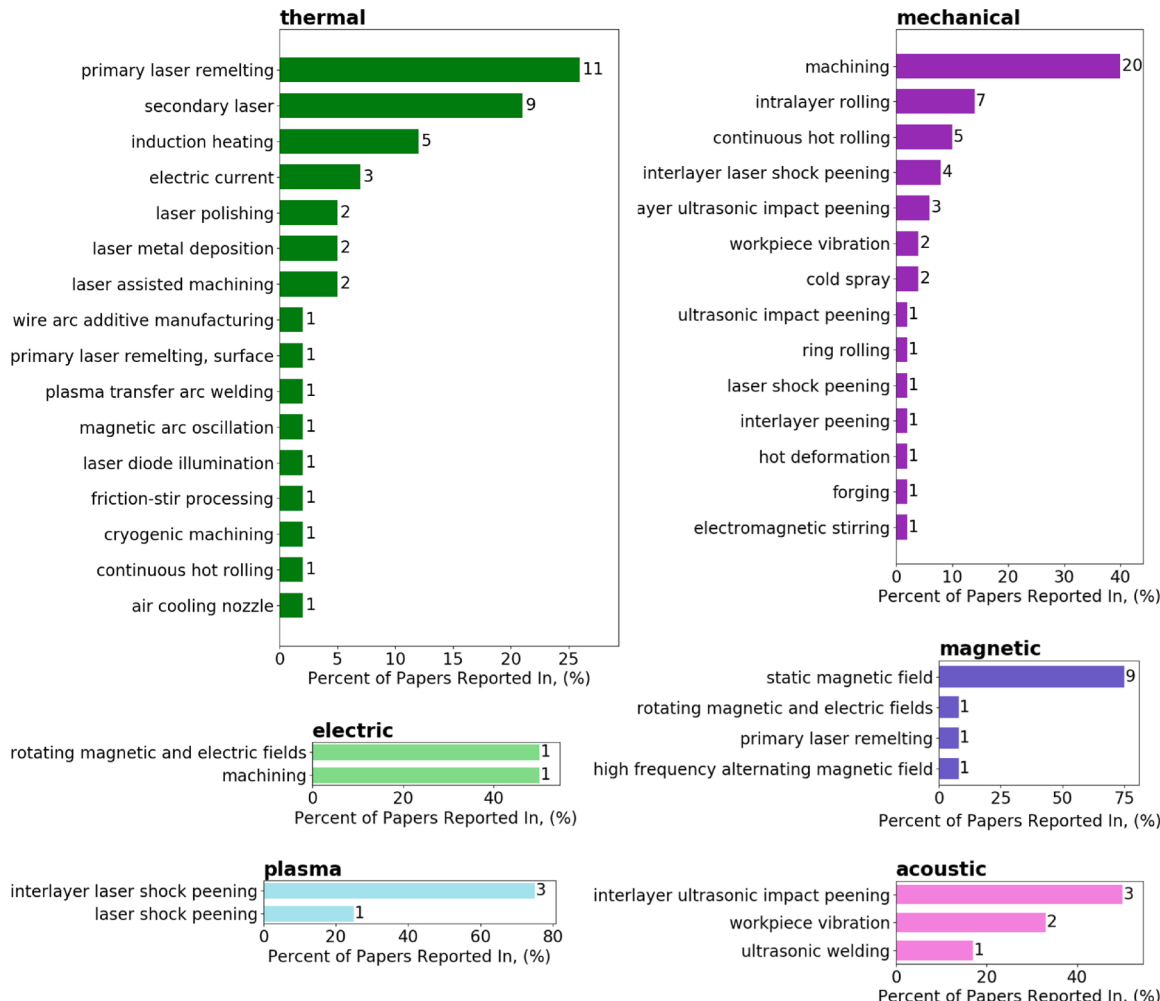


Fig. 8. Energy sources used in hybrid-AM processes. The two most common hybrid-AM processes are “AM + machining” and “AM + primary laser remelting”, followed closely by secondary laser processing and use of static magnetic fields.

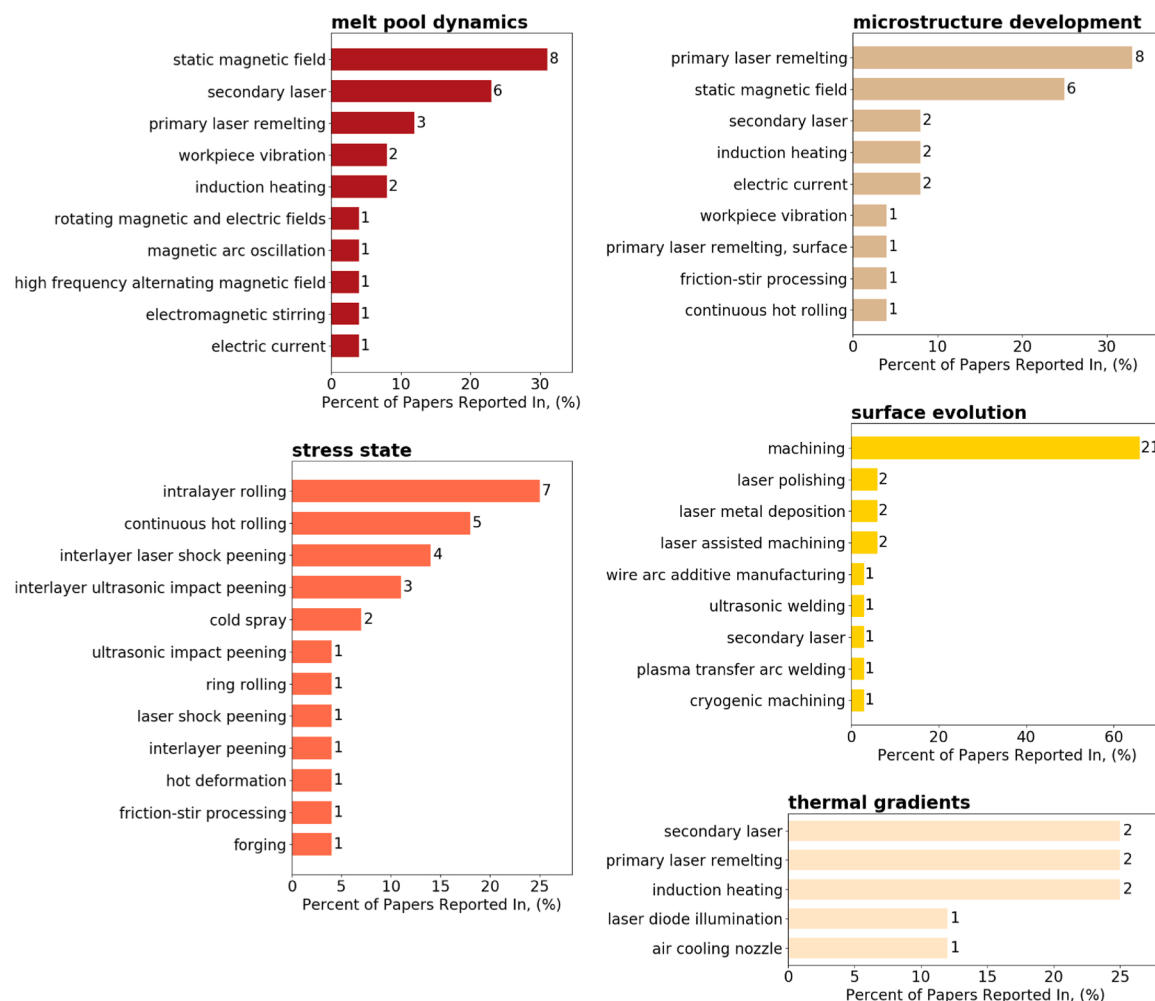


Fig. 9. Processes used to affect five physical mechanisms in hybrid-AM.

as well as decrease in anisotropy by controlling thermal gradients (further discussed in Section 4). In this case, the reduction of cracks and porosity probably contributes the most to the increase in UTS and YS. Titanium Gr 5 had the most mechanical properties studied across all mechanisms, which is shown by the large area coverage in Fig. 6. Both 316 L and Alloy 718 show significant gaps in reported mechanical properties, where the microstructure development and thermal gradients categories only have hardness reported for 316 L. However, it is noted that surface evolution had the largest effect on hardness for 316 L (increased by 100 HV), and melt pool dynamics showed the largest change in UTS for Alloy 718 (largest value by 200 MPa). More conclusions on the effect of mechanism choice on mechanical property can be drawn as gaps in knowledge are filled in for each material, and more specific relationships are discussed in Section 4.

3.2. Mechanism and energy source type

The types of energy sources utilized within each mechanism is shown in Fig. 7. Mechanical and thermal energy sources were the most widely used, which is attributed to ease of implementation. There is, however, a clear difference in which mechanisms they are used for.

Specifically, mechanical energy is used almost exclusively to create stress state and surface evolution changes, while thermal energy is used in every mechanism, exhibiting its versatility. Plasma and electric energies are the least commonly used: plasma has only been used to alter stress state, and electric energy has only been utilized to create differences in melt pool dynamics and surface evolution.

3.3. Energy source utilization in hybrid-AM processes

The utilization of energy sources in hybrid-AM processes is shown in Fig. 8. Thermal and mechanical energies are, respectively, most used to add heat when using a primary or secondary laser for remelting/heating or in the removal of material in machining. More specific applications are seen for acoustic, magnetic, plasma, and electric energies because of the increased difficulty in incorporating them into a hybrid-AM process. The most notable applications of the less popular energy sources are acoustic energy in ultrasonic impact peening, magnetic energy in the use of static magnetic fields to alter melt pool dynamics, and plasma energy used in laser shock peening.

4. Physical mechanisms of concern

In the previous section, the overarching relationships between properties, mechanism, energy source, and hybrid-AM process were presented. As known, there are many more specific relationships and examples within the PMEH framework. In the following five subsections, each mechanism will be discussed in detail, as well as the corresponding processes that drive the mechanism and their effects on material and part properties. It is noted here that the proposed definition of hybrid-AM readily presents two categories of processes: simultaneous and controlled processes (during the AM build process) and process chains (before or after the AM build process). While both process categories fit within the PMEH framework presented in Fig. 3, Sections 4.1–4.5 will discuss simultaneous processes and Section 5 will discuss

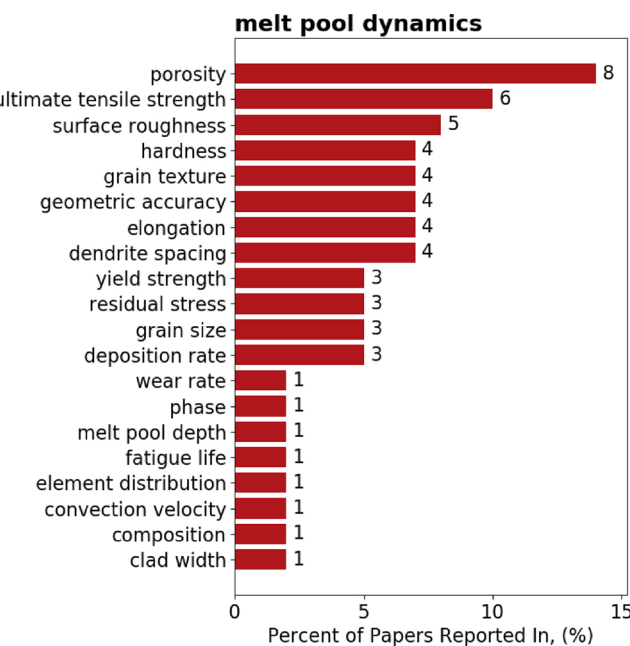


Fig. 10. Mechanical properties and process parameters (deposition rate, convection velocity) affected by melt pool dynamics.

process chains for clarity. The mechanisms are presented in the order shown in the PMEH framework in Fig. 3. The list of processes for each mechanism is shown in Fig. 9, which effectively summarizes the current state of the art in hybrid-AM.

4.1. Melt pool dynamics

While there are many physics associated with the melt pool, such as heat transfer, fluid dynamics, and capillary forces (Debroy et al., 2018), they all work together to determine the final size, shape, flow velocities, surface tension, and cooling rate of the melt pool. This section analyzes hybrid-AM processes that affect one or more of these fundamental aspects which ultimately determine the structure and properties of the final material (Olson, 1997).

Fig. 7 shows the percentage breakdown of the energy sources used to influence melt pool dynamics. It is clear that thermal energy is the most commonly used, which is most likely due to the ease of using a secondary laser to add energy into the system or using the same main laser to remelt solidified material. The second most used energy source is magnetic, wherein a static magnetic field can be used to influence the flow velocity of the melt pool through thermoelectric magnetohydrodynamic control. The last major energy source is mechanical, which makes up the last 12 percent of the utilized energy sources. A comprehensive list of processes is presented in Fig. 9. It is shown that the most frequently used processes are a secondary laser or a static magnetic field,

which aligns with the common use of thermal and magnetic energy. The following sections discuss the main effects of energy source on manipulating melt pool dynamics, specifically melt pool size and flow pattern. A full list of affected properties through manipulating melt pool dynamics is shown in Fig. 10, where porosity, ultimate tensile strength and surface roughness are the most frequently reported affected properties.

4.1.1. Melt pool size and deposition rate

Melt pool size in traditional AM is directly related to the amount of power being used in the build (Webster et al., 2020), where a larger melt pool will be able to handle an increased deposition rate. In hybrid-AM, a secondary energy source is used to augment the size of the melt pool in conjunction with the main processing source. Multiple techniques have been used: induction heating, secondary laser heating, and rotating magnetic and electric fields. Dalaee et al. (2020) used induction heating co-axially with a powder-blown system which increased melt pool depth from 0.03 mm to 0.5 mm and allowed a 3.6 times larger deposition rate overall. Another study by Nowotny et al. (2015) showed an increased deposition rate of 46% through heating of the substrate and deposition material in laser hot wire AM, which indicates a general increase in melt pool size.

The previous studies used indirect thermal energy to increase the melt pool size, whereas both Näsström et al. (2019) and Heeling and Wegener (2018) added thermal energy into their respective AM processes using direct heating via secondary laser beams in the leading and trailing positions. Näsström et al. (2019) demonstrated that the increased melt pool volume can reduce the melt wave amplitudes in WAAM, shown in a 35% decrease in standard deviation of measured melt profiles using a trailing laser beam, shown in Fig. 11. Heeling and Wegener (2018) additionally indicated that both a leading and trailing secondary laser beam with a small relative positional offset in SLM gives a smoother surface due to improved wetting behavior, as well as a larger chance for pores to escape given the larger reheated areas in the melt. Finally, Lu et al. (2019) utilized rotating electric and magnetic fields during DED to expand the melt pool to approximately 3 times larger due to the influence of electric and magnetic fields on the plasma above the melt pool. With increased melt pool size, the cooling speed became slower and the solidification mode was changed from ferritic-austenitic to austenitic-ferritic, resulting in an increase in hardness.

4.1.2. Melt pool flow pattern and velocity

The flow pattern and velocity of the melt pool in standard metal AM is mainly driven by the direction of deposition and convection forces in the melt pool (i.e., Marangoni convection) (Khalilah et al., 2016). Thermal and magnetic energy can be used to affect the flow pattern and velocity of the melt pool through induced thermal gradients, surface tension forces, and magnetohydrodynamic effects (Kao et al., 2020). The melt flow can be enhanced or inhibited depending on the secondary energy application, resulting in different heat transfer states of the melt pool as well as influences on microstructure through dendrite breaking.

Thermal energy sources such as primary laser remelting, secondary laser heating, and oscillating laser deposition generally led to an

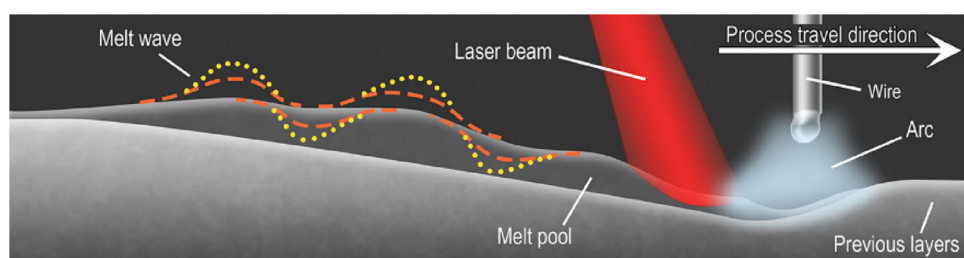


Fig. 11. Schematic of reduction in melt pool profile shapes using trailing laser beam (Näsström et al., 2019). Yellow dotted lines indicate larger waves, orange dashed lines indicate reduced wave amplitudes. (For interpretation of the references to color in this figure legend, the reader is referred to the web version of this article.)

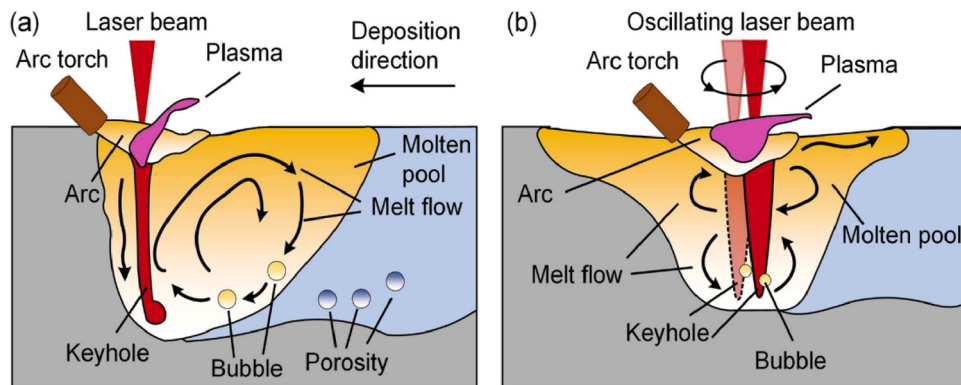


Fig. 12. Illustration of melt pool flow using (a) laser assisted hybrid WAAM and (b) oscillating laser assisted hybrid WAAM (Gong et al., 2020).

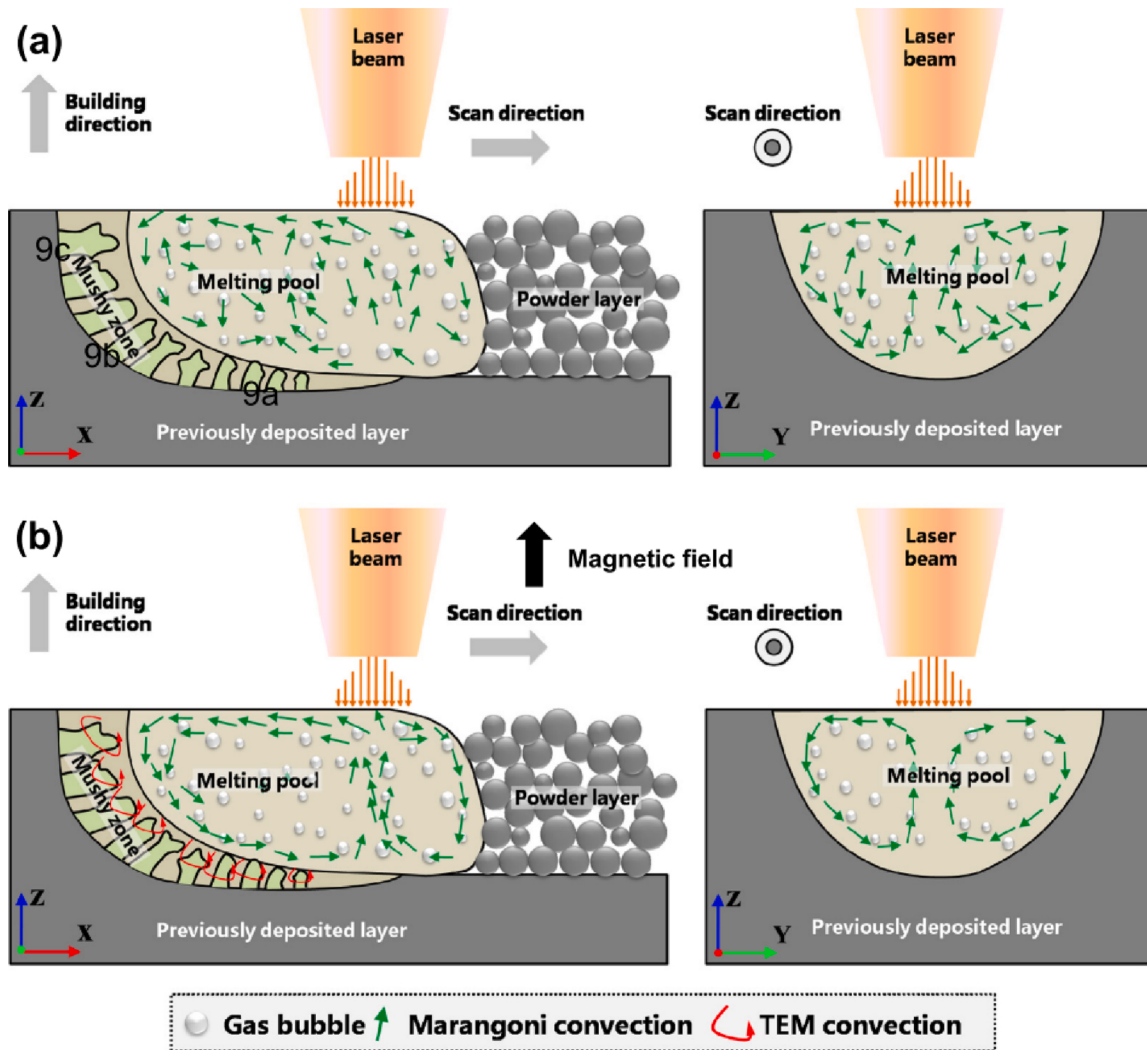


Fig. 13. Schematic of the effect of a static magnetic field on melt pool flow pattern during SLM. (a) Bubbles are trapped in Marangoni convection without magnetic field. (b) Damping of Marangoni convection by MHD and influence of TEMC caused by static magnetic field (Du et al., 2019).

improvement in the surface finish of the layer or part. For example, Zhao et al. (2019) used the primary processing beam in DED to remelt clads that resulted in a surface roughness decrease from $2.5 \mu\text{m}$ to $0.4 \mu\text{m}$. The remelting mechanism was earlier shown in laser polishing of SLS parts by Lamikiz et al. (2007), where the molten material flows from rough peaks and fills in valleys as surface tension forces bridge unevenness in previous layers. The melt pool is affected *in-situ* through use of a trailing

laser beam in WAAM by Näsström et al. (2019), shown again in Fig. 11, where the surface topology is decreased by 25% by mitigating noticeable waves created by the arc forces pushing on the melt pool. Another example of influencing the melt pool during deposition is by Gong et al. (2020), where an oscillating laser is used to induce a motion component perpendicular to the horizontal direction by changing its temperature distribution. This change in flow makes the melt pool shallower,

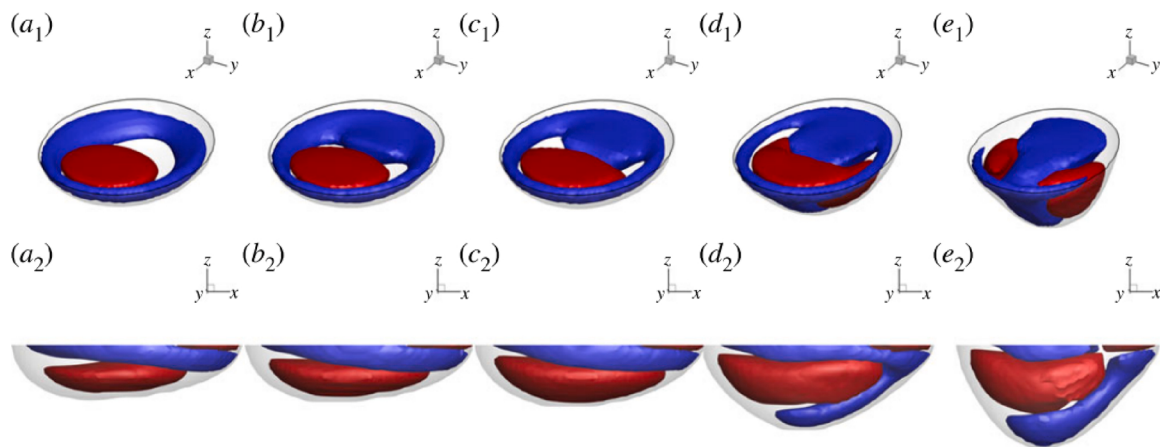


Fig. 14. Transition from Marangoni flow to TEMC flow with increasing magnetic field (a) 0 T, (b) 0.15 T, (c) 0.3 T, (d) 0.4 T, and (e) 0.5 T. Top row shows isosurfaces for flow in z direction and bottom row shows isosurfaces for flow in x -direction, red is positive and blue is negative (Kao et al., 2020). (For interpretation of the references to color in this figure legend, the reader is referred to the web version of this article.)

effectively improving surface accuracy. Pores are additionally mitigated because the keyhole is suppressed with distribution of heat from the oscillating laser, shown in Fig. 12.

The other main energy source used to affect the melt pool is magnetic energy, where both static and oscillating magnetic fields have been used. Zhou et al. (2020) indicated that a static magnetic field used during WAAM creates a significant tangential velocity in the melt pool, reducing its depth and increasing its width, leading to a smaller temperature gradient. In a separate application, Corradi et al. (2020) utilized oscillating magnetic fields to rapidly move the welding arc in WAAM; this resulted in a stirring effect and increased the convective flow. The forces that directly affect the melt pool using magnetic energy were more explicitly studied by Nie et al. (2020) and Du et al. (2019a). Both studies attributed changes in melt pool flow to a competition between two forces: magnetohydrodynamic damping (MHD) due to induced electromagnetic force in the bulk liquid and thermoelectric magnetic convection (TEMC) from the Seebeck effect. The general scale and effect of these forces is shown in Fig. 13.

MHD will restrain the standard Marangoni convection in the melt pool, decreasing its heat transfer and cooling rate. This restraint can result in reduced residual stress through increased time to fill interdendritic regions at the solidification front (Nie et al., 2020) or releasing bubbles normally trapped in the Marangoni vortex (Du et al., 2019). Du et al. (2019) showed that the melt pool velocity can be reduced by 83.9% using a static magnetic field of 0.12 T. TEMC increases the velocity at the

solidification front, interrupting a portion of elongated dendrites and resulting in grain refinement (Nie et al., 2020). While both of these studies highlight fundamental mechanisms that can be used in hybrid-AM, Kao et al. (2020) conducted the most thorough investigation of effects of static magnetic fields on molten pools through multi-physics simulations. Their study highlights the effect of static magnetic field direction and the resulting combined or inhibited flows within the melt pool, indicating that the bulk fluid flow can ultimately be controlled through directional magnetic fields by transitioning from Marangoni-dominated flow to TEMC dominated flow, shown in Fig. 14.

Changes in melt pool flow pattern and velocity can also directly affect microstructure through breaking of dendrites. This has been accomplished by using thermal and mechanical energy sources in hybrid-AM. Xiong et al. (2020) used primary laser remelting in conjunction with SLM, where previously formed columnar crystals are remelted and peeled off through a highly convective melt pool. The detached grains are engulfed in the molten pool and form free grains resulting in a fine grain zone. Mechanical energy sources were used by other researchers in a similar vein, where Liu et al. (2018) added electromagnetic stirring to DED, Zhang et al. (2019a) used part vibration in WAAM, and Todaro et al. (2020) used DED to deposit onto a workpiece actuated using an ultrasound sonotrode. Part vibration in the studies by Zhang et al. (2019a) and Todaro et al. (2020) had similar results to Xiong et al. (2020), where vibration led to nucleation of fine grains after dendrite arms were broken, shown in Fig. 15. In contrast, the

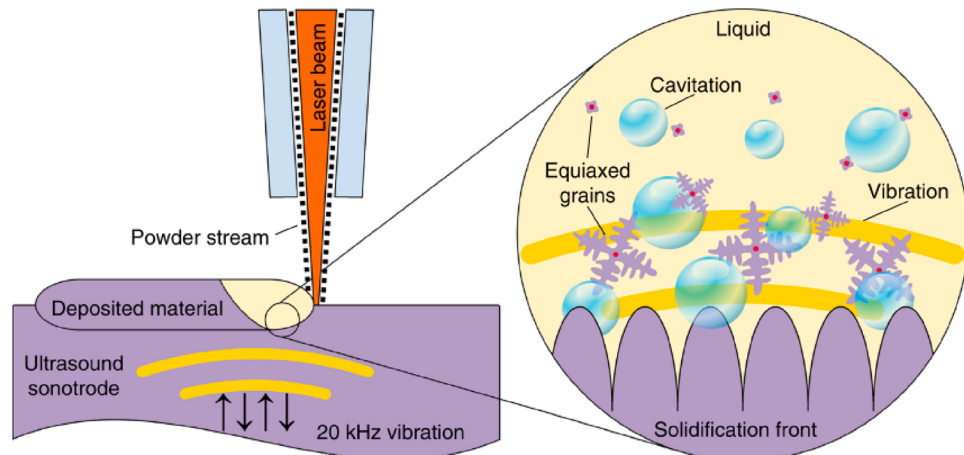


Fig. 15. Schematic of dendrite breaking through part vibration (Todaro et al., 2020). The melt is vigorously agitated, promoting grain refinement through nucleation of equiaxed grains via cavitation.

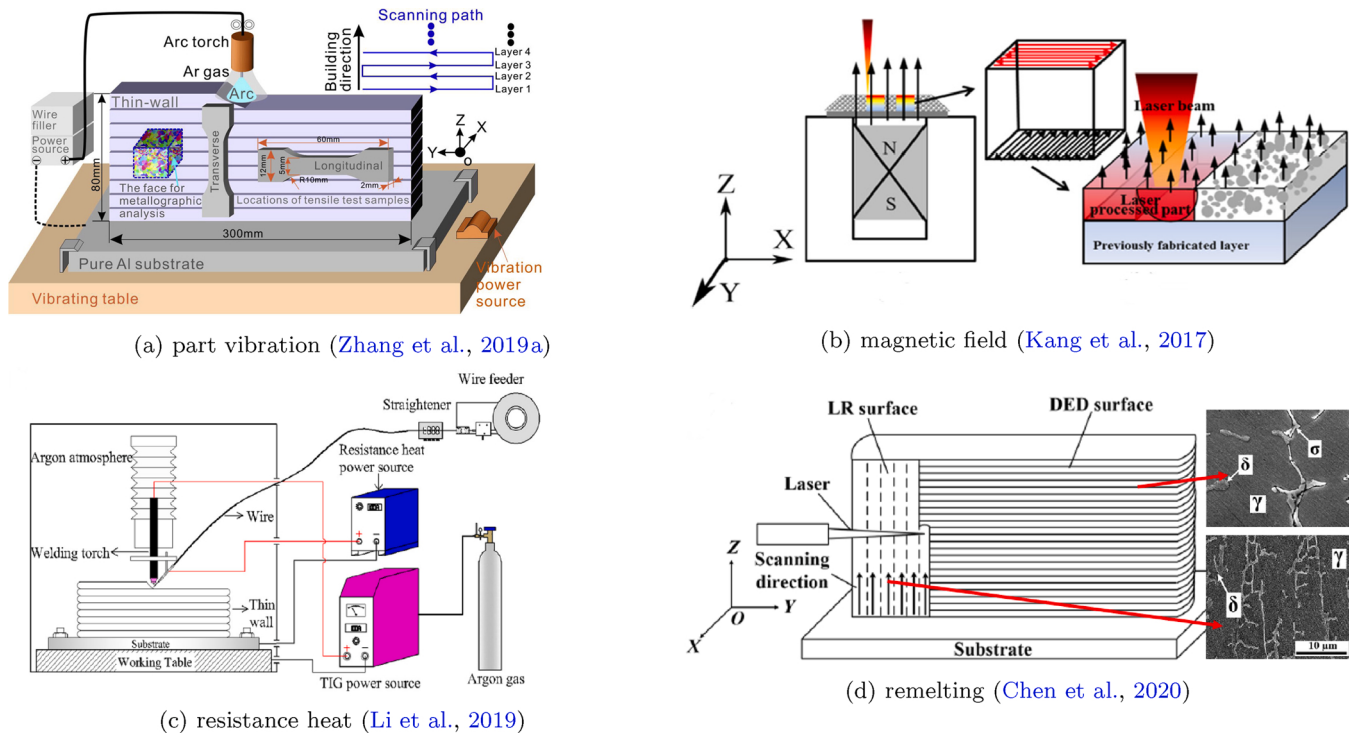


Fig. 16. Examples of hybrid-AM processes used to affect microstructure development.

electromagnetic stirring led to severe convection in the melt pool, where enriched alloying elements were moved away from interdendritic regions and the temperature gradient was increased at the solidification front.

In all, it is clear that multiple energy sources can be used to manipulate the melt pool in increasingly complex ways, which results in a variety of fundamental mechanisms that affect the final part quality in hybrid-AM.

4.2. Microstructure development

As one of five vital mechanisms used to influence material properties in hybrid-AM, microstructure development is defined as the act of changing micro scale structures of a material, mainly grain growth, element transition, texture or phase formation. In terms of AM, these changes occur through the course of cooling and have a significant influence on material properties.

As shown in Fig. 7, thermal energy is the most commonly used energy source to alter microstructure development followed by magnetic, mechanical and acoustic energy. The same types of energy sources are used for melt pool dynamics discussed in Section 4.1; but the amount of papers that reported using thermal energy in this case is more than twice of any other energy source. This is further reflected in Fig. 9, where processes that do not use thermal energy (static magnetic field, part vibration, friction-stir processing, and continuous hot rolling) account for only 36% of the processes utilized to alter microstructure development. Fig. 16 shows some examples of hybrid-AM processes using non-thermal and thermal energy sources. The first two utilize a vertical magnetic field (Kang et al., 2017) and vibration power (Zhang et al., 2019a), respectively. The last two utilize resistance heat (Li et al., 2019) and a secondary laser (Chen et al., 2020).

To characterize modifications in microstructure development, many investigations focus on grain size and shape, dendrite arm spacing, phase, texture, and porosity. Fig. 17 shows the percentage breakdown of properties investigated. Grain size is the most popular effect in terms of microstructure development, perhaps because grain refinement is relatively easy to achieve and effectively improves mechanical properties.

The following sections further expand upon the effects of energy source on microstructure development including grain size, grain orientation and texture, phase and element composition, and porosity distribution.

4.2.1. Grain size

Many current studies on manufacturing show that grain refinement can achieve comprehensive mechanical properties, i.e., both high strength and ductility (Guan and Tie, 2017). With respect to hybrid-AM, methods are used to create much finer and more homogeneous grain sizes by applying primary or secondary energy.

Primary laser remelting is a convenient technique used to melt coarse columnar grains and restrain grain growth due to high cooling rates induced by highly localized heating via laser power. Laser remelting strategies include surface remelting and inter-layer remelting. Surface remelting is only applied to the last (top or uppermost) layer of a part, but inter-layer remelting rescans other layers *in-situ* in addition to the surface layer. In terms of inter-layer remelting, Liu et al. (2019) indicated that laser remelting of each layer in SLM played a key role in grain size refinement with an increasing area fraction of equiaxed and fine grains. The shallower melt pool resulting from the second scan melted the coarse columnar grains at the top of the original melt pool line. This led to the formation of new equiaxed grains at the top of the re-scanned layer, while the original equiaxed grains remained unmelted at the lower regions. Furthermore, Griffiths et al. (2018) demonstrated that rescanning twice on each layer led to more grain refinement and homogenization, which is depicted clearly in Fig. 18.

Primary laser remelting, however, significantly slows down the AM process by rescanning the previous layer more than once. Thus, several secondary energy sources are utilized to affect grain size simultaneously without increasing the processing time. The study by Li et al. (2019) indicated that substrate, previous layers, and wire heated by 100 A electric current greatly refined coarse columnar grains, decreasing the width of β grains to 2 mm from 8 mm and further decreasing anisotropy in mechanical properties. The schematic illustration is shown in Fig. 16 (c). Du et al. (2019b) added a 120 mT vertical static magnetic field to SLM. The thermoelectric magnetic force (TEMF) was strong enough to break elongated columnar grains, causing its fraction to be reduced to

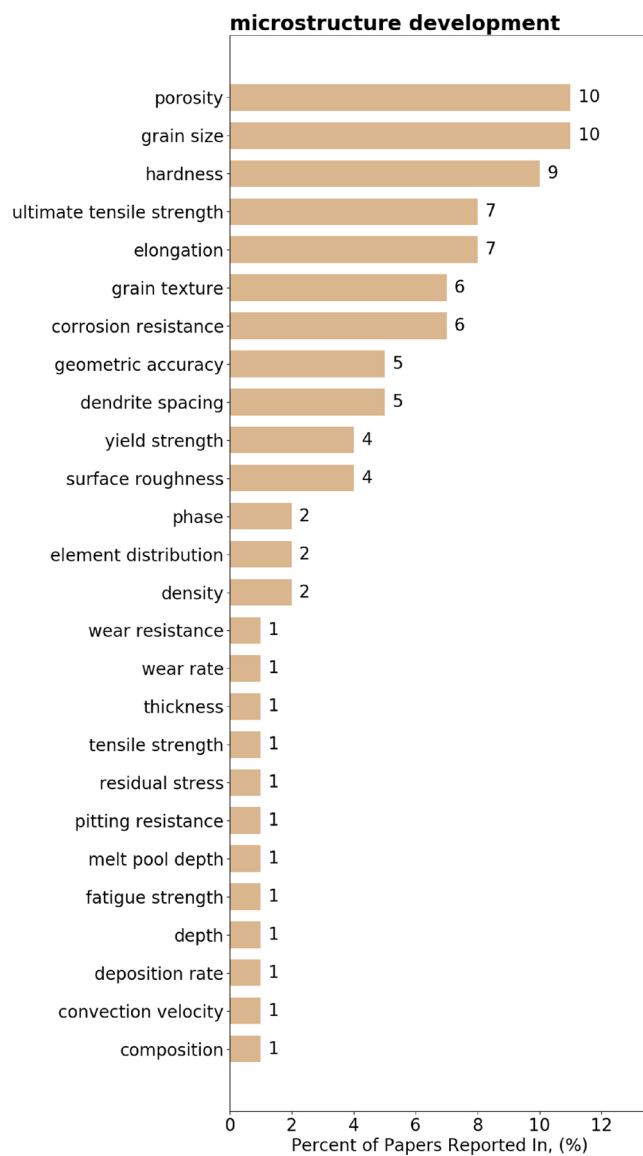


Fig. 17. Microstructure and mechanical properties affected by microstructure development. The three most commonly reported material properties are grain size, porosity, and hardness.

19% from 48%, as well as decreasing the dendrite spacing. The ultimate tensile strength (UTS) and elongation of magnetic field assisted AlSi10Mg samples increased from 325 MPa to 420 MPa and from 6% to 8.8%, respectively. Similarly, in the study by Nie et al. (2020), TEMF at the order of 10^6 Nm^{-3} interrupted grain growth and drastically refined grains. Zhang et al. (2019a) induced strong enough bending stress to break dendrite arms and form potential nuclei through part vibration during WAAM with a schematic shown in Fig. 16(a). It was presented that the average grain size can be reduced by 22.5% and the vibrated sample can achieve a UTS of 343 MPa with 22% elongation, which is much higher than those of wrought parts. Finally, Xie et al. (2016) applied hot rolling in WAAM to improve geometrical accuracy and mechanical properties. It was indicated that with finer and more homogeneous grains, the ultimate tensile strength of hybrid manufactured samples was increased by 6.6%.

4.2.2. Grain orientation and texture

Grain orientation in traditional metal AM is often controlled by changing process parameters, such as scanning strategies or laser power (Kirka et al., 2017). A part with uniform orientation of grains leads to

anisotropy in material properties. The most commonly used energy to influence grain orientation and form a highly oriented texture during hybrid-AM is magnetic energy, followed by thermal energy.

Al-Milaji et al. (2020) indicated that metal particles easily orient their magnetic axis parallel to the direction of applied external magnetic field during inject printing processes due to magnetostatic energy minimization. The manufactured films show high anisotropy of magnetic properties with improved saturation magnetization and susceptibility along this aligning direction. Similarly, Du et al. (2020) applied a 0.05 T or 0.1 T horizontal magnetic field to the DED manufacturing of Alloy 718, resulting in highly oriented grains and a (110) texture along the building direction. Furthermore, Wang and Shi (2019) applied a horizontal magnetic field with a much stronger strength of 1.0 T or 1.8 T, resulting in a (110) texture on the vertical cross-section, which is caused by both the heat flux (mainly along the building direction) and magnetic field that were perpendicular to each other.

Changing the laser power and heating area is also effective in altering grain orientation. Panteljev et al. (2017) indicated that remelting each layer was beneficial for grains to orient along the building direction across several layers. In addition, Koike et al. (2018) modified the dendrite growth direction by combining the remelting process with DED. Results indicated that the surface hardness increased by 26% due to more dendrites being directed to the hardest plane of (200), shown in Fig. 19. Finally, a study by Liu et al. (2019) showed that a texture along (100) plane in the samples built with a remelting strategy, wherein each layer was rescanned using the same toolpath as the former scan.

4.2.3. Phase and element composition

Phase transformation has been observed, modeled, and controlled in multiple studies using AM (Zhang et al., 2019b). Thermal energy is added in hybrid-AM through primary and secondary laser remelting, as well as resistance heat induced by electric current, in order to alter phase and element composition. Some studies improved microhardness through laser remelting based on these phase composition changes. For example, Yang et al. (2019) demonstrated that combining laser deposition and remelting led to the formation of hard phase Fe2B in samples which showed significant improvement in both microhardness and wear resistance. Surface quality was also improved in secondary laser remelting (LR), such as in the study by Chen et al. (2020), wherein secondary laser scanning in a direction parallel to deposition direction, shown in Fig. 16(d), led to improved surface quality. The deposited part showed a microhardness of 224 HV, which increased from 202 HV. This is mainly attributed to the increasing volume fraction of δ phases in the surface from 7.8% to 11.8% and the disappearing σ phases, shown in Table 1. A similar mechanism was shown by Liu et al. (2019), where each layer throughout the SLM process was rescanned with the same toolpath. The samples fabricated using this remelting strategy showed a microhardness improvement of 121.6 HV from 117.7 HV due to more Mg and Si dissolving in Al matrix resulting in solution strengthening.

Element composition modified by hybrid-AM can have a large impact on corrosion resistance. In a study by Zhang et al. (2020), metal wire was preheated by resistance in laser deposition, producing a hypo-eutectic structure with cobalt matrix in dendrite region and carbides in inter-dendrite, respectively. Such a structure indicated a different corrosion mechanism where the dendrite region was dissolved rather than the inter-dendrite region, resulting in much better corrosion resistance. In contrast, however, Vaithilingam et al. (2016) demonstrated that although better surface roughness is achieved through remelting of the top layer (surface remelting), it can also decrease corrosion resistance of Titanium Gr 2 parts due to increasing contents of Al and V in the top layer.

Other energy sources also present obvious alteration in element distribution. Kang et al. (2017) introduced a magnetic field along the building direction by mounting a permanent magnet under the substrate as shown in Fig. 16 (b), which resulted in the hardness at the bottom of

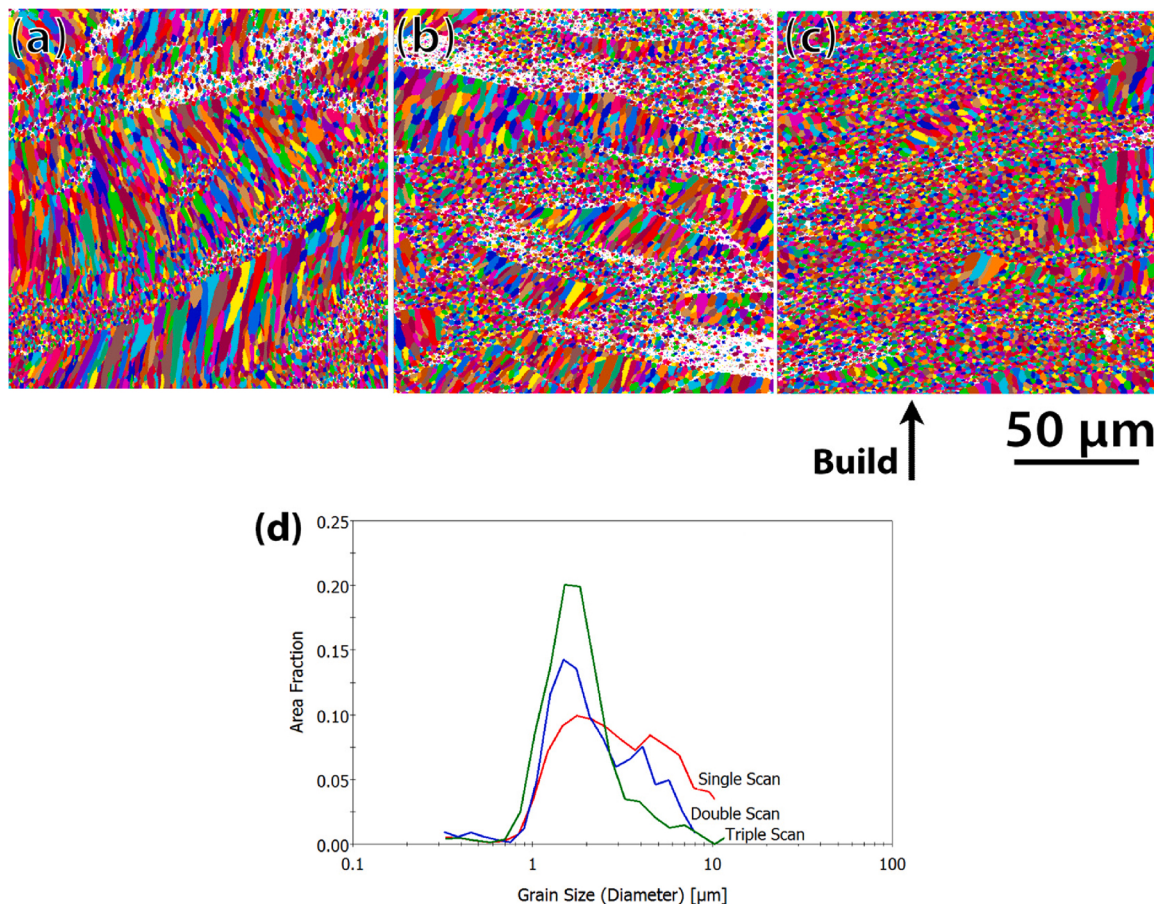


Fig. 18. EBSD grain maps of (a) single, (b) double, and (c) triple scans; (d) Distribution of area fractions vs. grain diameter (Griffiths et al., 2018).

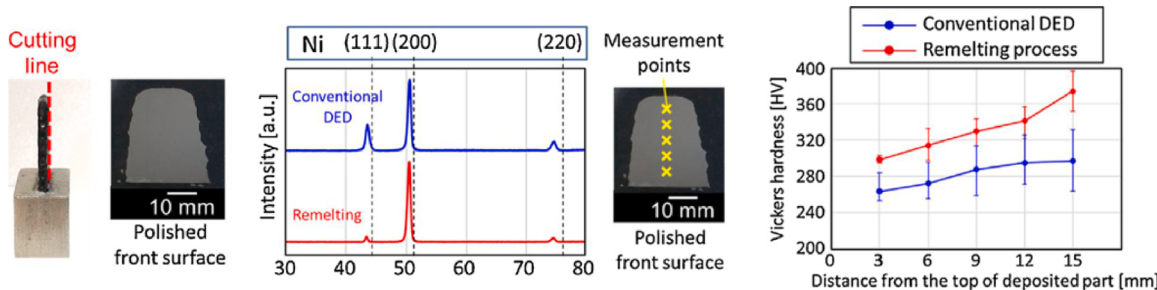


Fig. 19. Comparison of XRD analysis and hardness measurement on polished front surfaces of deposited part with conventional DED and DED combined with remelting process (Koike et al., 2018).

Table 1

Phase volume fraction and microhardness of DED 316 L and LR (Laser Remelting) surface (Chen et al., 2020).

Sample	δ phase/vol.%	σ phase/vol.%	Microhardness/HV
DED	7.8	3.0	202
LR	11.8	0	224

the sample to increase from 165 ± 36 HV to 535 ± 169 HV, attributed to the silicon content at the bottom of the sample increasing from 53.9% to 76.4%. An intensified fluid flow in the melt pool induced by TEMC led to a higher vaporization rate of Al and increased silicon content which resulted in larger grains, which is a different result from the study by Du et al. (2020) mentioned in Section 4.2.2. In the study by Wang and Shi (2019), the TEMC induced by external magnetic field significantly

restrained the microsegregation of Laves phase in γ matrix, forming a discontinuous morphology. Schirra et al. (2020) showed that continuous Laves phase improved crack initiation and propagation, significantly reducing fatigue life, UTS, ductility of wrought Alloy 718. Thus, less Laves phase with a discontinuous morphology could be beneficial to mechanical properties, i.e., UTS, ductility, fatigue life, and hot cracking resistance. Nie et al. (2020) indicated a more even distribution of Nb element in dendrite and inter-dendrite regions of the sample under a horizontal magnetic field of 0.55 T, shown in Fig. 20. However, a study by Zhang et al. (2019a) demonstrated that the influence of part vibration on the formation of strengthening phase was not significant. Thus, more studies should be conducted to study the effect of mechanical energy source on phase transformation to understand these differing results.

4.2.4. Porosity and pore distribution

In traditional AM, porosity has been given attention due to AM

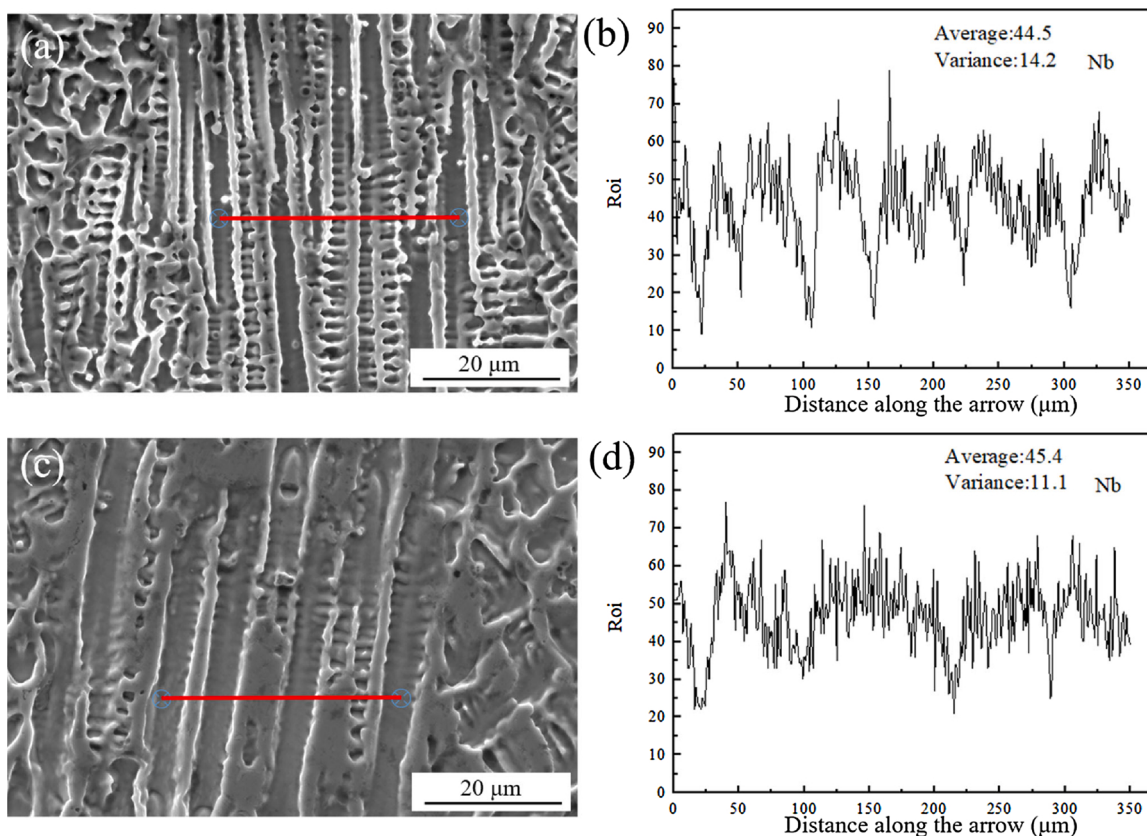


Fig. 20. SEM-EDS line scanning of the region within the laser remelted Alloy 718 substrate under different magnetic fields: (a, b) 0 T and (c, d) 0.55 T (Nie et al., 2020).

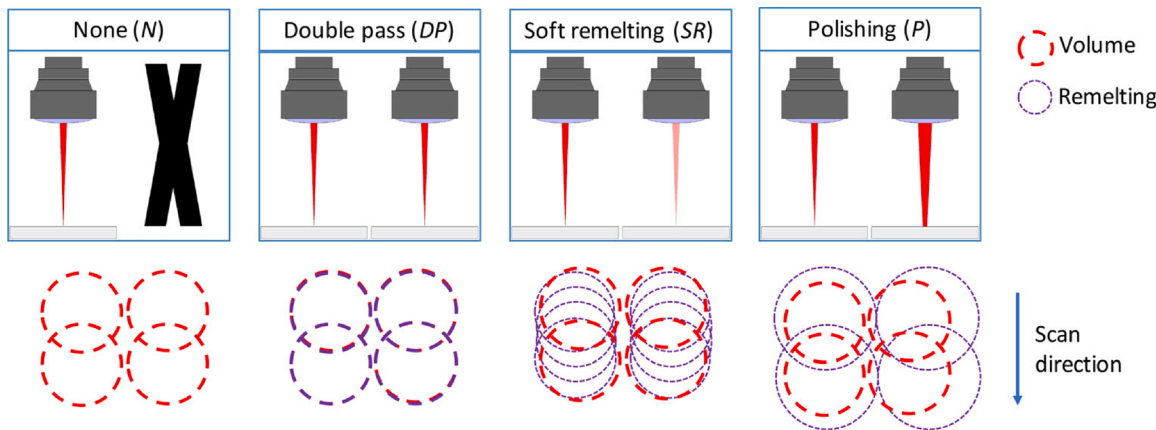


Fig. 21. Schematic representation of the volume and remelting passes applied in each strategy (Demir and Previtali, 2017).

processes' propensity to form pores (Webster et al., 2019) and its negative effect on mechanical properties (du Plessis et al., 2018). This property was frequently investigated in hybrid-AM in studies that utilized primary laser remelting, application of a static magnetic field, and part vibration.

Several different remelting strategies have been used to reduce porosity or modify pore distribution. For instance, Pantelićev et al. (2017) and Demir and Previtali (2017) both remelted each layer in a direction perpendicular to the previous scanning direction and demonstrated reduced porosity and larger grains than in SLMed parts. Pantelićev et al. (2017) showed that metallurgical pores and voids were filled in during the recoating and remelting each layer. Demir and Previtali (2017) applied three different remelting strategies by varying laser

parameters. The polishing strategy inducing a larger and shallower melt pool, which exhibited the smallest porosity and corresponded to the best average surface roughness, which decreased to 4 μm from about 8 μm, shown in Fig. 21.

Different from the previous studies, Gustmann et al. (2018) remelted every layer in the same direction as the previous scanning direction, resulting in the elimination of pores smaller than 100 μm when the input energy was 35.4 J/mm. The relative density of samples increased to $99.5 \pm 0.3\%$ from $98.9 \pm 0.1\%$ and grains were slightly refined. Similarly, Koike et al. (2018) applied the remelting process every 10 layers, showing that 61% of residual pores were removed.

Other secondary energy sources used are magnetic and acoustic energy. The study by Du et al. (2019) showed that bubbles trapped in the

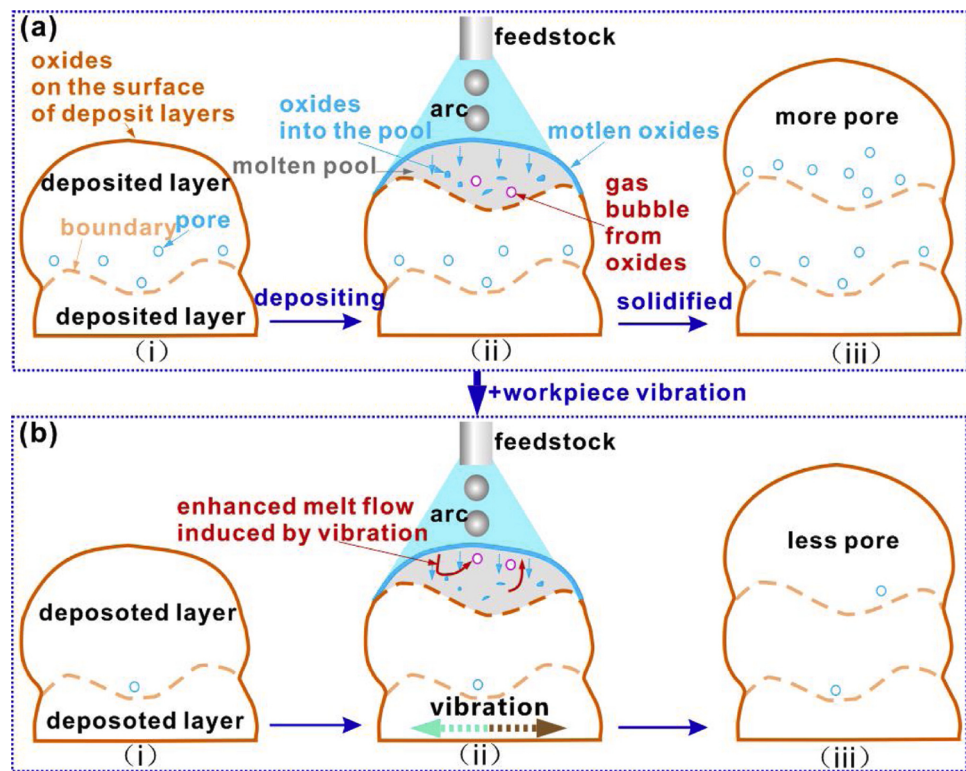


Fig. 22. The illustration of the decrease of porosity; (a) schematic cross section of the processing of a deposited layer without part vibration; (b) schematic cross section of the processing of a deposited layer with part vibration. (i): before processing, (ii): during processing, (iii): after processing (Zhang et al., 2019a).

melt pool could escape due to the damping effect induced by magnetic field on rapid Marangoni convection, resulting in a relative density increase to 99.6%, shown in Fig. 13. Kang et al. (2017) also applied the magnetic field to SLM but indicated an uneven distribution of pores where the bottom of the sample was less porous than the top. This was attributed to a larger silicon content at the bottom of the sample, which led to a lower thermal conductivity and a lower cooling rate, allowing more liquid to flow to the bottom of the sample and fill in pores. Finally, Zhang et al. (2019a) presented that the stirring effect induced by part vibration allowed oxide gas bubbles to escape from the melt pool, shown in Fig. 22, reducing the porosity from 6.66% to 1.52%.

4.3. Stress state

The third main mechanism that fundamentally alters AM materials through hybrid manufacturing is stress state. Four secondary energy sources are used to affect the stress state: mechanical, acoustic, plasma, and thermal. Fig. 7 shows the number of papers that reported use of each energy source. Mechanical energy sources are the most used, with 27 reported uses. The wide use of mechanical energy is expected as it is the most straightforward application of external energy to change the stress state of the workpiece. Acoustic, plasma, and thermal energies are combined within mechanical energy sources through ultrasonic vibration, laser shock peening, and hot rolling processes, respectively. These three main processes are also the most commonly used to affect the stress state. A full list of processes used to alter the stress state of a hybrid-AM material is shown in Fig. 9, where the processes are separated into categories of inter-layer processes (between multiple or singular layers) and surface modifications (which still reflect the result of the hybrid mechanism but not of bulk modifications). Four effects develop from the application of different energy sources in these processes: dynamic recrystallization, columnar grain growth breaking, conversion of residual stresses, and geometric accuracy and porosity improvement. The following sections highlight each of these effects and

the resulting affected material properties. A full list of affected material properties is shown in Fig. 23, where the most frequently reported affected properties are grain size (13 papers), hardness (12 papers), and ultimate tensile strength (10 papers).

4.3.1. Dynamic recrystallization

Dynamic recrystallization occurs when nucleation and growth of grains occurs during large deformation rather than during heat

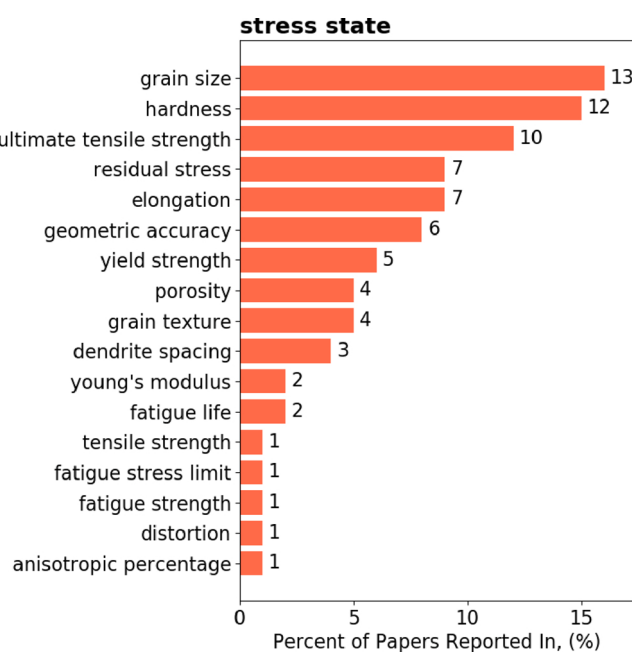


Fig. 23. Mechanical properties affected by the stress state.

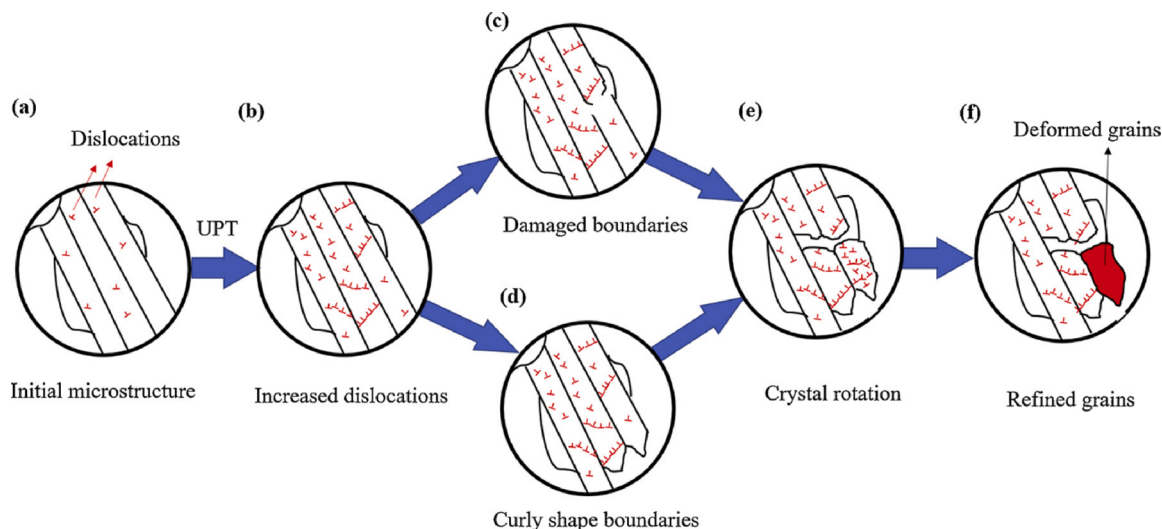


Fig. 24. Diagram of grain refinement using UIP (Gou et al., 2020).

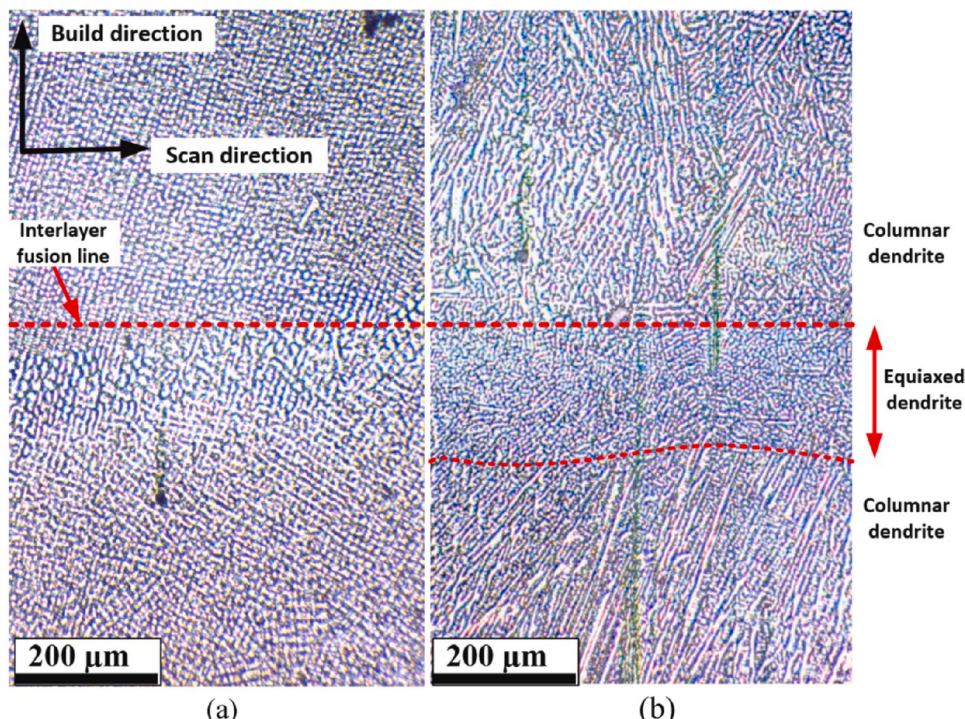


Fig. 25. Optical microscopy images of grain morphology in (a) LMD-only and (b) LMD and UIP, where layer of equiaxed grains prevents columnar grain growth in subsequent layers (Wang and Shi, 2020).

treatment (Huang and Logé, 2016). This mechanism occurs during ultrasonic impact peening (UIP), which uses acoustic energy to drive a small pin that mechanically deforms the metallic surface of the AM part. Gou et al. (2020) showed the effect of UIP as a surface treatment on single track depositions of Titanium Gr 5. High strain localization from UIP causes dislocation slip that leads to ultrasound-induced grain boundary sliding, crystal rotation and finally the formation of refined grains, shown in Fig. 24. Large induced residual stresses led to a decrease in β grain width from 1.8 mm to 1.3 mm (with a decrease in aspect ratio from 15.6 to 6.2, respectively), as well as a reduction in α bulge size from 50–70 μm to 10–30 μm and damaged/curly boundaries on originally lamellar structures. It is noted that large grain sizes here are due to using WAAM, where grains in the new layer nucleate at a previous layer and continue to grow up through multiple layers at a time. A similar

mechanism was shown by Wang and Shi (2019) in Titanium Gr 5, where UIP treatment after every deposition layer resulted in high compressive stress in interlayer regions; this provided a driving force for twinning and dynamic recrystallization. In this study, additional static recrystallization was observed in the rapid heating of subsequent layers in SLM. Both mechanisms worked together to refine grain size and create equiaxed grains at the interlayer regions.

4.3.2. Columnar grain growth breaking

In traditional metal AM, columnar grains are able to grow across long stretches of material in the direction of layer heating due to re-heating of subsequent layers (Parimi et al., 2014). This leads to anisotropy, one of the biggest challenges in metal AM. One way the re-growth of columnar grains can be hindered is by nucleating a layer of fine, equiaxed grains.

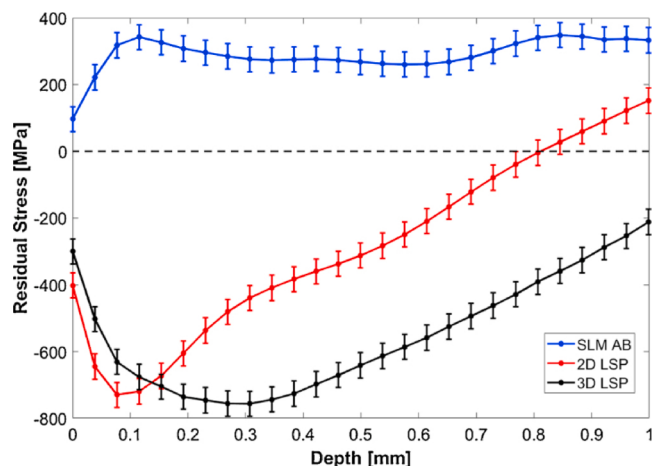


Fig. 26. Residual stress in samples using (a) SLM only (b) surface-treatment LSP and (c) inter-layer and surface-treatment LSP as a function of depth below the part surface (geometry of part is 1 in. cube) (Kalentics et al., 2020).

This has been accomplished in hybrid metal AM through interlayer UIP and interlayer rolling. A study on interlayer UIP was conducted by Wang and Shi (2020) that showed a fine equiaxed dendrite region approximately 200 μm deep within interlayer regions, shown in Fig. 25; this region of fine grains (around 10 μm) prevented columnar growth between layers.

Columnar grain growth breaking was also shown in interlayer hot rolling by Zhou et al. (2016) where larger rolling reduction led to a more uniform distribution of strain energy and dislocation density in the dynamic recrystallization region, ultimately resulting in highly refined grains on top of large columnar grains. Perhaps the most thorough study of this mechanism was performed by Donoghue et al. (2016), Colegrove et al. (2013) and Martina et al. (2015), though, where maps of strain and reconstruction of prior β grains were created from samples of interlayer rolling of Titanium Gr 5 in WAAM (Donoghue et al., 2016) and then mapped in conjunction with residual stresses in both Titanium Gr 5 (Martina et al., 2015) and steel (SupraMIG G3Si1/ER70S-6 wire) (Colegrove et al., 2013). This group showed that the “ratcheting” effect of β columnar grain regrowth was mitigated by nucleation of new β orientations associated with the $\alpha \rightarrow \beta$ phase transformation during reheating of the β transus temperature. This implies that rolling creates

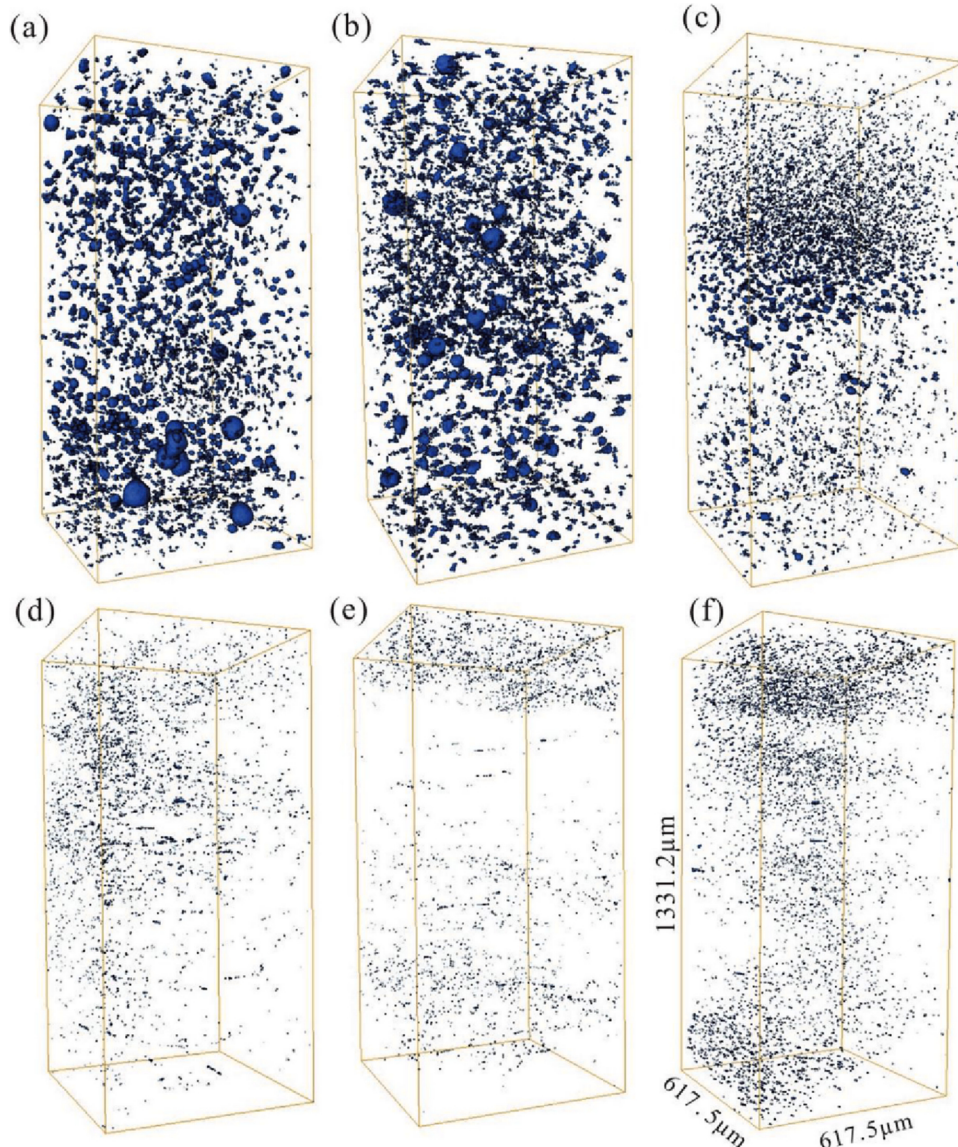


Fig. 27. Micropores in WAAM for (a) as deposited, (b) post-deposition heat treated, (c–e) 15 kN, 30 kN, and 45 kN inter-layer rolled, and (f) 45 kN rolled and heat treated (Gu et al., 2020).

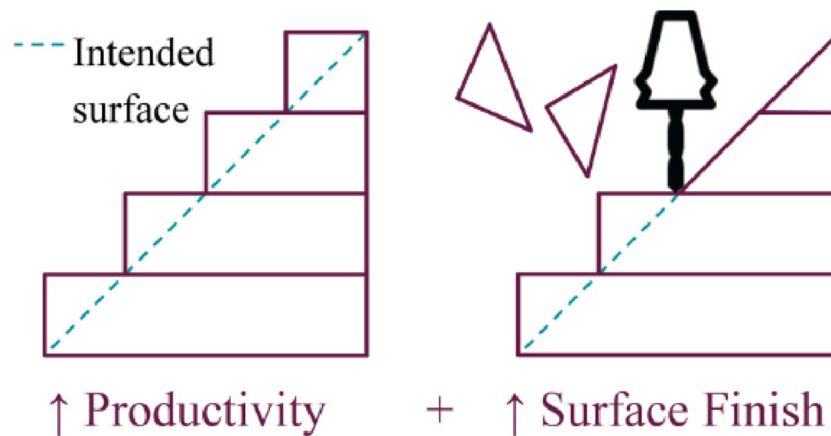


Fig. 28. Conceptual visualization of the hybrid surface evolution techniques (Du et al., 2016).

new β orientations and these grow in the subsequent heating step. This cyclic nucleation of weak textures and small grain sizes of 56–139 μm ensures the halting of β regrowth and large, columnar grains on the order of centimeters.

4.3.3. Conversion of residual stresses

Residual stresses build up in traditional metal AM from shrinkage during rapid solidification and cooling. Large tensile stresses are created on the surface of a part that are balanced by a large bending moment upwards when a part is removed or unclamped from the build plate (Li et al., 2019). This challenge has been addressed through metal hybrid-AM by converting tensile residual stresses to compressive stresses through UIP, laser shock peening (LSP), and interlayer rolling.

Zhou et al. (2020) modelled interlayer UIP with DED, showing that the plastic deformation zone (PDZ) can be increased through UIP frequency or amplitude increase causing stress relaxation to a certain depth and a fine-grained microstructure ($<25 \mu\text{m}$). The microstructure and stress relaxation can be applied to the full part by adjusting the thickness of each deposited layer to be less than the calculated PDZ. Interlayer rolling is similar in the fact that a compressive force is applied to the surface and results in conversion of tensile residual forces to compressive residual forces, or at the very least mitigation of the tensile stresses (Martina et al., 2013). Colegrove et al. (2013) shows a reduction in residual stress from 600 MPa to 250 MPa in carbon steel interlayer rolling with WAAM, where the peak stress is located at the interface of the baseplate and thin wall. The residual stress was calculated from residual elastic strain measurements using the SALSA neutron diffractometer at the Institut Laue-Langevin, France. It was determined that remelting during the welding process (producing tensile stresses at each layer) was in competition with the rolling steps (producing compressive stresses at each layer) to define the final stress state; whichever step affected the larger area (or depth in the thin wall case) would determine the final stress state (Martina et al., 2016). The same reduction in residual stress and competition between remelting and rolling was shown in Titanium Gr 5 WAAM by Martina et al. (2014) (500 MPa to 200 MPa) since distortion was not eliminated completely.

LSP has a mechanism different than direct application of force to create compressive stress, as in UIP and interlayer rolling. Metal materials are very stiff and thus will resist expansion from the plasma shockwave generated by LSP and will build a local compressive field (Hackel et al., 2018). In this way, tensile stresses can be mitigated or converted into compressive stresses across an AM part through interlayer LSP, shown in Fig. 26. For example, Kalentics et al. (2020) performed LSP at 10 layers and the final layer of 316 L parts, where the increase in fatigue life was more than 15 times compared to the as built part due to accumulation of compressive residual stresses and a reduction in porosity in the LSP affected zone.

Both Madireddy et al. (2019) and Sealy et al. (2016) modelled LSP with DED and SLM, respectively. Madireddy et al. (2019) specifically studied the effect of peening layer frequency in carbon steel, where LSP was applied once every 1, 5, and 10 layers in a part. More frequent peening led to a more sustained compressive stress band below the surface; however, only layer-by-layer peening induced compressive residual stresses that were not completely cancelled from heat or mechanical redistribution, suggesting that more frequent peening between layers or multiple peenings are necessary for full mitigation. Additionally, dramatic reversals in compressive residual stress is shown between layers, which could lead to short cycle fatigue failure. Sealy et al. (2016) investigated the effect of layer thickness on interlayer LSP in Titanium Gr 5, where thinner layers required higher peening such that a larger depth is affected and subsequent layer heating will not cancel out the formed compressive stresses, which is in agreement with Madireddy et al. (2019). Both of these studies led to the conclusion that an optimal peening condition can be defined for a given layer thickness and ultimately used to create a desired residual stress contour.

Finally, Lin et al. (2018) improved upon regular interlayer LSP by adding graphene layers during LSP, where graphene acts as a shock-loading transferor, allowing the shock wave to pass through and bounce back between the layers. This results in high density dislocation and nanotwinning structures around the graphene interface where a tensile stress of 150–200 MPa is reduced to compressive stress of 450 MPa. Microhardness and fatigue life were greatly improved due to the large amount of strain energy stored.

4.3.4. Geometric accuracy and porosity improvement

The last two effects of altering the stress state in hybrid-AM materials are greater geometric accuracy (Xie et al., 2014) and closing of porosity (Gu et al., 2020). Improved geometric accuracy is generally achieved through all previously discussed processes, but was specifically studied by Xie et al. (2016) in continuous hot rolling in WAAM. Their group developed a novel metamorphic rolling mechanism for various rolling configurations. It was shown that there was a 78% reduction in absolute error and standard deviation of bead heights after rolling. Grains additionally became equiaxed rather than columnar. As for reduction on porosity, Gu et al. (2020) showed that the size and number of micro-pores in Al-Cu0.3 alloy decreased with increasing rolling loads in WAAM (as voids in the metal were closed together), shown in Fig. 27, and Shchitsyn et al. (2020) demonstrated that peening leads to almost complete disappearance of pores with a 4.7% reduction in porosity compared to cold metal transfer (CMT) without peening.

4.4. Surface evolution

The surface evolution of AM metal parts in both PBF and DED

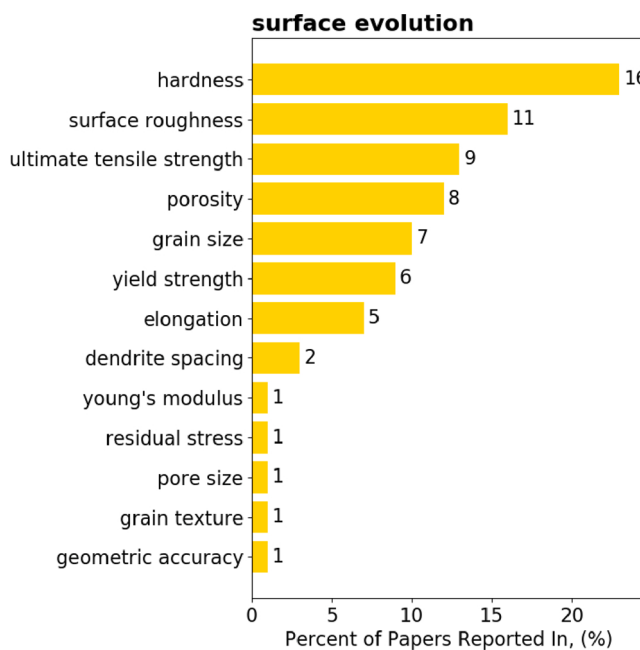


Fig. 29. Mechanical properties affected by surface evolution. Hardness and surface roughness are the most often reported properties.

methodologies is inherently dependent on processing and material conditions. These conditions are comprised of many factors. On the process side, elements such as energy source size and profile, gas flow, toolpath strategy, layer thickness and others contribute to the resultant surface. On the material side, elements such as material feedstock, size, geometry, and thermophysical properties all contribute to the final surface. In many instances, metal AM processes alone cannot achieve the required surface conditions while meeting an acceptable production rate. In fact, the latter is a key motivation for many of the hybrid-AM processes herein, as it can generally be stated that the production rate of metal AM processes is inversely related to the achievable process or surface fidelity.

The fact that a traditional machining process will achieve a significantly better surface roughness than can be achieved by AM alone led to the development of hybrid-AM machines that combine DED or PBF machines with an *in-situ* operation, or, conversely have incorporated DED or PBF equipment into a milling machine (Liou et al., 2007). The main process associated with the surface evolution mechanism is machining, which uses mechanical energy in the form of a rotating tool to remove material (Section 4.4.1) and exert better control over the evolution of the additive surface. This is conceptually represented by Du et al. (2016) in Fig. 28.

The machining process is considered to be concurrent with the additive process and has the ability to either intermittently or finally machine the component being produced. Other processes researched are laser ablation, laser assisted machining, and cryogenic machining (Sections 4.4.2 and 4.4.3). All of these processes focus on the increased control over the AM surface, and the breakdown of these processes and energy sources can be seen in Figs. 9 and 7. The list of properties that are affected by surface evolution are shown in Fig. 29, where hardness and surface roughness are the most reported. It should be noted that the motivation for this section is research primarily focused on surface evolution with respect to material properties. Research in Section 5 also largely addresses surface evolution; however, it is more specifically focused on aspects of the process such as increased production rate or accuracy.

4.4.1. Shearing methods

The combination of a metal additive process with *in-situ* shearing or

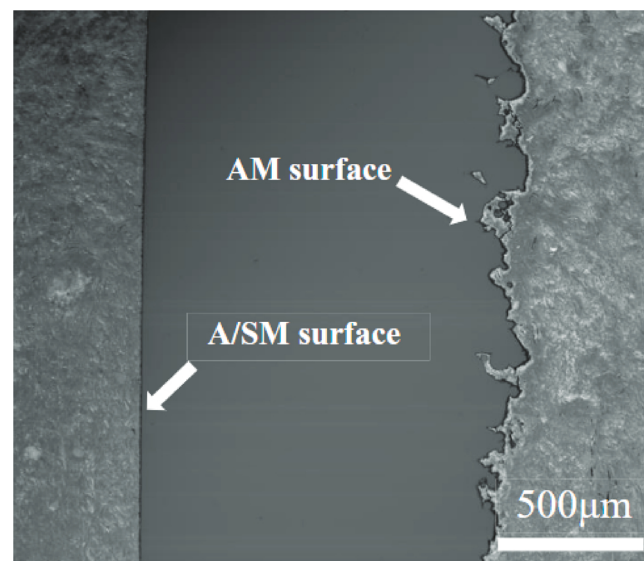


Fig. 30. Comparison of “as-built AM Surface” and hybrid processed machined surface (Du et al., 2016).

ablation methods, conceptualized by authors from the late 1990s to 2010, has paved the way for the subsequent work focused on resulting properties such as surface roughness, hardness, density, and residual stress.

Brown et al. (2018) evaluated the hybrid process of PBF and machining to overcome the limitations of high surface roughness and low dimensional accuracy in AM. The surface roughness and micro-hardness for Alloy 718 was presented. The surface roughness of the hybrid components was found to be $0.3 \mu\text{m} R_a$ compared to significantly higher starting values. Ye et al. (2017) used a pulse laser wire micro DED process with milling on a machine with a functional work envelope of $50 \times 50 \times 100 \text{ mm}$. A comparative example of as-deposited vs. machined surface finish can be seen in Fig. 30. They used 304 wire and substrates for their tests and reported an average grain size of $10 \mu\text{m}$. Yang et al. (2018) evaluated the densification, surface morphology, microstructure, and mechanical properties of 316 L produced on a hybrid manufacturing machine SVW80C-3D (Dalian Hybrid-wise Additive Manufacturing Technology Co., Ltd, China) which uses a laser powder DED method. It was discussed that the DED process alone results in low surface quality with adhered metal powder particles and a staircase effect. In comparison, the research presented a visual benchmark of the improved surface finish due to the addition of a machining operation.

Du et al. (2016) presented research on a hybrid-AM process using PBF and machining on a Sodick OPM250 with a 45,000 rpm spindle. Their investigation of 18Ni Maraging steel found that a density of 99.2% was achieved, and this was significantly better than an AM-only created component. The work presented a comparison of the additive surface and the hybrid surface noting that agglomerations and fused particles were removed in the hybrid process resulting in a smoother surface. Finally, the authors showed that the surface hardness after heat treatment achieved 649 HV with no significant difference between the side and top surfaces. Yamazaki (2016) presented the development of a hybrid multi-tasking machine tool with a fine and high speed laser deposition head into an INTEGREX 400 mill turn machining center. The author produced Alloy 718 samples and presented similar yield and ultimate tensile strength results to bar stock material. A hardness value of 240 HV was achieved which was the same as the bar stock.

The uptick in hybrid AM processes with machining has enabled components to be formed in a concurrent approach where additive and subtractive operations can be interchanged over the course of part production. Cortina et al. (2018b) studied the detailed impact of



Fig. 8. Micro machining of external features.

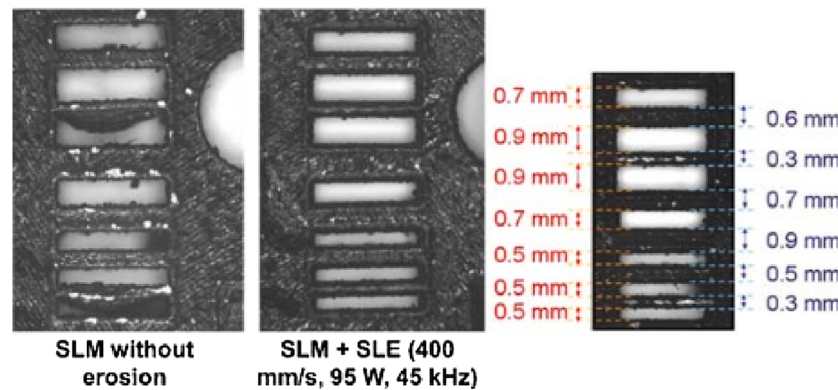


Fig. 31. Results from applying a laser erosion technique after powder bed fusion (Yasa et al., 2011).

different coolant types in these intermediate machining operations, as well as their impact on the resultant material and surfaces. The authors found that lower concentrations of oil fluid emulsions resulted in reduced porosity. The best results were achieved with an intermediate cleaning step using the laser to burn off any residual contaminants. The hardness varied with the scan direction of the PBF process and coolant method in the machining operation. Machining traditional wrought or cast materials is widely published research. There is more limited information on the settings and tool wear behavior for machining AM components. Yang et al. (2020) studied the combined impact of DED scanning strategies on densification reporting a density of 99.4% and the subsequent influence on surface finish with varying feed per tooth (f_z) values. It was found that f_z values of 0.2 mm resulted in the lowest surface roughness values in the presented work.

Wang et al. (2015) focused on some of the compounding issues in thermal distortion of the DED process. It was presented that a combination of integrated laser scanning and automated tool path generation could alleviate some of these challenges. Using a laser displacement sensor, a resolution of 10 μm was achieved. Heigel et al. (2018) focused on the relationship between residual stress in the PBF process and impact on the surface and accuracy of the machining process. The authors produced a series of Stainless Steel 17-4 PH cylinders which were then machined using a 3 axis machining center. Results showed the PBF samples were very rough before machining with an R_a value of 16.5 μm . The authors found that sample diameters shrunk and counter-acted the measured residual stress from the additive samples through cold working during the machining process.

4.4.2. Thermally modified shearing

While it is easier to fabricate hard-to-machine materials using AM, it is also possible to add thermal control to the machining process. Woo et al. (2020) used a laser assisted machining (LAM) process combined with DED to improve surface finish and reduce cutting forces by 40% by locally preheating the material before the rotating tool. Conversely, Moritz et al. (2020) combined DED and cryogenic machining to achieve a 1.5 μm surface roughness, eliminating the need for coolant that can create part contamination issues.

4.4.3. Ablation and acoustic methods

While the majority of research in the surface evolution category is conducted through mechanical energy and a shearing process, there are several researchers that have looked to thermal or acoustic processes to achieve control over the surface evolution mechanism. Yasa et al. (2011) combined a laser-based PBF machine with a secondary laser process of selective laser erosion to process 316 L. It was shown that the addition of the secondary process overcomes the high surface roughness limitations of the primary process. Additionally, the authors concluded that with this process, pin diameters down to 50 μm were achievable, while the additive process could only produce a minimum diameter of 400 μm pins, shown in Fig. 31. Friel and Harris (2013) present a hybrid process using ultrasonic consolidation. This process, coupled with machining is able to create dissimilar material joints, and multi-material components including embedded fiber cables. Bouet et al. (2019) combined a laser PBF process with a femtosecond laser with the intention of controlled surface quality to improve orthopedic integration of implants. The hybrid process was able to reduce the surface roughness from 12.7 μm R_a

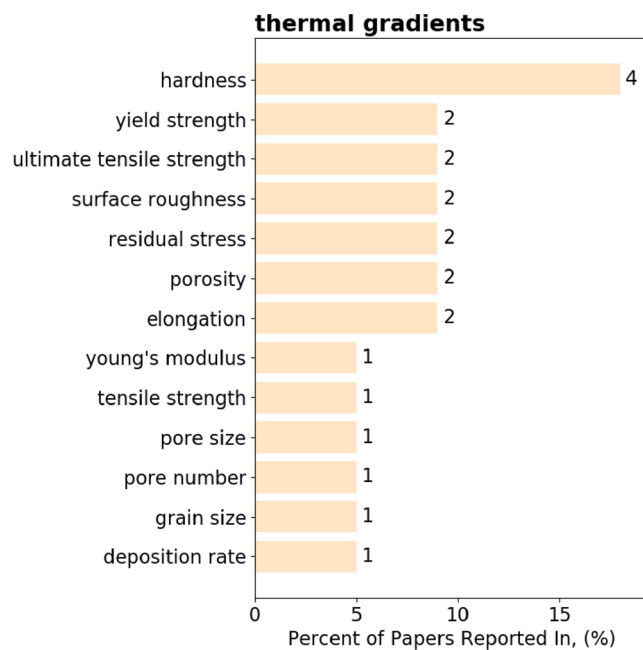


Fig. 32. Mechanical properties affected by thermal gradients. Hardness is the most reported material property. Overall there is a lack of investigation on controlling thermal gradients *in-situ* and their effect on material properties.

to $3.7 \mu\text{m}$ R_a .

4.5. Thermal gradients

While previous discussions in Sections 4.1 and 4.2 have included effects on thermal gradients through hybrid-AM processes, this section pertains to studies that have explicitly controlled or studied thermal gradients as a driving mechanism for resulting structures and properties in hybrid-AM materials. It is well established that heat accumulation in combination with fast cooling rates can lead to nonuniform properties as well as differing microstructure across a given geometry (Dass and Moridi, 2019). In order to overcome this, some researchers have used additional thermal energy to manipulate the thermal gradient in the melt zone or across multiple layers, resulting in changes of properties shown in Fig. 32. In contrast to mechanisms discussed in previous sections, only one type of energy was used to influence thermal gradients, unsurprisingly, thermal energy. The list of processes used to influence thermal gradients is shown in Fig. 9, where laser diode illumination and

air-cooling nozzle are introduced into hybrid-AM.

Highly local thermal energy was used by two groups (Heeling and Wegener, 2018) and Wu et al. (2020) through secondary laser sources. Heeling and Wegener (2018) used a secondary laser in conjunction with SLM, while Wu et al. (2020) used a secondary laser with WAAM. Heeling observed a homogenization of the temperature when the vicinity of the melt pool is heated with the secondary laser. In addition, improved wetting and a reduction in cooling speeds is noted. The reduced cooling speeds led to higher density, as more pores will escape during the lengthened solidification period. While Heeling and Wegener (2018) observed temperature homogenization, Wu et al. (2020) determined that the temperature gradient was actually higher in the secondary laser heated zone compared to the arc heated zone (105–106 K/m compared to 103–104 K/m). This led to greater undercooling and, thus, finer grains.

The remaining processes affect a much larger area, leading to changes in thermal gradients across multiple layers. For example, Xiao et al. (2020) used remelting with the primary laser in SLM, which reduces the cooling rate and thermal gradient of the part due to heat accumulation across the part. Similar heat accumulation is seen when coupling the process with induction heating, as in studies by Nowotny et al. (2015) and Seidel et al. (2018). Nowotny et al. (2015) demonstrated that the reduced temperature gradient (below 500 °C) reduces residual stresses because of prolonged cooling time within the temperature interval 500–800 °C for Alloy 625. Seidel et al. (2018) had agreeing results, where cracks were further suppressed due to the reduced thermal gradient between the melt pool and substrate, shown in Fig. 33.

A 90% reduction in residual stresses was also found by Roehling et al. (2019), where a set of laser diodes was used to selectively illuminate layers in PBF creating heating/cooling cycles with smaller temperature gradients. Finally, rather than controlling the temperature gradient with additional heat, Hackenhaar et al. (2020) used a cooling nozzle with shield gas to mitigate the heat accumulation across a part.

The area of thermal gradients in hybrid metal AM is essential given the resulting material structure directly depends on it. There is certainly a gap of knowledge considering the control of thermal gradients, as it was the smallest percentage of papers considered in this study at 7%. More work clearly needs to be done in this area and it would have a significant impact on the hybrid metal AM field.

5. Process chains

Hybrid-AM processes are motivated by the long time needed to manufacture a single part via PBF and DED alone (on the order of multiple hours depending on geometry), as well as the desire to increase

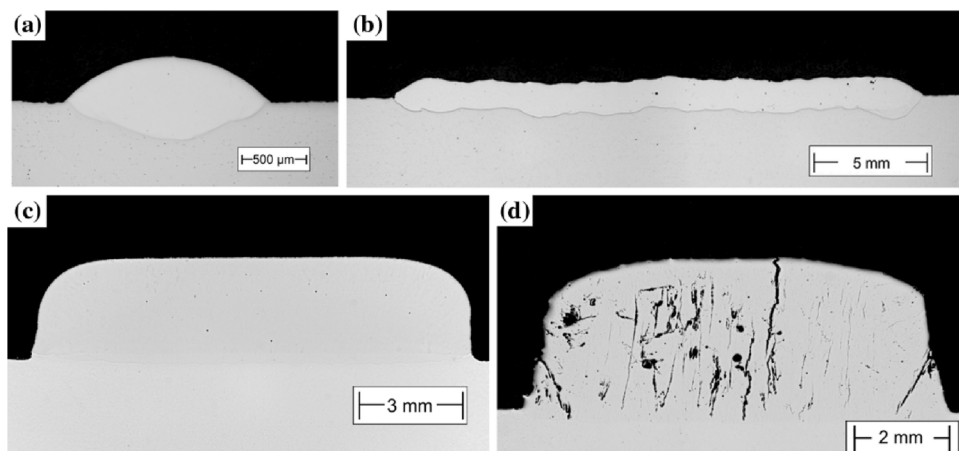


Fig. 33. Cross sections of (a,b) single layer and (c,d) multi-layer builds with (a,c) and without (b,d) induction heating. Crack suppression is clearly shown in (a) and (c). (Seidel et al., 2018).

complexity, flexibility in geometry, and build properties. Initial research in process chains mainly focused on the feasibility and advantages of integrating multiple processes on one machine (Chong et al., 2018). For example, one of the first mentions of hybrid-AM was by Kulkarni and Dutta (2000), where different milling strategies implemented in layer deposition were investigated.

The combination of process techniques increases manufacturing flexibility and reduces tooling change time, improving design options and speed of manufacture. One of the most common hybrid machine designs uses 3- or 5-axis CNC to accommodate direct deposition and inter-layer or finishing machining (Flynn et al., 2016). This has been realized in industry by multiple companies, but one of the first was DMG Mori Seiki AG where laser metal deposition (LMD) and milling were combined (Merklein et al., 2016). In a similar line of reasoning, challenges in AM, such as surface roughness, porosity, and anisotropy (Book and Sangid, 2016), have been addressed through process chain techniques, with the most popular combination being AM and machining.

This section will summarize research endeavors where a metal AM process is combined with another traditional unit manufacturing operation(s) in order to achieve improvements in geometric accuracy, production rate, or geometric flexibility. Overall, the discussed hybrid-AM techniques readily increase the functionality of AM and demonstrate the application of the PMEH framework to functional properties through mechanisms such as surface evolution (machining) and stress state (forging, incremental forming). While this section contains similar mechanisms highlighted in surface evolution in Section 4.4, the research described here will focus on series of processes, such as machining a part after it is built by AM, rather than *in-situ* processes such as intra-layer machining or laser ablation.

5.1. Geometric accuracy

Intra-layer machining to improve surface roughness and geometric accuracy has been discussed in Section 4.4, but it is time consuming. In order to meet specified tolerances and decrease overall process time, secondary machining operations are performed. Thus, both the flexibility of metal AM and machined surface quality is maintained. Some of the initial research publications on combining AM and machining to achieve higher precision components with improved surface quality began in the late 90s and early 2000s. Song et al. (1999) presented a hybrid-AM approach called “3D welding and milling” in 1999, and their work demonstrated the creation of an injection mold. Jeng and Lin (2001) also used injection molds manufactured by a hybrid machine to demonstrate improved surface finish and increased design flexibility through mold modification. Akula and Karunakaran (2006) built a 3-axis motion platform that integrated an arc welding system and a milling setup previously proposed. This work developed the process to “slice” a part geometry and produce the additive and subtractive tool-paths. It was also presented that, given stable processing conditions, the hybrid manufacturing process could deliver 100% density results and achieve accuracies comparable to those of a CNC machine.

Looking past machine integration and into further functionality, Cortina et al. (2018a) first produced cooling ducts by closing pre-milled cooling channels with DED to verify the functionality of milling + DED, and then generated an adaptive geometry with DED which performed better than the original part. The maximum temperature in the cooling fixture was lowered from 362.8 °C to 319.2 °C. Additionally, an important result of machining AM builds is the influence of anisotropic microstructure on secondary machining operations, which was demonstrated by Fernandez-Zelaia et al. (2019). This research group showed that machining forces are sensitive to the anisotropy driven by microstructure morphology and texture (long, columnar grains present in metal AM). Therefore, the build direction of AM parts and how they are finished is important to consider if AM + machining is utilized.

5.2. Production rate

Hybrid-AM machines inherently save time by integrating multiple tools into one processing area (i.e., DED and machining), but overall production rate can be further increased in process chains through use of standard pre-forms. This subsection first covers research on AM + forging and then AM + milling process chains with the goal to increase production rate. When it comes to using preforms in conjunction with AM, there are two processing routes: (1) forge the preform and then use AM to deposit features or (2) use AM to make the preform and then form the final part. Depending on the geometry, either strategy is viable, but the first increases production rate by taking advantage of standard preforms while the second increases control of material properties. Both Hirtler et al. (2020) and Meiners et al. (2020) utilized the first strategy, where a forged preform was used as a substrate for WAAM (Hirtler et al., 2020) or DED (Meiners et al., 2020). Successful parts were built in either case, however, Hirtler et al. (2020) found that heat input is sensitive to geometry, where an uneven heat input led to large deviations in mechanical properties across the part. The second strategy was used by Michl et al. (2020), where thick disk preforms were fabricated and then used for ring rolling. The resulting AM preforms had good forming behavior, and the hybrid process was largely successful; however, porosity defects occurred when the AM material did not receive heat treatment and there was a large variation in mechanical properties overall. Further research has been performed by Bambach et al. (2020) to address these issues through a study of hot deformation behavior of Titanium Gr 5 AM pre-forms, where a model is proposed that predicts flow stresses and microstructure evolution. This model can be implemented in process chain design to further improve mechanical properties and reduce variations.

Looking at milling integration after DED, Choi et al. (2001) implemented a CO₂ laser and wire feeder on a 3-axis milling machine. Using this device, they provided initial characterization of the tensile properties and found that the ultimate strength of deposited and machined material to be comparable to wrought properties. The use of wire is advantageous in terms of a simple feeding mechanism, as well as a higher deposition rate. Karakulak (2019) proposed a similar machine but demonstrated adaptive slicing through the integration of various cutting tools to be used programmatically, and presented a schematic of a 2.5 axis machine with an automatic tool changer, both of which decrease processing time and increase productivity.

5.3. Geometric flexibility

Another flexible manufacturing process complementary to AM is incremental forming (IF) (Emmens et al., 2010), where a piece of metal is plastically deformed in small steps to create a freeform 3D geometry. Multiple research groups have combined IF with metal AM in order to achieve improvements in the IF process along with greater geometric flexibility, while only one other group investigated AM + sheet metal bending (Huber et al., 2019). Huber et al. (2019) demonstrated appropriate deposition parameters (energy densities) for PBF on top of thin sheet metal, where the joint at the base of the AM part and top of the sheet metal must resist fracture from residual stresses and overcome lack of fusion. While this study intended for only sheet metal bending of the resulting part, it could easily be used for IF, which is shown by Pragana et al. (2020) and Ambrogio et al. (2019). Ambrogio et al. (2019) used PBF to locally thicken sheets for use in single point IF (SPIF) where excessive sheet thinning is a major challenge. In addition, they stated that the combination of highly flexible manufacturing will increase the typology of shapes that can be manufactured. Pragana et al. (2020) also investigated the use of IF + AM but took hybrid processing one step further and incorporated milling with the two flexible processes. In this way, one machine would be capable of forming, subtractive, and additive processing. However, one drawback that Pragana et al. (2020) found in IF + AM is that the highly anisotropic material from the as-built

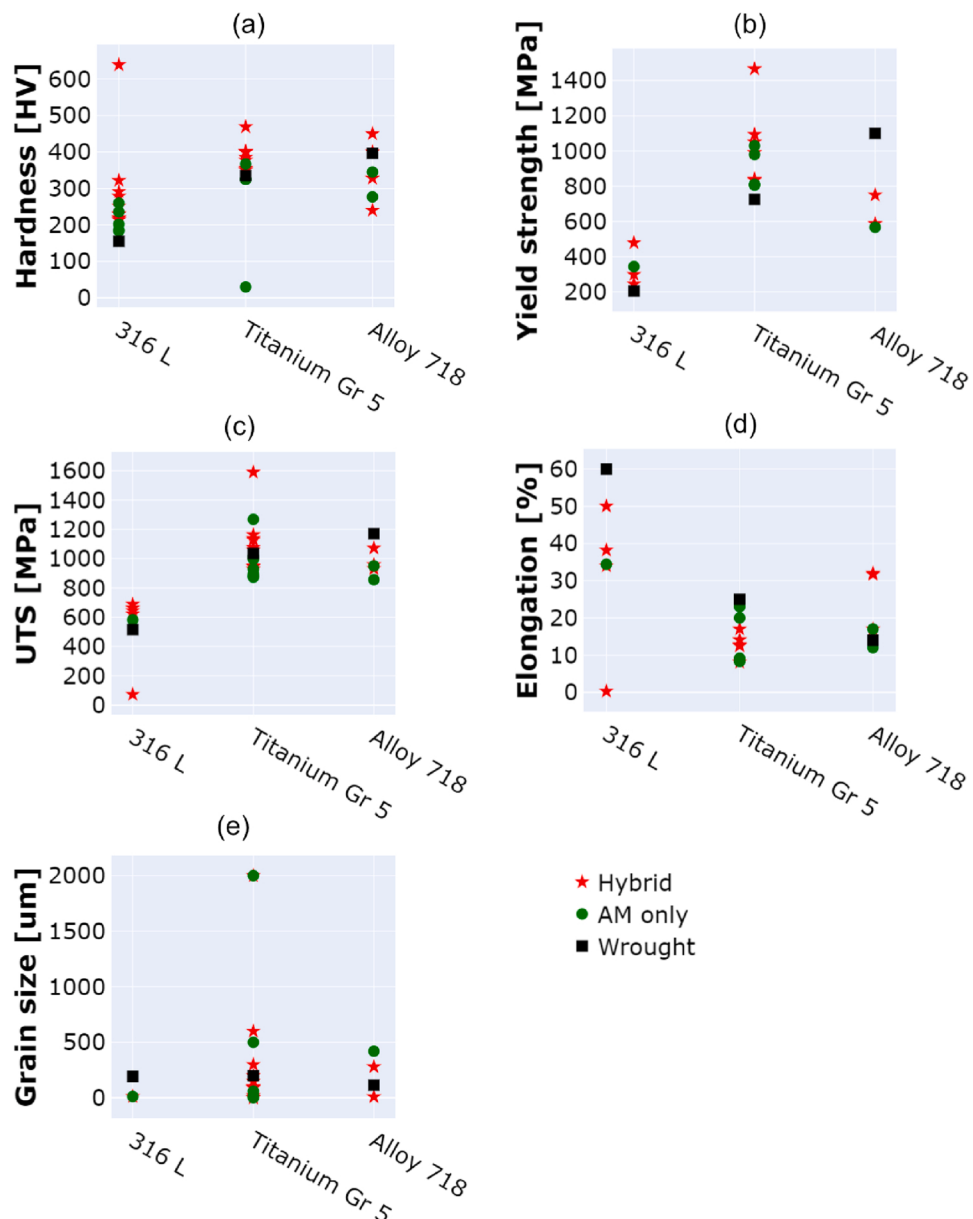


Fig. 34. Collection of reported values for hardness, yield strength, UTS, elongation, and grain size for 316 L, Titanium Gr 5, and Alloy 718. Red stars show hybrid-AM process properties reported in the paper, green circles show AM only processes (if reported in the paper), and black squares show wrought properties for each material. (For interpretation of the references to color in this figure legend, the reader is referred to the web version of this article.)

AM parts with pronounced primary dendrite directions can lead to fracture during IF.

Further geometric flexibility has been found in process chains by integrating 5-axis machines in hybrid-AM, where increased degrees of freedom for both AM and machining give increased geometric complexity. For example, Kerschbaumer and Ernst (2004) implemented DED and high-speed milling on a 5-axis CNC machine. This work enabled deposition of support-free components, demonstrated by a wine glass geometry that was produced (which would require support material in an AM only process). Further research on combining laser deposition and a 5-axis CNC machine was conducted by Liou et al. (2007), which addressed challenges such as sensor selection, part orientation, and part decomposition.

6. Summary and future outlook

With the continued increase in popularity of metal hybrid-AM, the

following discussion is devoted to summarizing general trends found in this study and identifying major gaps in knowledge in the field within the following topics: Improvement in material properties (Section 6.1), expansion of investigated materials (Section 6.2), distributions of energy types and mechanisms that reported resulting properties (Section 6.3), inconsistent findings in research (Section 6.4), process chain integration and improvement (Section 6.5), and looking to new processes in Section 6.6.

6.1. Improvement in material properties

Superior material properties can be achieved with hybrid-AM processing by taking advantage of mechanisms described in Section 4, such as manipulating the melt pool dynamics to control microstructure or by imposing a particular stress state preferred for fatigue resistance through a deformation process; however, there currently exist large variations in reported material properties. The individually reported mechanical

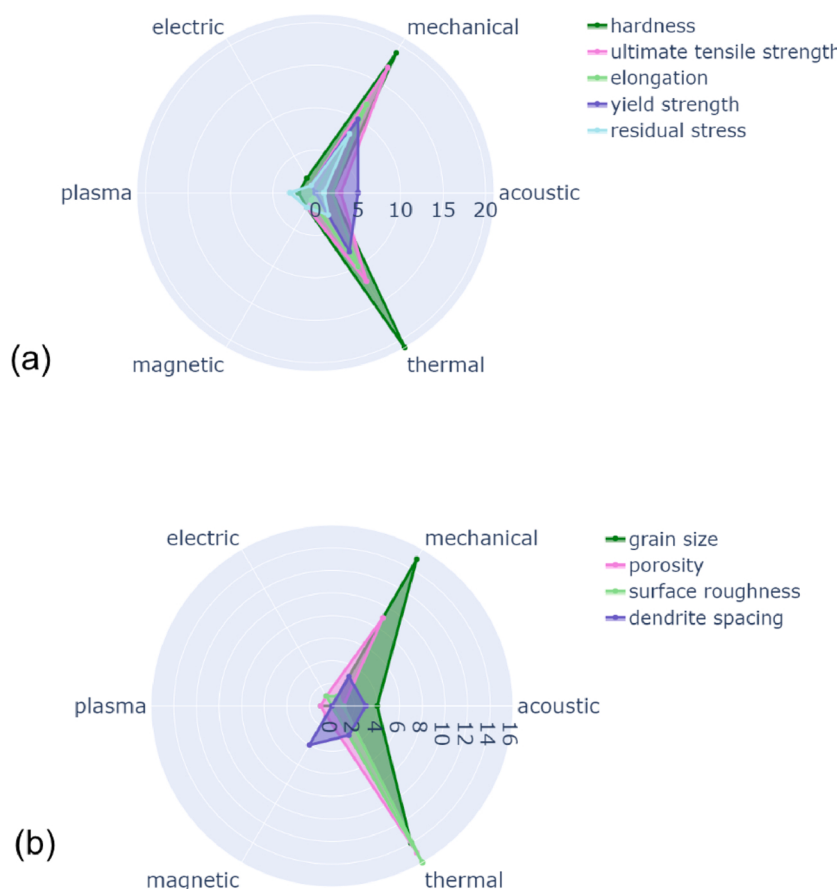


Fig. 35. Number of papers that reported (a) material properties and residual stress, and (b) microstructure as a function of energy source. It is evident that thermal and mechanical energy dominate in hybrid-AM processes. More consideration should be given to alternative energy sources to support innovation.

property values of 316 L, Titanium Gr 5, and Alloy 718 as results of hybrid-AM can be seen in Fig. 34 to be compared with values for AM processes only (if reported in the paper) and wrought properties. In general, the maximum mechanical property values are achieved through hybrid processes as opposed to only AM, with the exception of yield strength and UTS in Alloy 718 and elongations in 316 L and Titanium Gr 5.

Looking at the hardness and YS in Fig. 34(a) and (b), hybrid-AM improves both of these properties for 316 L and Titanium Gr 5 compared to wrought values, while both hardness and YS for Alloy 718 are either below or just comparable to wrought values. The lack of improvement in hardness and yield strength for Alloy 718 in hybrid-AM, as compared to wrought properties, is attributed to the lack of heat treatment afterwards. Fig. 34 (c) shows a large range for the ultimate strength in both 316 L and Titanium Gr 5, 73–688 MPa and 929–1163 MPa, respectively. This is most likely due to the introduction of porosity in the AM portion of the hybrid process, especially when cold spraying was implemented. While the hybrid processes can show superior properties, these materials can show inferior UTS values compared to wrought values without HIP or post-processing. For example, no UTS values reported for Alloy 718 were superior to that of the wrought material, which is again attributed to needed heat treatment.

Opposing trends are seen in elongation compared to hardness and YS, shown in (d), where reported elongation values are well below those of wrought materials for both 316 L and Titanium Gr 5, but the hybrid-AM elongation values for Alloy 718 are superior to wrought. This may be due to the inconsistency of elongation values reported as for a given dimension or until the breaking point. Finally, grain sizes have been reported smaller across the board of materials, shown in (e), which is due to the rapid solidification in AM processes (Debroy et al., 2018) that

continues to be reflected in hybrid-AM processes. The large ranges of achieved grain values in Titanium Gr 5 are attributed to its propensity to form very long, columnar β grains where the type of secondary process is critical to prevent these formations. Additionally, the growth of grains is achieved in hybrid-AM through thermal or mechanical inputs, which could increase the ranges of grains reported for Titanium Gr 5 and Alloy 718.

In all, hybrid-AM processes have the capability to improve material properties as compared to AM only processes, however the variation in material properties must be addressed.

6.2. Expansion of investigated materials

The most reported material for a single mechanism category is Titanium Gr 5, mainly due to a series of five papers by Cortina et al. (2018b) that showed an effective way to refine long, columnar grains through intralayer rolling. Both Titanium Gr 5 and 316 L were studied at least once in each mechanism category, however there are gaps among 304, Alloy 718, AlSi10Mg, and ER70S-6, identified in Fig. 4. 304 is minimally listed in mechanisms that utilize thermal energy because of its low thermal and electric conductivity and difficulty in phase strengthening. Instead, 304 is usually strengthened by rolling processes where the stress state is affected. The lack of research in Alloy 718 could be attributed to raw powder material cost and necessity of heat treatments in AM processing (Seow et al., 2019). Aluminum alloys also present difficulty in AM processing due to hot cracking, and to achieve appropriate mechanical properties must also be heat treated (Casati et al., 2018). Finally, ER70S-6 is a steel wire typically used in WAAM, so if the hybrid-AM process did not consider WAAM, then this material is not listed in that mechanism. For a list of all materials that have been

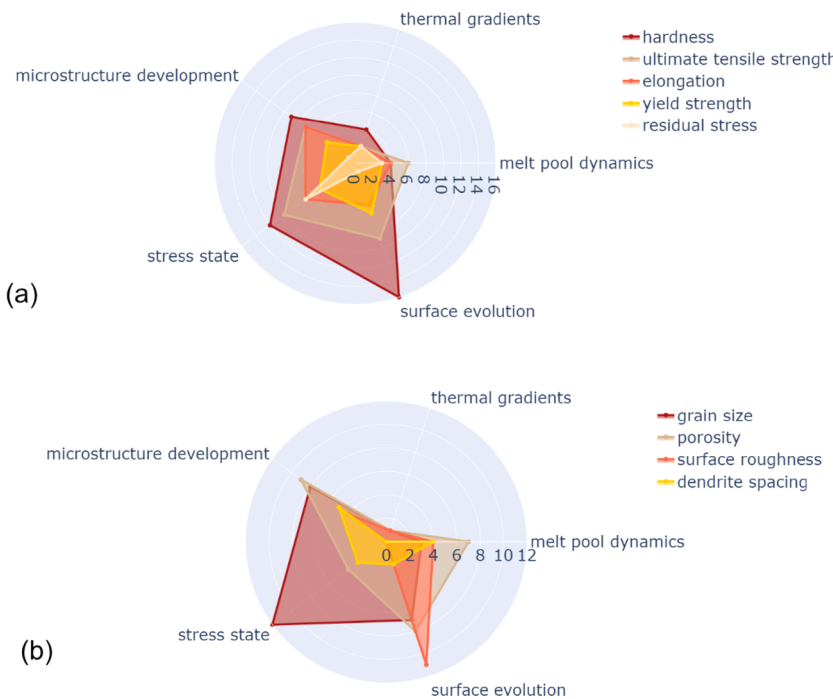


Fig. 36. Number of papers that reported (a) material properties and residual stress, and (b) microstructure as a function of mechanism within papers used in this study. The most reported property is hardness. While large area coverage is seen in (a) for mechanical properties, (b) shows a lack of characterization across mechanisms for selected microstructure properties. Both sets of properties should be reported in tandem for full understanding of material behavior.

investigated in hybrid-AM refer to the material data column in Appendix D. It is clear that a larger variety of materials should be implemented in metal hybrid-AM in order to expand design possibilities.

6.3. Distributions of energy types and mechanisms that reported resulting properties

The distribution of energy sources used in hybrid-AM with respect to mechanism is shown in Fig. 7, which highlights the major energy sources used overall as well as the most common energy sources for each physical mechanism. While thermal and mechanical energies were most used, larger interest is growing in using magnetic energy to alter the melt pool dynamics and microstructure development, as discussed in Sections 4.1 and 4.2 and shown in Fig. 7. Another opportunity presents itself in further exploration using acoustic energy, as in part vibration, where it is seen in Fig. 7 that acoustic energy is used in four out of five mechanisms but has a low number of papers it is reported in. Finally, the vast majority of papers analyzed in this study only use one additional energy source at a time, thus, there are a lot of opportunities for innovation and development of hybrid-AM processes that utilize two or more energy sources to solve different challenges or improve different properties at the same time, ultimately saving time and energy resources to fabricate a part. The disparity in energy source utilization is shown in greater detail in Fig. 35 where the number of papers that reported material and residual stress (a) and microstructure (b) properties are plotted with respect to energy source.

Fig. 36 further shows mechanism utilization, where the number of papers that report material properties and residual stress (a) and microstructure properties (b) are plotted with respect to mechanism. These charts overall show the major gaps in property reporting and mechanism or energy source usage. Specifically, mechanical properties are widely studied within each mechanism, shown in Fig. 36, where hardness was most frequently reported. In this same plot, it is evident that tensile properties (UTS, YS, elongation) should be studied more to supplement the hardness values and describe a given material's deformation behavior in full. There is also a clear lack in reported

microstructure properties such as surface roughness, dendrite spacing, and porosity which are all asymmetrically skewed to certain mechanisms. Moreover, there are generally less microstructure properties reported than mechanical properties.

To improve research in metal hybrid-AM, both sets of properties should be reported for a given material for complete understanding of material behavior. There is also opportunity to explore the use of thermal gradients in hybrid-AM, as it is the least reported mechanism overall, shown in Fig. 36. Finally, to reiterate, Fig. 35 shows that mechanical and thermal energy sources have the largest number of reported properties, with hardness and grain size reported the most. There is a clear need to explore both mechanical and microstructure properties when utilizing other energy sources, and expansion of energy source variety is critical.

6.4. Reported inconsistencies

The previous Section (6.3) identified gaps in knowledge of energy source types and mechanisms, and reported material properties with respect to the number of reported papers; however, this is only one metric to identify future research directions. The number of papers reported for a given topic should also be considered in context of inconsistencies reported in said literature. Therefore, here, we will detail inconsistencies found through this study to identify topics that should be pursued further as shown below.

- Both leading and trailing laser positions were investigated, but quantitative differences are limited.
- Experimental evidence of Marangoni versus TEMC dominated flow is needed, perhaps through in situ X-ray imaging.
- The effect of applying magnetic or mechanical energy to influence phase and composition changes had a large discrepancy and should be further investigated.
- Numerical prediction of LSP and intra-layer rolling should be implemented and improved in order to increase uniformity across a part.

- Opposing results were reported when using a secondary laser to control thermal gradients within the melt pool; this needs to be further investigated to realize the correct mechanism.

Considering Section 4.1, secondary laser beams were utilized frequently; however, the position of the laser beam was not consistent through all studies where both leading and trailing lasers were investigated. Surface roughness, melt wave amplitudes, and melt pool convection differed between the laser positions, and while qualitative comparisons can be made, further efforts should quantitatively determine the advantages of using a leading or trailing laser in conjunction with DED and LPBF. Additionally, the melt flow can be enhanced or inhibited through directional magnetic fields by transitioning from Marangoni-dominated flow to TEMC dominated flow, as discussed in Section 4.1.2. While there has been post-processed experimental data and thorough numerical simulations, it would be beneficial to utilize highspeed, *in-situ* X-ray, as in Webster et al. (2020), to directly verify the transition between the Marangoni-dominated flow to the TEMC-dominated flow.

As discussed in Section 4.2, the use of magnetic or mechanical energy led to differing levels of strengthening phase via application of static magnetic fields and part vibration, respectively. Magnetic fields had a large effect on phase and composition changes, while part vibration did not seem to have a significant effect. Further investigation on the influence of mechanical energy on phase transformation is, thus, recommended, particularly in conjunction with the study of its effectiveness with respect to the part size.

Looking at the stress state mechanism in Section 4.3, applying LSP (and intra-layer rolling) at more or less frequent points within the material led to larger or smaller bands of compressive stress. This inconsistency was exacerbated by cancellation of compressive stress through re-heating or mechanical redistribution. Further investigation should focus on the ability to have a better numerical prediction of compressive stress with respect to process variations and uncertainties, yielding an effective strategy to control the stress bands in order to overcome stress cancellation, as well as increase uniformity.

Finally, an inconsistency is noted with respect to the thermal gradient mechanism in Section 4.5, where temperature homogenization within the melt pool zone was observed using a secondary laser in one case, but another use led to a higher temperature gradient in the secondary laser heated zone. Further investigation into controlling thermal gradients within the melt pool is, thus, recommended.

6.5. Process chain integration and improvement

Research topics in hybrid-AM have expanded to more than just feasibility, owing to its increase in processing capabilities, and now include investigations into process integration (Strong et al., 2017) and their economic and environmental impact (Manogharan et al., 2016). Strong et al. (2018, 2019) developed multiple supply chain models to identify optimal locations for AM “hubs” within the U.S. to facilitate hybrid-AM collaborations, which would support existing machine shops and the demand for complex metal parts. While combining AM and traditional manufacturing has become integral in research, part design for hybrid-AM presents challenges where the process must be considered during product conception for efficient use of AM (Häfele et al., 2019). Part design for process chains has additionally been addressed by Ndi-p-Agbor et al. (2018) where a solution to Constraint Satisfaction Problem for Manufacturing was developed and can be used to make ‘smart’ manufacturing process sequence selection. Furthermore, economic or environmental benefits can only be realized if the hybrid-AM process is considered at initial design due to the high impact of part geometry on energy consumption (Ahmad and Enemuoh, 2020) and material efficiency (Wippermann et al., 2020).

In all, AM + traditional processes are widely implemented with a variety of processes, but typically suffer from the variation and

anisotropy in AM materials. It is important to explore more combinations of traditional and flexible manufacturing processes with AM in order to decrease single-part processing time, show successful incorporation into general manufacturing chains, and increase the variety of shapes able to be manufactured.

6.6. Looking to new processes

All of the processes analyzed in this study are shown in Fig. 9 by mechanism. While there is a myriad of processes, the four most widespread ones were machining, use of static magnetic field, primary laser remelting, and intralayer rolling. The following bulleted list summarizes the potential of high-impact secondary processes in hybrid AM and detailed discussions of each follow.

- Further utilization of lasers in surface evolution applications should be used to improve surface and material properties simultaneously.
- Controlling thermal gradients promises to decrease anisotropy and improve mechanical properties.
- Utilization of multiple lasers in secondary processing can greatly improve hybrid material processing time.
- Part vibration, secondary laser control, and application of magnetic fields were not commonly reported, but all showed vast improvement in part properties while being easily incorporated into AM setups.

The largest opportunity in process development is in surface evolution, where machining is utilized almost exclusively. It would be interesting to expand upon assisted machining, such as laser-assisted machining or laser polishing, which could improve both surface properties and material properties through better accuracy and grain refinement simultaneously. Additionally, there is a large need for research to be performed by controlling thermal gradients, which has great promise in decreasing part anisotropy and improving mechanical properties. It is also noted that primary laser remelting applied to multiple layers could significantly slow down the already slow AM process. Thus, multiple lasers used for remelting can speed up the processing time. It will also be beneficial to study the lasers’ interactions with each other and the resulting material properties. Furthermore, manipulation/control of volumetric energy density (VED) through use of multiple assisting lasers should be investigated. This could be accomplished by using both a leading and trailing laser to create a more uniform thermal gradient or melt pool dynamics in response to changes in part geometry.

While not commonly reported, there were three processes that stood out among others with promising potential: part vibration, secondary laser control, and magnetic fields. These three processes not only improved part properties overall but could easily be integrated into current AM machines. Part vibration is an innovative application of acoustic energy to encourage nucleation of new grains and dendrite breaking, promoting grain growth and preventing anisotropy in metal AM processes. However, the implementation of acoustic energy is challenged by its effectiveness when the physical size of the part increases. Magnetic fields were also used to promote dendrite breaking through changing flow patterns in the melt pool, which additionally could be used to control solidification rate, melt pool size, and cooling rate. Further research into better manipulation of the melt pool would thus have a great impact on metal hybrid-AM. Finally, the use of a secondary laser to control surface roughness *in-situ* should be explored further to mitigate the current necessity of post-processing all metal AM parts for use in industry. Control of the surface will not only give improved geometric accuracy and better fatigue life; it will also allow for surface patterning.

In summary, this study defined hybrid-AM as “*in-situ* or series combination of an additive manufacturing process and secondary energy sources in which physical mechanisms are fundamentally altered/

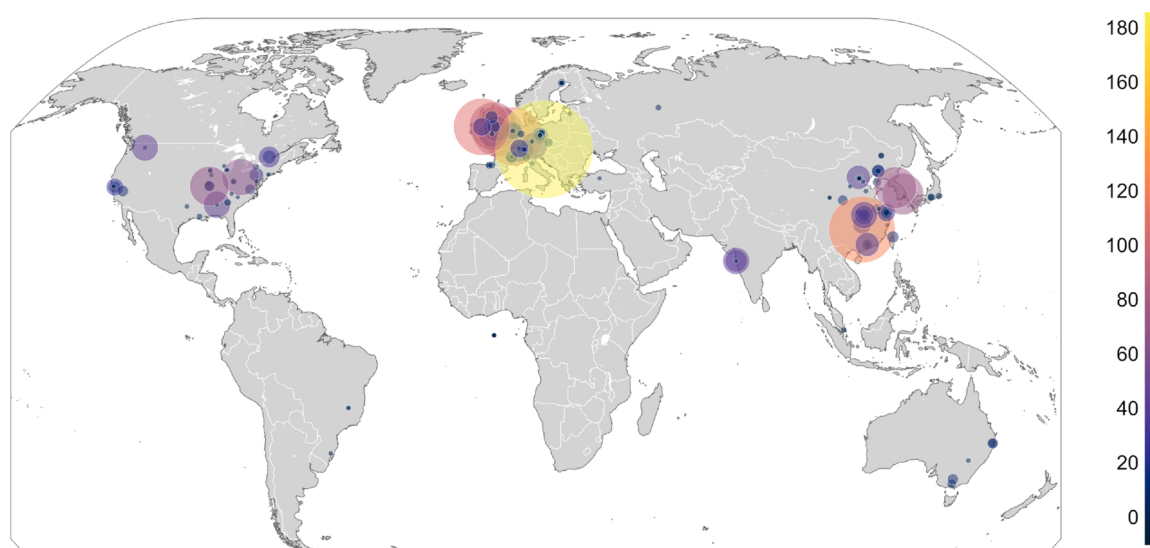


Fig. A.37. Map of locations affiliated with metal hybrid-AM research based on papers considered in this study. It shows a current snapshot of the hybrid AM research landscape which will expand and change as hybrid-AM becomes more popular. The color map and the size of the circle show the relative number of citations with respect to research location.

controlled to affect the resulting properties of the material and/or part.” This definition included *in-situ* secondary processes as well as process chains and further framed hybrid-AM processes through development of Property – Mechanism – Energy Source – hybrid-AM Process (PMEH) relationships in hybrid-AM. Additionally, five prominent unifying physical mechanisms were identified in this analysis: melt pool dynamics, microstructure development, stress state, surface evolution, and thermal gradients. Overall, there is a clear need for innovation in hybrid-AM. The PMEH framework can be used in a systematic way, particularly when the experimental exploration can be integrated with predictive numerical simulations, to delve into more complex or innovative solutions in addition to the identified general gaps in knowledge.

CRediT author statement

Samantha Webster: Conceptualization, Methodology, Investigation, Data Curation, Writing – Original Draft, Visualization, Project Administration.

Hui Lin: Conceptualization, Investigation, Data Curation, Writing – Original Draft, Visualization.

Fred Carter: Conceptualization, Investigation, Data Curation, Writing – Original Draft, Visualization.

Kornel Ehmann: Conceptualization, Writing – Review & Editing, Supervision.

Jian Cao: Conceptualization, Writing – Review & Editing, Supervision, Funding Acquisition.

Declaration of Competing Interest

The authors report no declarations of interest.

Acknowledgement

SW would like to acknowledge the National Science Foundation for the Graduate Fellowship (under Grant No. DGE-1842165) to allow her freely pursue her research interest; JC to the support of the Vannevar Bush Faculty Fellowship N00014-19-1-2642 for its encouragement and financial support for pursuing fundamental manufacturing science. The authors acknowledge support by the National Institute of Standards and Technology (NIST) – Center for Hierarchical Material Design (CHiMaD) under grant No.70NANB14H012and the National Science Foundation

Table C.1

Common and alternative name standards for materials analyzed in this study. Alloy 718 is not listed because it does not exist in these naming conventions.

Common name	SAE/AISI	EN #	JIS
Stainless Steel 316 L	316 L	1.4404	SUS316L
Stainless Steel 304	304	1.4301	SUS304
Ti-6Al-4V	Titanium Gr 5	3.7165	S Ti 6400
AlSiMg	A13600	3.2381	ADC3

(NSF) – Cyber-Physical Systems (CPS) under grant No.CPS/CMMI-1646592.

Appendix A. Current snapshot of hybrid-AM research landscape

Fig. A.37 shows the variety of research locations that published the hybrid-AM work, as well as the relative number of citations in each area.

Appendix B. Methods used to analyze data

In this study, multiple databases (Scopus, Web of Knowledge, and Google Scholar) were used for paper retrieval using keyword(s) of ‘metal hybrid manufacturing’, ‘hybrid additive manufacturing’ or ‘hybrid 3D printing’, etc. Moreover, in order to research more thoroughly, the references and citations for each paper searched out were also considered whether using hybrid-AM or not. Detailed information from over 100 papers that considered hybrid-AM was extracted manually, where terminology, properties, and units were standardized, and compiled in the data spreadsheet in [Appendix D](#). The extracted data include: material type, property, mechanism, energy source, process, basic information (author, publish year, group, affiliation), etc. Python codes were used to analyze statistics information, e.g., values of properties, number of papers reported, number of reported materials, affiliation distribution, etc. To note, some papers were left out of the analysis if insufficient information was given (i.e., material properties). Python codes were used to plot statistics information mainly present in [Section 2](#). The full code can be found in the supplementary material.

Appendix C. Material list

The common and alternative standard names for the six most used

Table D.1

Compiled data for over 100 papers analyzed in this study. Extracted and standardized data includes: paper reference, No. of citations, affiliation(s), mechanism(s), energy source(s), process, material, standardized property, property without hybrid (if reported), and the percent difference between the hybrid and AM-only property (if applicable).

Paper Reference	No. of Citations	Affiliation	Mechanism	Energy Source	Process	Material	Standardized Property	Standardized Quantitative Property	Standardized Units	Property without hybrid	Units	Property, [%] difference
Yasa, E., Kruth, J. P., & Deckers, J. (2011). Manufacturing by combining Selective Laser Melting and Selective Laser Erosion/laser remelting. <i>CIRP Annals – Manufacturing Technology</i> , 60(1), 263–266. https://doi.org/10.1016/j.cirp.2011.03.063	107	KU Leuven	Surface evolution	Thermal	Secondary laser	316 L	Surface roughness	1.500	[um], Ra	12	[um], Ra	-700.0%
					Microstructure development							
						316 L	Porosity	0.036	[%]	0.77	[%]	-0.7%
						316 L	Geometric accuracy	75.000	[um], features	450	[um]	-500.0%
Francis, R., Newkirk, J., & Liou, F. (2016). Investigation of forged-like microstructure produced by a hybrid manufacturing process. <i>Rapid Prototyping Journal</i> , 22(4), 717–726. https://doi.org/10.1108/RPJ-03-2015-0038	1	Missouri University of Science and Technology	Microstructure development	Thermal	Friction-stir processing	Titanium Gr 5	Grain size	1.500	[um]	16	[um]	-966.7%
					Stress state							
						Titanium Gr 5 Titanium Gr 5	Grain texture Hardness	Equiaxed 400.000	[HV]	–	–	–
Koike R Misawa T Aoyama T Kondo M. (2018). Controlling metal structure with remelting process in direct energy deposition of Inconel 625. <i>CIRP Annals</i> , 2018 vol: 67 (1) pp: 237–240. https://doi.org/10.1016/j.cirp.2018.04.061	4	Keio University	Microstructure development	Thermal	Primary laser remelting	Alloy 625	Porosity	0.017	[%]	–	–	–
		DMG Mori Seiki Co., Ltd.				Alloy 625	Hardness	375.000	[HV]	–	–	–
Qian, Y. P., Huang, J. H., Zhang, H. O., & Wang, G. L. (2008). Direct rapid high-temperature alloy prototyping by hybrid plasma-laser technology. <i>Journal of Materials</i>	9	Hubei University of Technology	Melt pool dynamics	Thermal	Secondary laser	Ni-based alloy	–	–	–	–	–	–

(continued on next page)

Table D.1 (continued)

Paper Reference	No. of Citations	Affiliation	Mechanism	Energy Source	Process	Material	Standardized Property	Standardized Quantitative Property	Standardized Units	Property without hybrid	Units	Property, [%] difference
Processing Technology, 208(1–3), 99–104. https://doi.org/10.1016/j.jmatprotec.2007.12.116		Huazhong University of Science and Technology										
Yasa, E., & Kruth, J. (2011). Application of Laser Re-Melting on Selective Laser Melting Parts. <i>Advances in Production Engineering & Management</i> , 6(4), 259–270	146	Catholic University of Leuven	Melt pool dynamics	Thermal	Primary laser remelting	316 L	Porosity	0.030	[%]	0.67	[%]	-0.6%
						316 L	Surface roughness	1.500	[μm], Ra	12	[μm]	-700.0%
Dalaee, M. T., Gloor, L., Leinenbach, C., & Wegener, K. (2020). Experimental and numerical study of the influence of induction heating process on build rates Induction Heating-assisted laser Direct Metal Deposition (IH-DMD). <i>Surface and Coatings Technology</i> , 384(August 2019), 125275. https://doi.org/10.1016/j.surcoat.2019.125275	2	Inspire AG	Melt pool dynamics	Thermal	Induction heating	F6NM	Porosity	100.000	[%]	-	-	-
		Institute of Machine Tools & Manufacturing Swiss Federal Laboratories for Materials Science and Technology				F6NM	Deposition rate	20.380	[g/min]	14.56	[g/min]	28.6%
						F6NM	Melt pool depth	500.000	[μm]	0.03	[mm]	94.0%
Näsström, J., Brückner, F., & Kaplan, A. F. H. (2019). Measuring the effects of a laser beam on melt pool fluctuation in arc additive manufacturing. <i>Rapid Prototyping Journal</i> , 25 (3), 488–495	1	Lulea University of Technology	Melt pool dynamics	Thermal	Secondary laser	316 L	Geometric accuracy	97.000	[μm], standard deviation	-	-	-

Table D.1 (continued)

Paper Reference	No. of Citations	Affiliation	Mechanism	Energy Source	Process	Material	Standardized Property	Standardized Quantitative Property	Standardized Units	Property without hybrid	Units	Property, [%] difference	
Nie Z Wang G McGuffin-Cawley J Narayanan B Zhang S Schwam D Kottman M Rong Y. (2016). Experimental study and modeling of H13 steel deposition using laser hot-wire additive	38	Tsinghua University	Melt pool dynamics	Thermal	Electric current	H13	Hardness	460.000	[HV]	-	-	-	
Heeling, T., & Wegener, K. (2018). The effect of multi-beam strategies on selective laser melting of stainless steel 316L. Additive Manufacturing, 22(February), 334–342. https://doi.org/10.1016/j.addma.2018.05.026	11	Institute of Machine Tools and Manufacturing	Melt pool dynamics	Thermal	Secondary laser	316 L	Surface roughness	-	-	-	-	-	
Nowotny, S., Brueckner, F., Thieme, S., Leyens, C., & Beyer, E. (2015). High-performance laser cladding with combined energy sources. Journal of Laser Applications, 27 (S1), S17001. https://doi.org/10.2351/1.4817455	11	Fraunhofer Institute Material and Beam Technology IWS	Melt pool dynamics	Thermal	Induction heating	316 L	Porosity	-	-	-	-	-	
Al-Milaji K Gupta S Pecharsky V Barua R Zhao H Hadimani R.(2020). Differential effect of magnetic alignment on additive manufacturing of magnetocaloric particles. AIP Advances 10, 015052. https://doi.org/10.1063/1.5130028	1	Virginia Commonwealth University	Microstructure development	Magnetic	Static magnetic field	Gd5Si4	-	-	-	-	-	-	
Griffiths S Rossell M Croteau J Vo N Dunand D Leinenbach C. (2018). Effect of laser rescanning	27	Department of Energy Iowa State University	Laboratory for Advanced Materials Processing	Microstructure development	Thermal	Primary laser remelting	Addalloy	Melt pool depth	35.000	[um]	50	[um]	-42.9%

(continued on next page)

Table D.1 (continued)

Paper Reference	No. of Citations	Affiliation	Mechanism	Energy Source	Process	Material	Standardized Property	Standardized Quantitative Property	Standardized Units	Property without hybrid	Units	Property, [%] difference
on the grain microstructure of a selective laser melted Al-Mg-Zr alloy. Materials Characterization. 143 (March): 34–42. https://doi.org/10.1016/j.matchar.2018.03.033		Laboratory of Photonic Materials and Characterization Electron Microscopy Center										
Xiong Z Zhang P Tan C Dong D Ma W Yu K. (2020). Selective Laser Melting and Remelting of Pure Tungsten. Advanced Engineering Materials, 22 (3). https://doi.org/10.1002/adem.201901352	1	Central South University	Melt pool dynamics	Thermal	Primary laser remelting	Tungsten	Porosity	1.600	[%]	98.1	[%]	0.3%
31		Guangdong Institute of New Materials				Tungsten	Surface roughness	10.620	[μm], Ra	14.72	[μm]	-38.6%
						Tungsten	Grain size	14.000	[μm]	29	[μm]	-107.1%
Zhang C Gao M Zeng X. (2019). Workpiece vibration augmented wire arc additive manufacturing of high strength aluminum alloy. Journal of Materials Processing Technology, 271, 85–92. https://doi.org/10.1016/j.jmatprotec.2019.03.028	7	Wuhan University Huazhong University of science and tech	Microstructure development	Acoustic	Workpiece vibration	Al-Mg	Grain size	29.800	[μm]	40.8	[μm]	-36.9%
Kang N Yuan H Coddet P Ren Z Bernage C Liao H Coddet C. (2017). On the texture, phase and tensile properties of commercially pure Ti produced via selective laser melting assisted by	17	University Bourgogne Franche-Comte	Melt pool dynamics	Mechanical		Al-Mg	Porosity	1.520	[%]	4.72	[%]	-3.2%
						Al-Mg	Ultimate tensile strength	343.000	[MPa]	313	[MPa]	8.7%
						Al-Mg	Yield strength	185.000	[Mpa]	80	[MPa]	56.8%
						Al-Mg	Elongation	22.000	[%]	22	[%]	0.0%

(continued on next page)

Table D.1 (continued)

Paper Reference	No. of Citations	Affiliation	Mechanism	Energy Source	Process	Material	Standardized Property	Standardized Quantitative Property	Standardized Units	Property without hybrid	Units	Property, [%] difference
static magnetic field Materials Science and Engineering C, 70: 405–407. https://doi.org/10.1016/j.msec.2016.09.011		Ecole Nationale d'Ingénieurs de Saint-Etienne (ENISE) Shanghai University,				Titanium Gr 2	Fracture strain	35	[%]	28	[%]	7.0%
Ortiz-Fernandez R Jodoin B. (2020) Hybrid Additive Manufacturing Technology: Induction Heating Cold Spray—Part II: Coating Mechanical Properties, Journal of Thermal Spray Technology 29 (4) 700–713. https://link.springer.com/content/pdf/10.1007/s1166-020-01006-9.pdf	0	University of Ottawa	Microstructure development	Thermal	Induction heating	SST-A5001 (99.8% Al) (Ti6Al4V substrate)	Hardness	47.000	[HV]	57	[HV]	-21.3%
						SST-A5001 (99.8% Al) (Ti6Al4V substrate)	Hardness	48.000	[HV]	55	[HV]	-14.6%
						SST-A5001 (99.8% Al) (Ti6Al4V substrate)	Adhesion strength	70	[Mpa]	44	[MPa]	37.1%
Gong, M., Meng, Y., Zhang, S., Zhang, Y., Zeng, X., &Gao, M. (2020). Laser- arc hybrid additive manufacturing of stainless steel with beam oscillation. Additive Manufacturing, 33 (March), 101180. https://doi.org/10.1016/j.addma.2020.101180	0	Wuhan National Laboratory for Optoelectronics	Melt pool dynamics	Thermal	Secondary laser	316 L	Surface roughness	42.000	[um], Ra	205	[um], Ra	-388.1%
		Huazhong University of Science and Technology				316 L	Grain texture	1.600	[%], cube	11.8	[%], cube	-10.2%
						316 L	Porosity	0.000	[%]	0	[%]	0.0%
						316 L	Ultimate tensile strength	622.000	[MPa]	582	[MPa]	6.4%
						316 L	Yield strength	299.000	[MPa]	344	[MPa]	-15.1%

(continued on next page)

Table D.1 (continued)

Paper Reference	No. of Citations	Affiliation	Mechanism	Energy Source	Process	Material	Standardized Property	Standardized Quantitative Property	Standardized Units	Property without hybrid	Units	Property, [%] difference
Zhang, Z., Sun, C., Xu, X., & Liu, L. (2018). Surface quality and forming characteristics of thin-wall aluminum alloy parts manufactured by laser assisted MIG arc additive manufacturing. International Journal of Lightweight Materials and Manufacture, 1(2), 89–95. https://doi.org/10.1016/j.ijlmm.2018.03.005	7	Dalian University of Technology	Melt pool dynamics	Thermal	Secondary laser	316 L	Elongation	34.000	[%]	34.4	[%]	-0.4%
Xie, Y., Zhang, H., & Zhou, F. (2016). Improvement in Geometrical Accuracy and Mechanical Property for Arc-Based Additive Manufacturing Using Metamorphic Rolling Mechanism. Journal of Manufacturing Science and Engineering, Transactions of the ASME, 138(11), 1–8. https://doi.org/10.1115/1.4032079	23	Huazhong University of Science and Technology	Microstructure development	Mechanical	Continuous hot rolling	AA6061	Surface roughness	0.190	[um], Ra	-	-	-
Näström, J., Brueckner, F., & Kaplan, A. F. H. (2019). Laser enhancement of wire arc additive manufacturing. Journal of Laser Applications, 31(2), 022307. https://doi.org/10.2351/1.5096111	1	Lulea University of Technology	Melt pool dynamics	Thermal	Secondary laser	316 L	Geometric accuracy	0.200	[mm]	2.4	[mm]	-1100.0%
33	Stress state	Thermal	304	1045	1045	1045	Geometric accuracy	0.120	[mm]	0.45	[mm]	-275.0%
							Yield strength	547.900	[MPa]	526.7	[MPa]	3.9%
							Ultimate tensile strength	816.700	[MPa]	765.9	[MPa]	6.2%
							Elongation	40.700	[%]	37.9	[%]	2.8%
							Geometric accuracy	0.100	[mm]	2.3	[mm]	-2200.0%
							Geometric accuracy	0.020	[mm], standard deviation	0.18	[mm]	-800.0%
							Grain texture	Equiaxed		Columnar		
							Porosity	0.000	[%]	-	-	-

(continued on next page)

Table D.1 (continued)

Paper Reference	No. of Citations	Affiliation	Mechanism	Energy Source	Process	Material	Standardized Property	Standardized Quantitative Property	Standardized Units	Property without hybrid	Units	Property, [%] difference
		Fraunhofer Institute for Material and Beam Technology Dresden										
Corradi, D. R., Bracarense, A. Q., Wu, B., Cuiuri, D., Pan, Z., & Li, H. (2020). Effect of Magnetic Arc Oscillation on the geometry of single-pass multi-layer walls and the process stability in wire and arc additive manufacturing. <i>Journal of Materials Processing Technology</i> , 283 (December 2019), 116723. https://doi.org/10.1016/j.jmatprotec.2020.116723	0	Federal University of Sao Joao del-Rei	Melt pool dynamics	Thermal	Magnetic arc oscillation	Low carbon steel	Geometric accuracy	250.000	[um], standard deviation	0.32	[mm], standard deviation	-28.0%
34		The University of Wollongong				Titanium Gr 5	Geometric accuracy	40.000	[um], standard deviation	0.43	[mm], standard deviation	-975.0%
		Federal University of Minas Gerais										
Nie, J., Chen, C., Shuai, S., Liu, X., Zhao, R., Wang, J., ... Ren, Z. (2020). Effect of Static Magnetic Field on the Evolution of Residual Stress and Microstructure of Laser Remelted Inconel 718 Superalloy. <i>Journal of Thermal Spray Technology</i> . https://doi.org/10.1007/s11666-020-01039-0	0	Shanghai University	Melt pool dynamics	Magnetic	Static magnetic field	Alloy 718	Residual stress	315.450	[MPa]	392.5	[MPa]	-24.4%
		University Bourgogne Franche-Comte	Microstructure development		Primary laser remelting	Alloy 718	Dendrite spacing	4.250	[um]	6.25	[um]	-47.1%
Du, D., Haley, J. C., Dong, A., Fautrelle, Y., Shu, D., Zhu, G., ... Lavernia, E. J. (2019). Influence of static magnetic field on microstructure and mechanical behavior of selective laser melted AlSi10Mg alloy. <i>Materials and Design</i> , 181. https://doi.org/10.1016/j.matdes.2019.108250	4	Shanghai Jiao Tong University	Melt pool dynamics	Magnetic	Static magnetic field	AlSi10Mg	Porosity	0.400	[%]	99.2	[%, relative density]	0.4%

(continued on next page)

Table D.1 (continued)

Paper Reference	No. of Citations	Affiliation	Mechanism	Energy Source	Process	Material	Standardized Property	Standardized Quantitative Property	Standardized Units	Property without hybrid	Units	Property, [%] difference
//doi.org/10.1016/j.matdes.2019.107923						AlSi10Mg	Dendrite spacing	400.000	[um]	450	[um], cellular dendrite spacing [%]	-12.5%
		University of California Irvine	Microstructure development			AlSi10Mg	Grain texture	19.000	[%], columnar grains	48	[%]	-29.0%
		Shanghai University				AlSi10Mg AlSi10Mg	Elongation Ultimate tensile strength	8.800 420.000	[%] [MPa]	6 325	[%] [MPa]	2.8% 22.6%
Liu, F., Cheng, H., Yu, X., Yang, G., Huang, C., Lin, X., & Chen, J. (2018). Control of microstructure and mechanical properties of laser solid formed Inconel 718 superalloy by electromagnetic stirring. Optics and Laser Technology, 99, 342–350. https://doi.org/10.1016/j.optlastec.2017.09.022	11	Nanchang Hangkong University	Melt pool dynamics	Mechanical	Electromagnetic stirring	Alloy 718	Fatigue life	82100.000	[cycles]	40900	[cycles]	50.2%
		Shenyang Aerospace University				Alloy 718	Phase	2.390	[%], laves phase	5.49	[%], laves phase	-3.1%
		Northwestern Polytechnic University				Alloy 718	Residual stress	358.000	[MPa]	223	[MPa]	37.7%
						Alloy 718 Alloy 718	Hardness Ultimate tensile strength	328.000 1072.000	[HV] [MPa]	277 950	[HV] [MPa]	15.5% 11.4%
						Alloy 718	Elongation	32.000	[%]	12	[%]	20.0%
Lu, Y., Sun, G., Wang, Z., Zhang, Y., Su, B., Feng, A., & Ni, Z. (2019). Effects of electromagnetic field on the laser direct metal deposition of austenitic stainless steel. Optics and Laser Technology, 119 (January). https://doi.org/10.1016/j.optlastec.2019.105586	0	Southeast University	Melt pool dynamics	Magnetic	Rotating magnetic and electric fields	316 L	Residual stress	-75.300	[MPa]	-29.11	[MPa]	61.3%
		Guangdong University of Technology Wenzhou University				316 L	Hardness	218.940	[HV]	183.84	[HV]	16.0%
	1	Tianjin University	Stress state	Mechanical		Titanium Gr 5		9600		-	-	-

(continued on next page)

Table D.1 (continued)

Paper Reference	No. of Citations	Affiliation	Mechanism	Energy Source	Process	Material	Standardized Property	Standardized Quantitative Property	Standardized Units	Property without hybrid	Units	Property, [%] difference
Gou, J., Wang, Z., Hu, S., Shen, J., Tian, Y., Zhao, G., Chen Y. (2020). Effects of ultrasonic peening treatment in three directions on grain refinement and anisotropy of cold metal transfer additive manufactured Ti-6Al-4V thin wall structure. <i>Journal of Manufacturing Processes</i> , 54 (June) pp: 148–157. https://doi.org/10.1016/j.jmapro.2020.03.010					Ultrasonic impact peening		Grain size (length)		[um], beta phase			
						Titanium Gr 5	Grain size (width)	1800	[um], beta phase	–	–	–
						Titanium Gr 5	Grain size	20.000	[um]	60	[um], alpha bulge	–200.0%
						Titanium Gr 5	Ultimate tensile strength	1059.000	[MPa]	996	[MPa]	5.9%
						Titanium Gr 5	Elongation	8.090	[%]	8.28	[%]	–0.2%
						Titanium Gr 5	Anisotropic percentage	0.800	[%]	6	[%]	–5.2%
Kao, A., Gan, T., Tonry, C., Krastins, I., & Pericleous, K. (2020). Thermoelectric magnetohydrodynamic control of melt pool dynamics and microstructure evolution in additive manufacturing. <i>Philosophical Transactions of the Royal Society A: Mathematical, Physical and Engineering Sciences</i> , 378(2171). https://doi.org/10.1098/rsta.2019.0249	0	University of Greenwich	Melt pool dynamics	Magnetic	Static magnetic field	AlSi10Mg	–	–	–	–	–	–
Zhou, X. M., Zhang, H. O., Wang, G. L., Liang, L. Y., Fu, Y. H., Bai, X. W., & Wang, X. P. (2020). Numerical simulation and experimental investigation of arc based additive manufacturing assisted with	3	Huazhong University of Science and Technology	Melt pool dynamics	Magnetic	Static magnetic field	ER70S-6	Clad width	10.000	[mm]	8	[mm]	20.0%

Table D.1 (continued)

Paper Reference	No. of Citations	Affiliation	Mechanism	Energy Source	Process	Material	Standardized Property	Standardized Quantitative Property	Standardized Units	Property without hybrid	Units	Property, [%] difference
Colegrove, P. A., Coules, H. E., Fairman, J., Martina, F., Kashoob, T., Mamash, H., & Cozzolino, L. D. (2013). Microstructure and residual stress improvement in wire and arc additively manufactured parts through high-pressure rolling. Journal of Materials Processing Technology, 213(10), 1782–1791. https://doi.org/10.1016/j.jmatprotec.2013.04.012	123	Cranfield University	Stress state	Mechanical	Continuous hot rolling	ER70S-6	Residual stress	250.000	[MPa]	600	[MPa]	-140.0%
Zhou, X., Zhang, H., Wang, G., Bai, X., Fu, Y., & Zhao, J. (2016). Simulation of microstructure evolution during hybrid deposition and micro-rolling process. Journal of Materials Science, 51(14), 6735–6749. https://doi.org/10.1007/s10853-016-9961-0	16	Huazhong University of Science and Technology	Stress state	Mechanical	Continuous hot rolling	ER70S-6	Hardness ER70S-6 Grain size	250.000 6.000	[HV] [um]	180 8	[HV] [um]	28.0% -33.3%
Wu, D., Liu, D., Niu, F., Miao, Q., Zhao, K., Tang, B., Bi, G., Ma, G. (2019). Al-Cu alloy fabricated by novel laser-tungsten inert gas hybrid additive manufacturing. Additive Manufacturing, 32 (November 2019) 100954. https://doi.org/10.1016/j.addma.2019.100954	3	Dalian University of Technology	Thermal gradients	Thermal	Secondary laser	ER2319 (nealy2219-Al)	Grain size	14.400	[um]	20.2	[um]	-40.3%
37	University of South China	Shanghai Aerospace Equipment Manufacturer Co. Ltd., Singapore Institute of Manufacturing Technology				ER2319 (nealy2219-Al)	Pore number	0.820	[%]	-	-	-
							Pore size	200.000	[um]	-	-	-
							Yield strength	155.500	[MPa]	108	[MPa]	30.5%

(continued on next page)

Table D.1 (continued)

Paper Reference	No. of Citations	Affiliation	Mechanism	Energy Source	Process	Material	Standardized Property	Standardized Quantitative Property	Standardized Units	Property without hybrid	Units	Property, [%] difference
Xiao Z Chen C Hu Z Zhu H Zeng X.(2020). Effect of rescanning cycles on the characteristics of selective laser melting of Ti6Al4V. Optics and Laser Technology,122, https://doi.org/10.1016/j.optlastec.2019.105890	0	Huazhong University of Science and T	Thermal gradients	Thermal	Primary laser remelting	ER2319 (nealy2219-Al) ER2319 (nealy2219-Al) ER2319 (nealy2219-Al)	Ultimate tensile strength Elongation Hardness	301.500 12.800 92.600	[MPa] [%] [HV]	240 10.7 -	[MPa] [%] -	20.4% 2.1% -
Zhou, C., Jiang, F., Xu, D., Guo, C., Zhao, C., Wang, Z., & Wang, J. (2020). A calculation model to predict the impact stress field and depth of plastic deformation zone of additive manufactured parts in the process of ultrasonic impact treatment. Journal of Materials Processing Technology, 280(August 2019). https://doi.org/10.1016/j.jmatprotec.2020.116599	38	Harbin Engineering University	Stress state	Mechanical	Interlayer ultrasonic impact peening	Titanium Gr 5 Titanium Gr 5 Titanium Gr 5 Titanium Gr 5	Yield strength Ultimate tensile strength Hardness Residual stress	1466.000 1590.000 401.280 625.000	[MPa] [MPa] [HV] [MPa]	1030 1268 -	[MPa] [MPa] -	29.7% 20.3% -
Wang, Y., & Shi, J. (2019). Microstructure and Properties of Inconel 718 Fabricated by Directed Energy Deposition with In-Situ Ultrasonic Impact Peening. Metallurgical	0	University of Cincinnati	Stress state	Mechanical	Interlayer ultrasonic impact peening	304 304 304 304	Young's modulus Hardness Dendrite spacing Yield strength Yield strength	200.000 300.000 25.000 370.000 690.000	[GPa] [HV] [um] [MPa] [MPa]	- -	- -	- -

(continued on next page)

Table D.1 (continued)

Paper Reference	No. of Citations	Affiliation	Mechanism	Energy Source	Process	Material	Standardized Property	Standardized Quantitative Property	Standardized Units	Property without hybrid	Units	Property, [%] difference		
and Materials Transactions B: Process Metallurgy and Materials Processing Science, 50(6), 2815–2827. https://doi.org/10.1007/s11663-019-01672-3														
Gu, J., Yang, S., Gao, M., Bai, J., Zhai, Y., & Ding, J. (2020). Micropore evolution in additively manufactured aluminum alloys under heat treatment and inter-layer rolling. Materials and Design, 186, 108288. https://doi.org/10.1016/j.matdes.2019.108288	2	Yanshan University	Stress state	Mechanical	Intralayer rolling	Al-Cu6.3	Acoustic	Alloy 718 Alloy 718 Alloy 718 Alloy 718	Hardness Dendrite spacing Grain size Grain texture	450.000 10.000 280.000 <1 1 1>	[HV] [um] [um] <1 0 0>	345 – 420	[HV] – [um]	23.3% – –50.0%
Kalentics, N., de Seijas, M. O. V., Griffiths, S., Leinenbach, C., & Logé, R. E. (2020). 3D laser shock peening – A new method for improving fatigue properties of selective laser melted parts. Additive Manufacturing, 33(January), 101112. https://doi.org/10.1016/j.addma.2020.101112	3	EPFL	Stress state	Mechanical	Interlayer laser shock peening	316 L	Northeastern University Cranfield University	Al-Cu6.3 Al-Cu6.3	Ultimate tensile strength Porosity	340.000 0.100	[MPa] [%]	290 –	[MPa] –	14.7% –
Shchitsyn, Y. D., Krivonosova, E. A., Trushnikov, D. N., Ol'shanskaya, T. V., Kartashov, M. F.,	0	National Research Polytechnic University	Stress state	Mechanical	Interlayer peening	Ti-Al-2V	Empa-swiss federal laboratories	316 L 316 L 316 L 316 L	Residual stress Porosity Hardness Grain size	-750.000 0.160 322.000 13.270	[MPa] [%] [HV] [um]	340 99.82 236 12.25	[MPa] [%] [HV] [um]	145.3% 0.0% 26.7% 7.7%

(continued on next page)

Table D.1 (continued)

Paper Reference	No. of Citations	Affiliation	Mechanism	Energy Source	Process	Material	Standardized Property	Standardized Quantitative Property	Standardized Units	Property without hybrid	Units	Property, [%] difference
&Neulybin, S. D. (2020). Use of CMT-Surfacing for Additive Formation of Titanium Alloy Workpieces												
Lin, D., Motlag, M., Saei, M., Jin, S., Rahimi, R. M., Bahr, D., &Cheng, G. J. (2018). Shock engineering the additive manufactured graphene-metal nanocomposite with high density nanotwins and dislocations for ultra-stable mechanical properties. <i>Acta Materialia</i> , 150, 360–372. https://doi.org/10.1016/j.actamat.2018.03.013	19	Purdue University	Stress state	Mechanical	Interlayer laser shock peening	4140	Residual stress	-450.000	[MPa]	175	[MPa]	138.9%
				Plasma		4140 4140	Hardness Fatigue stress limit	652.000 750.000	[HV] [MPa]	581 600	[VHN] [MPa]	10.9% 20.0%
40 Madireddy, G., Li, C., Liu, J., &Sealy, M. P. (2019). Modeling thermal and mechanical cancellation of residual stress from hybrid additive manufacturing by laser peening. <i>Nano Jishu Yu Jingmi Gongcheng/ Nanotechnology and Precision Engineering</i> , 2 (2), 49–60. https://doi.org/10.1016/j.npe.2019.07.001	3	University of Nebraska	Stress state	Mechanical	Interlayer laser shock peening	52100	Residual stress	-1250.000	[MPa]	1000	[MPa]	180.0%
		Autodesk Sentient Science Corporation		Plasma								
Wang, Y., &Shi, J. (2020). Recrystallization behavior and tensile properties of laser metal deposited Inconel 718 upon in-situ ultrasonic impact peening and heat treatment. <i>Materials Science and Engineering A</i> , 786 (January), 139434. https://doi.org/10.1016/j.msea.2020.139434	0	University of Cincinnati	Stress state	Acoustic	Interlayer ultrasonic impact peening	Alloy 718	Yield strength	750.000	[MPa]	567	[MPa]	24.4%
				Mechanical		Alloy 718		958.000	[MPa]	856	[MPa]	10.6%

(continued on next page)

Table D.1 (continued)

Paper Reference	No. of Citations	Affiliation	Mechanism	Energy Source	Process	Material	Standardized Property	Standardized Quantitative Property	Standardized Units	Property without hybrid	Units	Property, [%] difference
							Ultimate tensile strength					
						Alloy 718	Young's modulus	150.000	[GPa]	175	[GPa]	-16.7%
						Alloy 718	Dendrite spacing	7.000	[um]	7	[um]	0.0%
						Alloy 718	Grain size	10.000	[um]	-	-	-
						Alloy 718	Elongation	17.000	[%]	17	[um]	0.0%
Yang X Liu J Cui X Jin G Liu Z Chen Y Feng X. (2019). Effect of remelting on microstructure and magnetic properties of Fe-Co-based alloys produced by laser additive manufacturing. Journal of Physics	14	College of Material Science and Chemical Engineering, Harbin Engineering	Microstructure development	Thermal	Primary laser remelting	(Fe60Co35Ni5) 73.5S i13.5B9CuMo3	Hardness	975.000	[HV]	900	[HV0.3]	7.7%
Hackel, L., Rankin, J. R., Rubenchik, A., King, W. E., & Matthews, M. (2018). Laser peening: A tool for additive manufacturing post-processing. Additive Manufacturing, 24(May), 67–75. https://doi.org/10.1016/j.addma.2018.09.013	25	Curtiss Wright Surfae Technologies	Stress state	Mechanical	Laser shock peening	316 L	Fatigue life	2000000.000	[cycles]	100000	[cycles]	95.0%
		Lawrence Livermore National Laboratory		Plasma		316 L	-	-	-	-	-	-
Roehling, J. D., Smith, W. L., Roehling, T. T., Vrancken, B., Guss, G. M., McKeown, J. T., ... Matthews, M. J. (2019). Reducing residual stress by selective large-area diode surface heating during laser powder bed fusion additive manufacturing. Additive Manufacturing, 28 (January), 228–235. http://doi.org/10.1016/j.addma.2019.05.009	9	Lawrence Livermore National Laboratory	Thermal gradients	Thermal	Laser diode illumination	316 L	Residual stress	13.000	[MPa]	134	[MPa]	-930.8%
		University of California				316 L	Hardness	230.000	[HV]	260	[HV]	-13.0%
Hackenhaar, W., Mazzaferro, J. A. E., Montevercchi, F.,	1	Federal Univesity of Rio Grande do Sul	Thermal gradients	Thermal	Air cooling nozzle	AWS ER70S-6	-	-	-	-	-	-

(continued on next page)

Table D.1 (continued)

Paper Reference	No. of Citations	Affiliation	Mechanism	Energy Source	Process	Material	Standardized Property	Standardized Quantitative Property	Standardized Units	Property without hybrid	Units	Property, [%] difference
&Campatelli, G. (2020). An experimental-numerical study of active cooling in wire arc additive manufacturing. Journal of Manufacturing Processes, 52(October 2019), 58–65. https://doi.org/10.1016/j.jmapro.2020.01.051		University of Firenze										
Seidel, A., Finaske, T., Straubel, A., Wendrock, H., Maiwald, T., Riede, M., ... Leyens, C. (2018). Additive Manufacturing of Powdery Ni-Based Superalloys Mar-M-247 and CM 247 LC in Hybrid Laser Metal Deposition. Metallurgical and Materials Transactions A: Physical Metallurgy and Materials Science, 49(9), 3812–3830. https://doi.org/10.1007/s11661-018-4777-y	1	Fraunhofer Institute for Material and Beam Technology	Thermal gradients	Thermal	Induction heating	MAR-M-247	Young's modulus	161.000	[GPa]	108	[GPa]	32.9%
		Technische Universität Dresden Lulea University of Technology Leibniz-Institut für Festkörper und Werkstoffforschung				MAR-M-247	Tensile strength	980.000	[MPa]	918	[MPa]	6.3%
						MAR-M-247	Elongation	5.000	[%]	3.3	[%]	1.7%
Zhao Y Sun J Guo K Li J. (2019). Investigation on the effect of laser remelting for laser cladding nickel based alloy. Journal of Laser Applications 31, 022512, https://doi.org/10.2351/1.5096126	3	Shandong University	Thermal gradients	Thermal	Primary laser remelting	Ni-based alloy	Surface roughness	0.443	[um], Ra	2.498	[um]	-463.9%
						Ni-based alloy	Hardness	550.000	[HV]	627	[HV]	-14.0%
Zhang Z Kong F Kovacevic R. (2020). Laser hot-wire cladding of Co-Cr-W metal cored wire. Optics and Lasers in Engineering, 128:105998. https://doi.org/10.1016/j.optlasteng.2020.105998	0	Southern Methodist University	Microstructure development	Thermal	Electric current	WT-6	Hardness	490.000	[HV]	-	-	-

Table D.1 (continued)

Paper Reference	No. of Citations	Affiliation	Mechanism	Energy Source	Process	Material	Standardized Property	Standardized Quantitative Property	Standardized Units	Property without hybrid	Units	Property, [%] difference
org/10.1016/j.jophtlaseng.2019.105998. (no comparison between hot/cold wire)						WT-6	Corrosion resistance	-286.000	[V vs.SCE], self-corrosion potential, single layer, lower	-	-	-
						WT-6	Corrosion resistance	0.063	[$\mu\text{A}/\text{cm}^2$], self-corrosion current, single layer, lower	-	-	-
						WT-6	Pitting resistance	0.596	[V vs.SCE], self-corrosion potential, single layer	-	-	-
Li Z Liu C Xu T Ji L Wang D Lu J Ma S Fan H. (2019). Reducing arc heat input and obtaining equiaxed grains by hot-wire method during arc additive manufacturing titanium alloy. Materials Science and Engineering A, 742: 287–294. https://doi.org/10.1016/j.msea.2018.11.022	26	Beijing Institute of Technology	Microstructure development	Thermal	Electric current	Titanium Gr 5	Grain size	0.890	[μm]	1.1	[μm]	-23.6%
						Titanium Gr 5	Grain size	2000.000	[μm]	-	-	-
						Titanium Gr 5	Ultimate tensile strength	929.000	[MPa], longitudinal	873	[MPa], L	6.0%
						Titanium Gr 5	Ultimate tensile strength	944.000	[MPa], transverse	929	[MPa], T	1.6%
						Titanium Gr 5	Yield strength	835.000	[MPa], longitudinal	806	[MPa], L	3.5%
						Titanium Gr 5	Yield strength	840.000	[MPa], transverse	810	[MPa], T	3.6%
						Titanium Gr 5	Elongation	12.600	[%], longitudinal	23	[%], L	-82.5%
						Titanium Gr 5	Elongation	12.800	[%], transverse	9.17	[%], T	28.4%
Chen, X., Chen, B., Cheng, X. et al. Microstructure and properties of hybrid additive manufacturing 316L component by directed energy deposition and laser remelting. J. Iron Steel Res. Int. 27, 842–848	0	Beihang University	Microstructure development	Thermal	Secondary laser	316 L	Phase	8.900	[vol.%], volume fraction of δ phase	7.8	[vol.%]	1.1%

(continued on next page)

Table D.1 (continued)

Paper Reference	No. of Citations	Affiliation	Mechanism	Energy Source	Process	Material	Standardized Property	Standardized Quantitative Property	Standardized Units	Property without hybrid	Units	Property, [%] difference
(2020). https://doi.org/10.1007/s42243-020-00396-y		Commercial Aircraft Engine Manufacturing Co., Ltd.,				316 L	Phase	0.000	[vol.%], volume fraction of σ phase	3	[vol.%]	-3.0%
						316 L	Hardness	214.000	[HV]	202	[HV]	5.6%
						316 L	Corrosion resistance	-0.170	[VSCE]	-0.15	[VSCE]	11.8%
						316 L	Corrosion resistance	0.700	[VSCE]	0.47	[VSCE]	32.9%
Kang N Coddet P Wang J Yuan H Ren Z Liao H Coddet C. (2017). A novel approach to in-situ produce functionally graded silicon matrix composite materials by selective laser melting. 72: 251–258. https://doi.org/10.1016/j.comstruct.2017.03.096	13	University of Belfort-Montbeliard	Melt pool dynamics	Magnetic	Static magnetic field	50% Al, 50% Si (wt) substrate: pure Al	Hardness	387.000	[HV], top of melt	194	[HV0.2], top	49.9%
44		Shanghai University	Microstructure development			50% Al, 50% Si (wt) substrate: pure Al	Hardness	535.000	[HV], bottom of melt	165	[HV0.2], bottom	69.2%
						50% Al, 50% Si (wt) substrate: pure Al	Composition	65.000	[%]	54	[%]	11.0%
						50% Al, 50% Si (wt) substrate: pure Al	Wear rate	7.000	[* E4 mm ³ /N/m]	8.2	[* E4 mm ³ /N/m]	-17.1%
Du, D., Dong, A., Shu, D. et al. Influence of Static Magnetic Field on the Microstructure of Nickel-Based Superalloy by Laser-Directed Energy Deposition. Metall and Mat Trans A 51, 3354–3359 (2020). https://doi.org/10.1007/s11661-020-05783-4	0	Shanghai Jiao Tong University	Melt pool dynamics	Magnetic	Static magnetic field	Alloy 718	Dendrite spacing	4.000	[um]	-	-	-
						Alloy 718	Dendrite spacing	4.600	[um]	-	-	-
		University of California, Irvine,	Microstructure development			Alloy 718	Convection velocity	2.610	[m/s]	3.33	[m/s]	-27.6%
Liu B Li B Li Z. (2019). Selective laser remelting of an additive layer	9	North University of China	Microstructure development	Thermal	Primary laser remelting	AlSi10Mg	Hardness	121.600	[HV]	117.7	[HV0.3]	3.2%

(continued on next page)

Table D.1 (continued)

Paper Reference	No. of Citations	Affiliation	Mechanism	Energy Source	Process	Material	Standardized Property	Standardized Quantitative Property	Standardized Units	Property without hybrid	Units	Property, [%] difference
manufacturing process on AlSi10Mg. Results in Physics, 12 (December 2018) pp: 982–988. https://doi.org/10.1016/j.rinp.2018.12.018						AlSi10Mg	Surface roughness	9.940	[um], Ra	13.34	[um]	-34.2%
						AlSi10Mg	Porosity	0.700	[%]	97	[%]	2.3%
						AlSi10Mg	Density	2.660	[g/cm ³]	2.6	[g/cm ³]	2.3%
						AlSi10Mg	Grain size			-	-	-
						AlSi10Mg	Element distribution			-	-	-
Martina, F., Colgrove, P., Roy, M., & Williams, S. (2014). Residual Stress Reduction in High Pressure Interpass Rolled Wire+Arc Additive Manufacturing Ti-6Al-4V Components. Solid Freeform Fabrication Proceedings, 89–94	14	Cranfield University	Stress state	Mechanical	Intralayer rolling	Titanium Gr 5	Residual stress	200.000	[MPa]	500	[MPa]	-150.0%
45		The University of Manchester										
Zhang, H., Wang, X., Wang, G., & Zhang, Y. (2013). Hybrid direct manufacturing method of metallic parts using deposition and micro continuous rolling. Rapid Prototyping Journal, 19 (6), 387–394	28	Huazhong University of Science and Technology	Stress state	Mechanical	Continuous hot rolling	-	Tensile strength	42.000	[kN]	31	[kN]	26.2%
Martina, F., Colegrave, P. A., Williams, S. W., & Meyer, J. (2015). Microstructure of Interpass Rolled Wire + Arc Additive Manufacturing Ti-6Al-4V Components. Metallurgical and Materials Transactions A: Physical Metallurgy and Materials Science, 46(12), 6103–6118. https://doi.org/10.1007/s11661-015-3172-1	92	Cranfield University	Stress state	Mechanical	Intralayer rolling	Titanium Gr 5	Grain size	100.000	[um]	-	-	-
						Titanium Gr 5	Grain texture	Equiaxed		Columnar		

(continued on next page)

Table D.1 (continued)

Paper Reference	No. of Citations	Affiliation	Mechanism	Energy Source	Process	Material	Standardized Property	Standardized Quantitative Property	Standardized Units	Property without hybrid	Units	Property, [%] difference	
Xie, Y., Zhang, H., Wang, G., & Zhou, F. (2014). A novel metamorphic mechanism for efficient additive manufacturing of components with variable wall thickness. Solid Freeform Fabrication Symposium	1	Huazhong University of Science and Technology	Stress state	Mechanical	Continuous hot rolling	Steel	Geometric accuracy	500.000	[um], standard deviation	2	[mm]	-300.0%	
Colegrove, P. A., Martina, F., Roy, M. J., Szost, B. A., Terzi, S., Williams, S. W., ... Jarvis, D. (2014). High pressure interpass rolling of Wire + Arc additively manufactured titanium components. Advanced Materials Research, 996, 694–700. https://doi.org/10.4028/www.scientific.net/AMR.996.694	29	Cranfield University	Stress state	Mechanical	Intralayer rolling	Titanium Gr 5	Grain size	89.000	[um]	-	-	-	
Donoghue, J., Antonysamy, A. A., Martina, F., Colegrove, P. A., Williams, S. W., & Prangnell, P. B. (2016). The effectiveness of combining rolling deformation with Wire-Arc Additive Manufacture on β -	87	The University of Manchester ESA-ESTEC	Stress state	Mechanical	Intralayer rolling	Titanium Gr 5	Grain size	100.000	[um]	2000	[um]	-1900.0%	
Martina, Filomeno; Williams, Stewart W.; Colegrove, P. (2013). Improved Microstructure and Increased Mechanical Properties. 24th International SFF Symposium 2014, (August), 490–496	24	Cranfield University	Stress state	Mechanical	Intralayer rolling	Titanium Gr 5	Geometric accuracy	90.000	[um], standard deviation	0.19	[mm]	-111.1%	
							Titanium Gr 5	Hardness	377.000	[HV]	367	[HV]	2.7%
							Titanium Gr 5	Elongation	12.500	[%]	20	[%]	-7.5%
							Titanium Gr 5	Ultimate tensile strength	1075.000	[MPa]	880	[MPa]	18.1%
							Titanium Gr 5	Yield strength	990.000	[MPa]	810	[MPa]	18.2%

(continued on next page)

Table D.1 (continued)

Paper Reference	No. of Citations	Affiliation	Mechanism	Energy Source	Process	Material	Standardized Property	Standardized Quantitative Property	Standardized Units	Property without hybrid	Units	Property, [%] difference
Martina, F., Roy, M. J., Szost, B. A., Terzi, S., Colegrave, P. A., Williams, S. W., ... Hofmann, M. (2016). Residual stress of as-deposited and rolled wire+arc additive manufacturing Ti-6Al-4V components. <i>Materials Science and Technology (United Kingdom)</i> , 32(14), 1439–1448. https://doi.org/10.1080/02670836.2016.1142704	44	Cranfield University	Stress state	Mechanical	Intralayer rolling	Titanium Gr 5	Residual stress	200.000	[MPa]	500	[MPa]	-150.0%
Sealy, M. P., Madireddy, G., Li, C., & Guo, Y. B. (2016). Finite element modeling of hybrid additive manufacturing by laser shock peening. Solid Freeform Fabrication 2016: Proceedings of the 27th Annual International Solid Freeform Fabrication Symposium – An Additive Manufacturing Conference, SFF 2016, (August), 306–316	8	The University of Manchester European Space Agency Airbus Groups Innovation FRM II TU Munich	Stress state	Mechanical	Interlayer laser shock peening	Titanium Gr 5	-	-	-	-	-	-
Bai, X. W., Zhang, H. O., & Wang, G. L. (2013). Electromagnetically confined weld-based Additive Manufacturing. <i>Procedia CIRP</i> , 6, 515–520. https://doi.org/10.1016/j.procir.2013.03.084	8	University of Alabama	Huazhong University of Science and Technology	Melt pool dynamics	Magnetic	High frequency alternating magnetic field	ER70S-6	-	-	-	-	-
Jayasheelan Vaithilingam, Ruth D. Goodridge,	64	The University of Nottingham	Microstructure development	Thermal		Titanium Gr 5	Surface roughness	2.200	[μm], Ra	3.4	[μm]	-54.5%

(continued on next page)

Table D.1 (continued)

Paper Reference	No. of Citations	Affiliation	Mechanism	Energy Source	Process	Material	Standardized Property	Standardized Quantitative Property	Standardized Units	Property without hybrid	Units	Property, [%] difference
Richard J.M. Hague, Steven D.R. Christie, Steve Edmondson. (2016). The effect of laser remelting on the surface chemistry of Ti6Al4V components					Primary laser remelting, surface							
Pantélejev, Libor, Daniel Koutný, David Paloušek, and Jozef Kaiser. (2017). Mechanical and Microstructural Properties of 2618 Al-Alloy Processed by SLM Remelting Strategy. Materials Science Forum, 891 (March 2017): 343–49. https://doi.org/10.4028/www.scientific.net/MSF.891.343	9	Brno University of Technology	Microstructure development	Thermal	Primary laser remelting	2618Al	Ultimate tensile strength	24.000	[MPa]	273	[MPa]	-1037.5%
						2618Al	Elongation	0.300	[%]	0.6	[%]	-0.3%
Demir A Previtali B. (2017). Investigation of remelting and preheating in SLM of 18Ni300 maraging steel as corrective and preventive measures for porosity reduction. International Journal of Advanced Manufacturing Technology, 93 (5–8): 2697–2709	33	Politecnico di Milano	Microstructure development	Thermal	Primary laser remelting	18Ni300	Surface roughness	4.000	[µm], Ra	8	[µm]	-100.0%
						18Ni300	Density	8.005	[g/cm³]	7.983	[g/cm³]	0.3%
Wang, Yachao and Jing Shi. (2019). Texture control of Inconel 718 superalloy in laser additive manufacturing by an external magnetic field. Journal of Materials Science 54: 9809–9823. https://doi.org/10.1007/s10853-019-03569-7	2	University of Cincinnati	Microstructure development	Magnetic	Static magnetic field	Alloy 718	Misorientation angle	19	[°]	32	[°]	-68.4%
			Melt pool dynamics			Alloy 718	Multiple of uniform density	5.25		3.01		-42.7%
Tobias Gustmann, Holger Schwab, Uta Kühn, Simon Pauly, (2018). Selective laser remelting of an additively manufactured	14	Institute for Complex Materials	Microstructure development	Thermal	Primary laser remelting	81.95Cu-11.85Al-3.2Ni-3Mn	Grain size	84.000	[µm]	45	[µm]	46.4%

(continued on next page)

Table D.1 (continued)

Paper Reference	No. of Citations	Affiliation	Mechanism	Energy Source	Process	Material	Standardized Property	Standardized Quantitative Property	Standardized Units	Property without hybrid	Units	Property, [%] difference
Cu-Al-Ni-Mn shape-memory alloy, Materials &Design, 153: 129–138. https://doi.org/10.1016/j.matdes.2018.05.010						81.95Cu-11.85Al-3.2Ni-3Mn 81.95Cu-11.85Al-3.2Ni-3Mn 81.95Cu-11.85Al-3.2Ni-3Mn 81.95Cu-11.85Al-3.2Ni-3Mn 81.95Cu-11.85Al-3.2Ni-3Mn 81.95Cu-11.85Al-3.2Ni-3Mn 81.95Cu-11.85Al-3.2Ni-3Mn	Porosity Ultimate tensile strength Elongation Compressive fracture strength Compressive fracture strain	0.500 492.000 9.000 1512 13	[%] [MPa] [%] [MPa] [MPa]	98.9 617 8.2 1511 14	[%] [MPa] [%] [MPa] [%]	0.6% −25.4% 0.8% 0.1% −1.0%
R. Ortiz-Fernandez, B. Jodoin. (2020). Hybrid Additive Manufacturing Technology: Induction Heating Cold Spray—Part I: Fundamentals of Deposition Process, J. Therm. Spray Technol. (2020) 29:684–699. https://doi.org/10.1007/s11666-020-01005-w	0	University of Ottawa	Microstructure development	Thermal	Induction heating	SST-A5001 (99.8% Al) (Ti6Al4V substrate)	Porosity	0.000	[%]	—	—	—
						SST-A5001 (99.8% Al) (Ti6Al4V substrate) SST-A5001 (99.8% Al) (Ti6Al4V substrate)	Thickness Deposition rate	1027.000 77	[um] [%]	698 52	[um] [%]	32.0% 25.0%
Yang, Y., Gong, Y., Qu, S. et al. Densification, mechanical behaviors, and machining characteristics of 316L stainless steel in hybrid additive/subtractive manufacturing. Int J Adv Manuf Technol 107, 177–189 (2020). https://doi.org/10.1007/s00170-020-05033-2	0	Northeastern University	Surface evolution	Electric	Machining	316 L	Porosity	0.600	[%]	—	—	—

(continued on next page)

Table D.1 (continued)

Paper Reference	No. of Citations	Affiliation	Mechanism	Energy Source	Process	Material	Standardized Property	Standardized Quantitative Property	Standardized Units	Property without hybrid	Units	Property, [%] difference
						316 L	Hardness	251.000	[HV]	–	–	–
						316 L	Yield strength	479.180	[MPa]	–	–	–
						316 L	Ultimate tensile strength	688.370	[MPa]	–	–	–
						316 L	Surface roughness	1.890	[um], Ra	–	–	–
Moritz, J., Seidel, A., Kopper, M., Bretschneider, J., Gumpinger, J., Finaske, T., Riede, M., Schneeweß, M., López, E., Brückner, F., Leyens, C., Rohr, T., &Ghidini, T. (2020). Hybrid manufacturing of titanium	0	Fraunhofer Institute for Material and Beam Technology	Surface evolution	Thermal	Cryogenic machining	Titanium Gr 23	Surface roughness	0.500	[um], Ra	–	–	–
Woo, W. S., Kim, E. J., Jeong, H. I., &Lee, C. M. (2020). Laser-Assisted Machining of Ti-6Al-4V Fabricated by DED Additive Manufacturing. International Journal of Precision Engineering and Manufacturing – Green Technology, 7(3), 559–572. https://doi.org/10.1007/s40684-020-00221-7	0	Changwon National University	Surface evolution	Thermal	Laser assisted machining	Titanium Gr 5	Surface roughness	0.250	[um], Ra	–	–	–
Bouet, G., Cabanettes, F., Bidron, G., Guignandon, A., Peyroche, S., Bertrand, P., Vico, L., &Dumas, V. (2019). Laser-Based Hybrid Manufacturing of Endosseous Implants: Optimized Titanium Surfaces	1	University of Lyon	Surface evolution	Thermal	Laser assisted machining	Titanium Gr 5	Hardness	400.000	[HV]	–	–	–
Dilberoglu, U. M., Haseltalab, V., Yaman, U., &Dolen, M. (2019). Simulator of an additive and subtractive type of hybrid manufacturing system. Procedia	0	Middle East Technical University	Surface evolution	Mechanical	Machining	–	–	–	–	–	–	–

Table D.1 (continued)

Paper Reference	No. of Citations	Affiliation	Mechanism	Energy Source	Process	Material	Standardized Property	Standardized Quantitative Property	Standardized Units	Property without hybrid	Units	Property, [%] difference
Manufacturing, 38(Fair 2019), 792–799												
Brown, D., Li, C., Liu, Z. Y., Fang, X. Y., & Guo, Y. B. (2018). Surface integrity of Inconel 718 by hybrid selective laser melting and milling. <i>Virtual and Physical Prototyping</i> , 13 (1), 26–31. https://doi.org/10.1080/17452759.2017.1392681	16	The University of Alabama	Surface evolution	Mechanical	Machining	Alloy 718	Surface roughness	0.300	[Ra], um	–	–	–
Cortina, M., Arrizubieta, J. I., Ukar, E., & Lamikiz, A. (2018). Analysis of the influence of the use of cutting fluid in hybrid processes of machining and Laser Metal Deposition (LMD). <i>Coatings</i> , 8(2)	6	University of the Basque Country	Surface evolution	Mechanical	Machining	Alloy 718	Hardness	400.000	[HV]	–	–	–
Heigel, J. C., Phan, T. Q., Fox, J. C., & Gnaupel-Herold, T. H. (2018). Experimental Investigation of Residual Stress and its Impact on Machining in Hybrid Additive/Subtractive Manufacturing. <i>Procedia Manufacturing</i> , 26, 929–940. https://doi.org/10.1016/j.promfg.2018.07.120	6	National Institute of Standards and Technology	Surface evolution	Mechanical	Machining	Alloy 17-4 PH	Residual stress	150	[MPa], Hoop Stress	15	[um]	#DIV/0!
Yang, Y., Gong, Y., Qu, S., Rong, Y., Sun, Y., & Cai, M. (2018). Densification, surface morphology, microstructure and mechanical properties of 316L fabricated by hybrid manufacturing. <i>International Journal of Advanced Manufacturing Technology</i> , 97(5–8), 2687–2696. https://doi.org/10.1007/s00364-018-1600-0	8	Northeastern University	Surface evolution	Mechanical	Machining	316 L	Porosity	0.200	[%]	–	–	–

(continued on next page)

Table D.1 (continued)

Paper Reference	No. of Citations	Affiliation	Mechanism	Energy Source	Process	Material	Standardized Property	Standardized Quantitative Property	Standardized Units	Property without hybrid	Units	Property, [%] difference
org/10.1007/s00170-018-2144-1						316 L	Yield strength	245.210	[MPa]	-	-	-
Ye, Z. peng, Zhang, Z. jing, Jin, X., Xiao, M. Z., & Su, J. zhou. (2017). Study of hybrid additive manufacturing based on pulse laser wire depositing and milling. International Journal of Advanced Manufacturing Technology, 88(5–8), 2237–2248. https://doi.org/10.1007/s00170-016-8894-8	12	Beijing Institute of Technology	Surface evolution	Mechanical	Machining	304	Ultimate tensile strength	644.010	[MPa]	-	-	-
						316 L	Elongation	50.030	[%]	-	-	-
Yamazaki, T. (2016). Development of A Hybrid Multi-tasking Machine Tool: Integration of Additive Manufacturing Technology with CNC Machining. Procedia CIRP, 42(Isem XVIII), 81–86. https://doi.org/10.1016/j.procir.2016.02.193	43	Yamazaki Mazak Corporation	Surface evolution	Mechanical	Machining	Alloy 718	Grain size	10	[um], length	-	-	-
						304	Grain size	3	[um], width	-	-	-
Du, W., Bai, Q., & Zhang, B. (2016). A Novel Method for Additive/Subtractive Hybrid Manufacturing of Metallic Parts. Procedia Manufacturing, 5, 1018–1030. https://doi.org/10.1016/j.promfg.2016.08.067	34	Dalian University of Technology	Surface evolution	Mechanical	Machining	Alloy 718	Ultimate tensile strength	931.000	[MPa]	-	-	-
						Alloy 718	Elongation	31.700	[%]	-	-	-
						Alloy 718	Hardness	240.000	[HV]	-	-	-
Wang, Z., Liu, R., Sparks, T., Liu, H., & Liou, F. (2015). Stereo vision based hybrid	10	Missouri University of Science and Technology	Surface evolution	Mechanical	Machining	H13	Porosity	0.800	[%]	-	-	-
						18Ni300	Hardness	650.000	[HV]	-	-	-

(continued on next page)

Table D.1 (continued)

Paper Reference	No. of Citations	Affiliation	Mechanism	Energy Source	Process	Material	Standardized Property	Standardized Quantitative Property	Standardized Units	Property without hybrid	Units	Property, [%] difference
manufacturing process for precision metal parts. Precision Engineering, 42, 1–5 Friel, R. J., & Harris, R. A. (2013). Ultrasonic additive manufacturing A hybrid production process for novel functional products. Procedia CIRP, 6 (1), 35–40. https://doi.org/10.1016/j.procir.2013.03.004	44	Loughborough University	Surface evolution	Acoustic	Ultrasonic welding	Aluminium	Surface roughness	3.250	[Ra], um	–	–	–
Karunakaran, K. P., Suryakumar, S., Pushpa, V., & Akula, S. (2010). Low cost integration of additive and subtractive processes for hybrid layered manufacturing. Robotics and Computer-Integrated	186	Indian Institute of Technology	Surface evolution	Mechanical	Machining	ER70S-6	–	–	–	–	–	–
Liou, F., Slattery, K., Kinsella, M., Newkirk, J., Chou, H. N., & Landers, R. (2007). Applications of a hybrid manufacturing process for fabrication of metallic structures. Rapid Prototyping Journal, 13 (4),	69	University of Missouri	Surface evolution	Mechanical	Machining	Tool Steel	–	–	–	–	–	–
Akula, S., & Karunakaran, K. P. (2006). Hybrid adaptive layer manufacturing: An Intelligent art of direct metal rapid tooling process. Robotics and Computer-Integrated Manufacturing, 22(2), 113–123. https://doi.org/10.1016/j.rcim.2005.02.006	73	Indian Institute of Technology	Surface evolution	Mechanical	Machining	ER70S-6	Porosity	0.000	[%]	–	–	–
Kerschbaumer, M., & Ernst, G. (2004). Hybrid manufacturing process for rapid high performance tooling combining high	14	Joenneum Research Forschungsgesellschaft	Surface evolution	Mechanical	Machining	ER70S-6	Hardness	221.000	[HV]	–	–	–

(continued on next page)

Table D.1 (continued)

Paper Reference	No. of Citations	Affiliation	Mechanism	Energy Source	Process	Material	Standardized Property	Standardized Quantitative Property	Standardized Units	Property without hybrid	Units	Property, [%] difference
speed milling and laser cladding. ICALEO 2004 – 23rd International Liou, F. W., Choi, J., Landers, R. G., Janardhan, V., Balakrishnan, S. N., & Agarwal, S. (2001). Research and development of a hybrid rapid manufacturing process. Proceedings of the Twelfth Annual Solid	51	University of Missouri	Surface evolution	Mechanical	Machining	–	–	–	–	–	–	–
Choi, D. S., Lee, S. H., Shin, B. S., Whang, K. H., Song, Y. A., Park, S. H., & Jee, H. S. (2001). Development of a direct metal freeform fabrication technique using CO ₂ laser welding and milling technology. Journal of Materials Processing Technology, 113(1–3), 273–279. https://doi.org/10.1016/S0924-0136(01)00652-5	74	Korea Institute of Machinery and Materials	Surface evolution	Mechanical	Machining	ER70S-6	Grain size	10.000	[μm]	30	[μm]	–200.0%
Jeng, J. Y., & Lin, M. C. (2001). Mold fabrication and modification using hybrid processes of selective laser cladding and milling. Journal of Materials Processing Technology, 110(1), 98–103	104	National Taiwan University of Science and Technology	Surface evolution	Mechanical	Machining	Fe (72 wt.%), Ni (10 wt.%), and Cr (18 wt. %)	ER70S-6	Ultimate tensile strength	546.230	[MPa]	56	[kg/mm ²]
Karunakaran, K. P., Shanmuganathan, P. V., JadHAV, S. J., Bhaduria, P., & Pandey, A. (2000). Rapid prototyping of metallic parts and moulds.	38	Indian Institute of Technology	Surface evolution	Mechanical	Machining	Fe (72 wt.%), Ni (10 wt.%), and Cr (18 wt. %)	ER70S-6	Elongation	52.000	[%]	30	[%]
							ER70S-6	Hardness	305.800	[HV]	348	[HV], micro-hardness 300gf

Table D.1 (continued)

Paper Reference	No. of Citations	Affiliation	Mechanism	Energy Source	Process	Material	Standardized Property	Standardized Quantitative Property	Standardized Units	Property without hybrid	Units	Property, [%] difference
Journal of Materials Processing Technology, 105(3), Song, Y., Park, S., & Jee, H. (1999). 3D Welding and Milling-A Direct Approach for Fabrication of Injection Molds. Proceedings of the Solid Freeform Fabrication Symposium. University of Texas at Austin, 793–800. http://utwired.engr.utexas.edu/lff/symposium/proceedingsArchive/pubs/Manuscripts/1999/1999-092-Song.pdf	14	Korea Institute of Science and Technology	Surface evolution	Mechanical	Machining	ER70S-6	Ultimate tensile strength	588.400	[MPa]	–	–	–
Yin, S., Yan, X., Jenkins, R., Chen, C., Kazasidis, M., Liu, M., ... Lupoi, R. (2019). Hybrid additive manufacture of 316L stainless steel with cold spray and selective laser melting: Microstructure and mechanical properties. Journal of Materials Processing Technology, 273 (January), 116248. https://doi.org/10.1016/j.jmatprotec.2019.05.029	5	Trinity College Dublin	Stress state	Mechanical	Cold spray	316 L	Hardness	305.000	[HV]	–	–	–
National Engineering Laboratory for Modern Materials Surface Engineering Universite Bourgogne Franche-Comte State Key Laboratory of Advanced Special Steels						316 L	Hardness	291.49	[HV], for Cold spray layer as fabricated	–	–	–
						316 L	Hardness	219.17	[HV], for SLM layer as fabricated	–	–	–
						316 L	Ultimate tensile strength	73	[MPa], cold spray as fabricated	–	–	–
						316 L	Ultimate tensile strength	663	[MPa], SLM as fabricated	–	–	–
						316 L	Elongation	0.27	[%], cold spray as fabricated	–	–	–
						316 L	Elongation	38.21	[%], SLM as fabricated	–	–	–

Table D.1 (continued)

Paper Reference	No. of Citations	Affiliation	Mechanism	Energy Source	Process	Material	Standardized Property	Standardized Quantitative Property	Standardized Units	Property without hybrid	Units	Property, [%] difference
Hirtler, M., Jedynak, A., Sydow, B., Sviridov, A., &Bambach, M. (2020). A study on the mechanical properties of hybrid parts manufactured by forging and wire arc additive manufacturing. Procedia Manufacturing, 47(2019), 1141–1148. https://doi.org/10.1016/j.promfg.2020.04.136	0	Brandenburg University of Technology Cottbus-Senftenberg	Stress state	Mechanical	Forging	AlSi12	Grain size	4.1	[um], after forging	–	–	–
Michl, D., Sydow, B., &Bambach, M. (2020). Ring rolling of pre-forms made by wire-arc additive manufacturing. Procedia Manufacturing, 47(2019), 342–348. https://doi.org/10.1016/j.promfg.2020.04.275	0	SMS group CmbH	Stress state	Mechanical	Ring rolling	ER70S-6	Grain size	16	[um], ring rolled axial direction	–	–	–
Cortina, M., Arrizubieta, J. I., Calleja, A., Ukar, E., &Alberdi, A. (2018). Case study to illustrate the potential of conformal cooling channels for hot stamping dies manufactured using hybrid process of laser metal deposition (LMD) and milling. Metals, 8(2). https://doi.org/10.3390/met8020102	12	University of the Basque Country	Surface evolution	Mechanical	Machining	316 L	Pore size	100	[um]	–	–	–

(continued on next page)

Table D.1 (continued)

Paper Reference	No. of Citations	Affiliation	Mechanism	Energy Source	Process	Material	Standardized Property	Standardized Quantitative Property	Standardized Units	Property without hybrid	Units	Property, [%] difference
Fernandez-Zelaia, P., Nguyen, V., Zhang, H., Kumar, A., & Melkote, S. N. (2019). The effects of material anisotropy on secondary processing of additively manufactured CoCrMo. Additive Manufacturing, 29(June), 100764. https://doi.org/10.1016/j.addma.2019.06.015	2	Innovation-Industrial Systems Unit Georgia Institute of Technology	Surface evolution	Mechanical	Machining	CoCrMo	Young's modulus	235	[GPa], 12 direction	-	-	-
Bambach, M., Sizova, I., Szyndler, J., Bennett, J., Cao, J., Papke, T., & Merklein, M. (2020). On the hot deformation behavior of Ti-6Al-4V made by additive manufacturing. Journal of Materials Processing Technology	0	Bradenburg University of Technology Cottbus-Senftenberg	Stress state	Mechanical	Hot deformation	Titanium Gr 5	Flow stress	90	[MPa], DED	117	[MPa]	27.0%
Todaro, C. J., Easton, M. A., Qiu, D., Zhang, D., Bermingham, M. J., Lui, E. W., ... Qian, M. (2020). Grain structure control during metal 3D printing by high-intensity ultrasound. Nature Communications, 11(1), 1–9. https://doi.org/10.1038/s41467-019-13874-z	16	RMIT University	Melt pool dynamics	Acoustic	Workpiece vibration	Titanium Gr 5	Grain texture	Equiaxed	Columnar			
		The University of Queensland		Mechanical		Titanium Gr 5	Grain size	100	[um]	500	[um]	80.0%
						Titanium Gr 5	Yield strength	1094	[MPa]	980	[MPa]	10.4%
						Titanium Gr 5	Ultimate tensile strength	1137	[MPa]	1015	[MPa]	10.7%

(continued on next page)

Table D.1 (continued)

Paper Reference	No. of Citations	Affiliation	Mechanism	Energy Source	Process	Material	Standardized Property	Standardized Quantitative Property	Standardized Units	Property without hybrid	Units	Property, [%] difference
Dalaee, M., Cheitani, F., Arabi-Hasemi, A., Rohrer, C., Weisse, B., Leinenbach, C., &Wegener, K. (2020). Feasibility study in combined direct metal deposition (DMD) and plasma transfer arc welding (PTA) additive manufacturing. International Journal of Advanced Manufacturing Technology, 106(9–10), 4375–4389. https://doi.org/10.1007/s00170-019-04917-2	1	Institute of Machine Tools &Manufacturing (IWF), ETH Zuerich	Surface evolution	Thermal	Plasma transfer arc welding	415	Surface roughness	9.5	[Ra], um PTA	–	–	–
		Inspire AG				415	Surface roughness	4.5	[Ra], um DMD	–	–	–
		Stellba AG				415	Grain size	1250	[um], PTA	–	–	–
		Empa				415	Hardness	308	[HV], for PTA	–	–	–
						415	Hardness	330	[HV], for DMD	–	–	–
						415	Yield strength	845	[MPa]	–	–	–
						415	Ultimate tensile strength	897	[MPa]	–	–	–
Chen, L., Richter, B., Zhang, X., Ren, X., &Pfefferkorn, F. E. (2020). Modification of surface characteristics and electrochemical corrosion behavior of laser powder bed fused stainless-steel 316L after laser polishing. Additive Manufacturing, 32 (November 2019), 101013. https://doi.org/10.1016/j.addma.2019.101013	1	Jiangsu University	Surface evolution	Thermal	Laser polishing	316 L	Porosity	0.2	[%]	–	–	–
		University of Wisconsin Madison				316 L	Surface roughness	0.49	[Ra], um	4.88	[Ra], um As printed	–895.9%
						316 L	Hardness	278.4	[HV]	185.6	[HV]	33.3%
Liu, Q., Wang, Y., Zheng, H., Tang, K., Ding, L., Li, H., &Gong, S. (2016). Microstructure and mechanical properties of LMD-SLM hybrid forming Ti6Al4V alloy. Materials	27	AVIC Beijing Aeronautical Manufacturing Technology Research Institute	Surface evolution	Thermal	Laser metal deposition	Titanium Gr 5	–	–	–	–	–	–

Table D.1 (continued)

Paper Reference	No. of Citations	Affiliation	Mechanism	Energy Source	Process	Material	Standardized Property	Standardized Quantitative Property	Standardized Units	Property without hybrid	Units	Property, [%] difference
Science and Engineering A, 660, 24–33. https://doi.org/10.1016/j.msea.2016.02.069		Beihang University				Titanium Gr 5	Grain size	200	[um], PBF width	–	–	–
						Titanium Gr 5	Grain size	300	[um], DED width	–	–	–
						Titanium Gr 5	Porosity	0.5	[%]	–	–	–
						Titanium Gr 5	Ultimate tensile strength	950	[MPa]	895	[MPa], forging	5.8%
						Titanium Gr 5	Elongation	17	[%]	–	–	–
						Titanium Gr 5	Hardness	385	[HV], for SLM	325	[HV], for rolled plate	15.6%
						Titanium Gr 5	Hardness	355	[HV], for DMD	325	[HV], for rolled plate	8.5%
Tian, Y., Gora, W. S., Cabo, A. P., Parimi, L. L., Hand, D. P., Tammas-Williams, S., & Prangnell, P. B. (2018). Material interactions in laser polishing powder bed additive manufactured Ti6Al4V components. Additive Manufacturing, 20, 11–22. https://doi.org/10.1016/j.addma.2017.12.010	11	University of Manchester	Surface evolution	Thermal	Laser polishing	Titanium Gr 5	Surface roughness	1.65	[Ra], um	21.46	[Ra], um as deposited	-1200.6%
		Heriot-Watt University GKN Aerospace				Titanium Gr 5	Hardness	469	[HV]	–	–	–
						Titanium Gr 5	Residual stress	350	[MPa]	–	–	–
Schneider, J., Seidel, A., Gumpinger, J., Riede, M., López, E., Brueckner, F., & Leyens, C. (2019). Advanced manufacturing approach via the combination of selective laser melting and laser metal deposition. Journal of Laser Applications, 31 (2), 022317. https://doi.org/10.2351/1.5096123	1	Fraunhofer Institute for Materials and Beam Technology	Surface evolution	Thermal	Laser metal deposition	316 L	Hardness	230	[HV]	–	–	–
		Technische Universitaet Dresden ESA				316 L	Dendrite spacing	0.77	[um], SLM	–	–	–
						316 L	Dendrite spacing	4.45	[um], DED	–	–	–

(continued on next page)

Table D.1 (continued)

Paper Reference	No. of Citations	Affiliation	Mechanism	Energy Source	Process	Material	Standardized Property	Standardized Quantitative Property	Standardized Units	Property without hybrid	Units	Property, [%] difference
		Lulea University of Technology										
Shi, X., Ma, S., Liu, C., Wu, Q., Lu, J., Liu, Y., & Shi, W. (2017). Selective laser melting-wire arc additive manufacturing hybrid fabrication of Ti-6Al-4V alloy: Microstructure and mechanical properties. <i>Materials Science and Engineering A</i> , 684 (December 2016), 196–204. https://doi.org/10.1016/j.msea.2016.12.065	42	Beijing Institute of Technology	Surface evolution	Thermal	Wire arc additive manufacturing	Titanium Gr 5	Grain size	150	[μm], PBF width	–	–	–
						Titanium Gr 5	Grain size	600	[μm], DED width	–	–	–
						Titanium Gr 5	Yield strength	1050	[Mpa]	–	–	–
						Titanium Gr 5	Ultimate tensile strength	1163	[Mpa]	–	–	–
						Titanium Gr 5	Elongation	14.1	[%]	–	–	–
60	Yin, S., Yan, X., Chen, C., Jenkins, R., Liu, M., & Lupoi, R. (2018). Hybrid additive manufacturing of Al-Ti6Al4V functionally graded materials with selective laser melting and cold spraying. <i>Journal of Materials Processing Technology</i> , 255 (November 2017), 650–655. https://doi.org/10.1016/j.jmatprotec.2018.01.015	The University of Dublin	Stress state	Mechanical	Cold spray	Titanium Gr 5	Porosity	0.22	[%]	–	–	–
		Universite-de Technologie Belfort-Montbeliard				Al + Al2O3	Porosity	0.57	[%]	–	–	–
						Titanium Gr 5	Hardness	350	[HV]	325	[HV]	7.1%
						Al + Al2O3	Hardness	50	[HV]	30	[HV]	40.0%

materials in this study are shown in **Table C.1**. The SAE/AISI standard naming practice is used throughout this work for consistency.

Appendix D. Reported data and paper information for metal hybrid-AM

Compiled data for over 100 papers analyzed in this study are shown in Table C.1. Extracted and standardized data includes: paper reference, No. of citations, affiliation(s), mechanism(s), energy source(s), process, material, standardized property, property without hybrid (if reported), and the percent difference between the hybrid and AM-only property (if applicable). If a paper did not report any standardized properties, the process type is still recorded and included in the analysis of the distribution of mechanism and energy source types.

For further reference, both the standardized and the non-standardized data extracted from papers (including author notes on papers) can be found at the following link: <https://docs.google.com/spreadsheets/d/18xHKnwyjvdPG95m6TZ9UI5Emll98dt2enUae44o3U6M/edit?usp=sharing>.

The best way to use **Table D.1** is interactively through the google link. Data can be filtered by any category for quick exploration.

Appendix E. Average values of reported mechanical properties for 316 L, alloy 718, and Titanium Gr 5

Table E.1

Table E.1

Mechanical properties reported for each mechanism for the three most investigated materials. Averages were calculated for each property if it was reported in more than one paper for any given mechanism.

Material	Property	Mechanism	Values	Average	Std. dev	
316 L	Hardness	Melt pool dynamics	622		622	0
		Melt pool dynamics	299		299	0
		Surface evolution	479	245	362	117
		Melt pool dynamics	219		219	0
		Thermal gradients	230		230	0
	Elongation	Microstructure developments	214		214	0
		Stress state	322	291	219	278
		Surface evolution	251	639	278	230
		Melt pool dynamics	34		34	0
		Stress state	0	38	19	19
		Surface evolution	50		50	0
Alloy 718	Ultimate tensile strength	Melt pool dynamics	1072		1072	0
		Stress state	958		958	0
		Surface evolution	931		931	0
		Stress state	750		750	0
		Surface evolution	587		587	0
	Yield strength	Melt pool dynamics	328		328	0
		Surface evolution	400	240	320	80
		Melt pool dynamics	32		32	0
		Stress state	17		17	0
		Surface evolution	32		32	0
Titanium Gr 5	Ultimate tensile strength	Melt pool dynamics	1137		1137	0
		Thermal gradients	1590		1590	0
		Microstructure developments	929	944	937	8
		Stress state	1059	1075	1067	8
		Surface evolution	1128	950	1163	1080
	Yield strength	Melt pool dynamics	1094		1094	0
		Thermal gradients	1466		1466	0
		Microstructure developments	835	840	838	3
		Stress state	990		990	0
		Surface evolution	1050		1050	0
	Hardness	Thermal gradients	401		401	0
		Microstructure developments	400		400	0
		Stress state	400	377	350	376
		Surface evolution	400	385	355	469
		Microstructure developments	13	13	13	0
	Elongation	Stress state	8	13	10	2
		Surface evolution	17	14	16	1

Appendix F. Supplementary data

Supplementary data associated with this article can be found, in the online version, at <https://doi.org/10.1016/j.jmatprotec.2021.117048>.

References

- Ahmad, N., Enemuoh, E.U., 2020. Energy modeling and eco impact evaluation in direct metal laser sintering hybrid milling. *Heliyon* 6, e03168. <https://doi.org/10.1016/j.heliyon.2020.e03168>.
- Akula, S., Karunakaran, K.P., 2006. Hybrid adaptive layer manufacturing: an intelligent art of direct metal rapid tooling process. *Robot. Comput.-Integr. Manuf.* 22, 113–123. <https://doi.org/10.1016/j.rcim.2005.02.006>.
- Al-Milaji, K.N., Gupta, S., Pecharsky, V.K., Barua, R., Zhao, H., Hadimani, R.L., 2020. Differential effect of magnetic alignment on additive manufacturing of magnetocaloric particles. *AIP Adv.* 10. <https://doi.org/10.1063/1.5130028>.
- Ambrogio, G., Gagliardi, F., Muzzupappa, M., Filice, L., 2019. Additive-incremental forming hybrid manufacturing technique to improve customised part performance. *J. Manuf. Process.* 37, 386–391. <https://doi.org/10.1016/j.jmapro.2018.12.008>.
- Bambach, M., Sizova, I., Sznydler, J., Bennett, J., Cao, J., Papke, T., Merklein, M., 2020. On the hot deformation behavior of Ti-6Al-4V made by additive manufacturing. *J. Mater. Process. Technol.*
- Bennett, J.L., Wolff, S.J., Hyatt, G., Ehmann, K., Cao, J., 2017. Thermal effect on clad dimension for laser deposited Inconel 718. *J. Manuf. Process.* 28, 550–557. <https://doi.org/10.1016/j.jmapro.2017.04.024>.
- Book, T.A., Sangid, M.D., 2016. Evaluation of select surface processing techniques for in situ application during the additive manufacturing build process. *JOM* 68, 1780–1792. <https://doi.org/10.1007/s11837-016-1897-y>.
- Bouet, G., Cabanettes, F., Bidron, G., Guignandon, A., Peyroche, S., Bertrand, P., Vico, L., Dumas, V., 2019. Laser-based hybrid manufacturing of endosteous implants: optimized titanium surfaces for enhancing osteogenic differentiation of human mesenchymal stem cells. *ACS Biomater. Sci. Eng.* 5, 4376–4385. <https://doi.org/10.1021/acsbiomaterials.9b00769>.

- Brown, D., Li, C., Liu, Z.Y., Fang, X.Y., Guo, Y.B., 2018. Surface integrity of Inconel 718 by hybrid selective laser melting and milling. *Virtual Phys. Prototyp.* 13, 26–31. <https://doi.org/10.1080/17452759.2017.1392681>.
- Casati, R., Nasab, M.H., Coduri, M., Tirelli, V., Vedani, M., 2018. Effects of platform pre-heating and thermal-treatment strategies on properties of alsi10mg alloy processed by selective laser melting. *Metals* 8, 954. <https://doi.org/10.3390/met8110954>.
- Chen, S., Tong, Y., Liaw, P.K., 2018. Additive manufacturing of high-entropy alloys: a review. *Entropy* 20. <https://doi.org/10.3390/e20120937>.
- Chen, X.h., Chen, B., Cheng, X., Li, G.C., Huang, Z., 2020. Microstructure and properties of hybrid additive manufacturing 316L component by directed energy deposition and laser remelting. *J. Iron Steel Res. Int.* <https://doi.org/10.1007/s42243-020-00396-y>.
- Choi, D.S., Lee, S.H., Shin, B.S., Whang, K.H., Song, Y.A., Park, S.H., Jee, H.S., 2001. Development of a direct metal freeform fabrication technique using CO₂ laser welding and milling technology. *J. Mater. Process. Technol.* 113, 273–279. [https://doi.org/10.1016/S0924-0136\(01\)00652-5](https://doi.org/10.1016/S0924-0136(01)00652-5).
- Chong, L., Ramakrishna, S., Singh, S., 2018. A review of digital manufacturing-based hybrid additive manufacturing processes. *Int. J. Adv. Manuf. Technol.* 95, 2281–2300. <https://doi.org/10.1007/s00170-017-1345-3>.
- Chu, W.S., Kim, C.S., Lee, H.T., Choi, J.O., Park, J.I., Song, J.H., Jang, K.H., Ahn, S.H., 2014. Hybrid manufacturing in micro/nano scale: a review. *Int. J. Precis. Eng. Manuf. – Green Technol.* 1, 75–92. <https://doi.org/10.1007/s40684-014-0012-5>.
- Cockroft, M., Latham, D., 1968. Ductility and the workability of metals. *J. Inst. Metals* 96, 33–39.
- Colegrove, P.A., Coules, H.E., Fairman, J., Martina, F., Kashoob, T., Mamash, H., Cozzolino, L.D., 2013. Microstructure and residual stress improvement in wire and arc additively manufactured parts through high-pressure rolling. *J. Mater. Process. Technol.* 213, 1782–1791. <https://doi.org/10.1016/j.jmatprotec.2013.04.012>.
- Corradi, D.R., Bracarense, A.Q., Wu, B., Cuiuri, D., Pan, Z., Li, H., 2020. Effect of magnetic arc oscillation on the geometry of single-pass multi-layer walls and the process stability in wire and arc additive manufacturing. *J. Mater. Process. Technol.* 283, 116723. <https://doi.org/10.1016/j.jmatprotec.2020.116723>.
- Cortina, M., Arrizubieta, J.I., Calleja, A., Ukar, E., Alberdi, A., 2018a. Case study to illustrate the potential of conformal cooling channels for hot stamping dies manufactured using hybrid process of laser metal deposition (LMD) and milling. *Metals* 8. <https://doi.org/10.3390/met8020102>.
- Cortina, M., Arrizubieta, J.I., Ruiz, J.E., Ukar, E., Lamikiz, A., 2018b. Latest developments in industrial hybrid machine tools that combine additive and subtractive operations. *Materials* 11. <https://doi.org/10.3390/ma11122583>.
- Dalaee, M., Cheaitani, F., Arabi-Hashemi, A., Rohrer, C., Weisse, B., Leinenbach, C., Wegener, K., 2020. Feasibility study in combined direct metal deposition (DMD) and plasma transfer arc welding (PTA) additive manufacturing. *Int. J. Adv. Manuf. Technol.* 106, 4375–4389. <https://doi.org/10.1007/s00170-019-04917-2>.
- Dass, A., Moridi, A., 2019. State of the art in directed energy deposition: from additive manufacturing to materials design. *Coatings* 9, 1–26. <https://doi.org/10.3390/COATINGS9070418>.
- Debroy, T., Wei, H.L., Zuback, J.S., Mukherjee, T., Elmer, J.W., Milewski, J.O., Beese, A.M., Wilson-heid, A., De, A., Zhang, W., 2018. Progress in materials science additive manufacturing of metallic components – process, structure and properties. *Prog. Mater. Sci.* 92, 112–224. <https://doi.org/10.1016/j.pmatsci.2017.10.001>.
- Demir, A.G., Previtali, B., 2017. Investigation of remelting and preheating in SLM of 18Ni300 maraging steel as corrective and preventive measures for porosity reduction. *Int. J. Adv. Manuf. Technol.* 93, 2697–2709. <https://doi.org/10.1007/s00170-017-0697-z>.
- Donoghue, J., Antonymsamy, A.A., Martina, F., Colegrove, P.A., Williams, S.W., Prangnell, P.B., 2016. The effectiveness of combining rolling deformation with wire-arc additive manufacture on β -grain refinement and texture modification in Ti-6Al-4V. *Mater. Charact.* 114, 103–114. <https://doi.org/10.1016/j.matchar.2016.02.001>.
- Du, D., Dong, A., Shu, D., Wang, D., Zhu, G., Sun, B., Lavernia, E.J., 2020. Influence of static magnetic field on the microstructure of Nickel-based superalloy by laser-directed energy deposition. *Metall. Mater. Trans. A: Phys. Metall. Mater. Sci.* 51, 3354–3359. <https://doi.org/10.1007/s11661-020-05783-4>.
- Du, D., Haley, J.C., Dong, A., Faurelle, Y., Shu, D., Zhu, G., Li, X., Sun, B., Lavernia, E.J., 2019. Influence of static magnetic field on microstructure and mechanical behavior of selective laser melted AlSi10Mg alloy. *Mater. Des.* 181. <https://doi.org/10.1016/j.matdes.2019.107923>.
- Du, W., Bai, Q., Zhang, B., 2016. A novel method for additive/subtractive hybrid manufacturing of metallic parts. *Proc. Manuf.* 5, 1018–1030. <https://doi.org/10.1016/j.promfg.2016.08.067>.
- Emmens, W.C., Sebastiani, G., van den Boogaard, A.H., 2010. The technology of incremental sheet forming—a brief review of the history. *J. Mater. Process. Technol.* 210, 981–997. <https://doi.org/10.1016/j.jmatprotec.2010.02.014>.
- Fernandez-Zelaia, P., Nguyen, V., Zhang, H., Kumar, A., Melkote, S.N., 2019. The effects of material anisotropy on secondary processing of additively manufactured CoCrMo. *Addit. Manuf.* 29, 100764. <https://doi.org/10.1016/j.addma.2019.06.015>.
- Flynn, J.M., Shokrani, A., Newman, S.T., Dhokia, V., 2016. Hybrid additive and subtractive machine tools – research and industrial developments. *Int. J. Mach. Tools Manuf.* 101, 79–101. <https://doi.org/10.1016/j.ijmachtools.2015.11.007>.
- Friel, R.J., Harris, R.A., 2013. Ultrasonic additive manufacturing a hybrid production process for novel functional products. *Procedia CIRP* 6, 35–40. <https://doi.org/10.1016/j.procir.2013.03.004>.
- Gong, M., Meng, Y., Zhang, S., Zhang, Y., Zeng, X., Gao, M., 2020. Laser-arc hybrid additive manufacturing of stainless steel with beam oscillation. *Addit. Manuf.* 33, 101180. <https://doi.org/10.1016/j.addma.2020.101180>.
- Gou, J., Wang, Z., Hu, S., Shen, J., Tian, Y., Zhao, G., Chen, Y., 2020. Effects of ultrasonic peening treatment in three directions on grain refinement and anisotropy of cold metal transfer additive manufactured Ti-6Al-4V thin wall structure. *J. Manuf. Process.* 54, 148–157. <https://doi.org/10.1016/j.jmapro.2020.03.010>.
- Griffiths, S., Rossell, M.D., Croteau, J., Vo, N.Q., Dunand, D.C., Leinenbach, C., 2018. Effect of laser rescanning on the grain microstructure of a selective laser melted Al-Mg-Zr alloy. *Mater. Charact.* 143, 34–42. <https://doi.org/10.1016/j.matchar.2018.03.033>.
- Gu, D.D., Meiners, W., Wissenbach, K., Poprawe, R., 2012. Laser additive manufacturing of metallic components: materials, processes and mechanisms. *Int. Mater. Rev.* 57, 133–164. <https://doi.org/10.1179/1743280411Y.0000000014>.
- Gu, J., Yang, S., Gao, M., Bai, J., Zhai, Y., Ding, J., 2020. Micropore evolution in additively manufactured aluminum alloys under heat treatment and inter-layer rolling. *Mater. Des.* 186, 108288. <https://doi.org/10.1016/j.matedes.2019.108288>.
- Guan, R.G., Tie, D., 2017. A Review on Grain Refinement of Aluminum Alloys: Progresses, Challenges and Prospects. <https://doi.org/10.1007/s40195-017-0565-8>.
- Gustmann, T., Schwab, H., Kühn, U., Pauly, S., 2018. Selective laser remelting of an additively manufactured Cu-Al-Ni-Mn shape-memory alloy. *Mater. Des.* 153, 129–138. <https://doi.org/10.1016/j.matedes.2018.05.010>.
- Hackel, L., Rankin, J.R., Rubenchik, A., King, W.E., Matthews, M., 2018. Laser peening: a tool for additive manufacturing post-processing. *Addit. Manuf.* 24, 67–75. <https://doi.org/10.1016/j.addma.2018.09.013>.
- Hackenhaar, W., Mazzaferra, J.A., Montevechi, F., Campatelli, G., 2020. An experimental-numerical study of active cooling in wire arc additive manufacturing. *J. Manuf. Process.* 52, 58–65. <https://doi.org/10.1016/j.jmapro.2020.01.051>.
- Häfele, T., Schneberger, J.H., Kaspar, J., Vielhaber, M., Griebsch, J., 2019. Hybrid additive manufacturing – Process chain correlations and impacts. *Proc. CIRP* 84, 328–334. <https://doi.org/10.1016/j.cirproc.2019.04.220>.
- Heeling, T., Wegener, K., 2018. The effect of multi-beam strategies on selective laser melting of stainless steel 316L. *Addit. Manuf.* 22, 334–342. <https://doi.org/10.1016/j.addma.2018.05.026>.
- Heigel, J.C., Phan, T.Q., Fox, J.C., Gnaupel-Herold, T.H., 2018. Experimental investigation of residual stress and its impact on machining in hybrid additive/subtractive manufacturing. *Proc. Manuf.* 26, 929–940. <https://doi.org/10.1016/j.promfg.2018.07.120>.
- Hill, R., 1952. On discontinuous plastic states, with special reference to localized necking in thin sheets. *J. Mech. Phys. Solids* 1, 19–30. [https://doi.org/10.1016/0022-5096\(52\)90003-3](https://doi.org/10.1016/0022-5096(52)90003-3).
- Hirtler, M., Jedynak, A., Sydow, B., Sviridov, A., Bambach, M., 2020. A study on the mechanical properties of hybrid parts manufactured by forging and wire arc additive manufacturing. *Proc. Manuf.* 47, 1141–1148. <https://doi.org/10.1016/j.promfg.2020.04.136>.
- Huang, K., Logé, R.E., 2016. A review of dynamic recrystallization phenomena in metallic materials. *Mater. Des.* 111, 548–574. <https://doi.org/10.1016/j.matedes.2016.09.012>.
- Huber, F., Papke, T., Kerkien, M., Tost, F., Geyer, G., Merklein, M., Schmidt, M., 2019. Customized exposure strategies for manufacturing hybrid parts by combining laser beam melting and sheet metal forming. *J. Laser Appl.* 31, 022318. <https://doi.org/10.2351/1.15096115>.
- Jeng, J.Y., Lin, M.C., 2001. Mold fabrication and modification using hybrid processes of selective laser cladding and milling. *J. Mater. Process. Technol.* 110, 98–103. [https://doi.org/10.1016/S0924-0136\(00\)00850-5](https://doi.org/10.1016/S0924-0136(00)00850-5).
- Kalentics, N., de Sejas, M.O.V., Griffiths, S., Leinenbach, C., Logé, R.E., 2020. 3D laser shock peening – a new method for improving fatigue properties of selective laser melted parts. *Addit. Manuf.* 33, 101112. <https://doi.org/10.1016/j.addma.2020.101112>.
- Kang, N., Coddet, P., Wang, J., Yuan, H., Ren, Z., Liao, H., Coddet, C., 2017. A novel approach to in-situ produce functionally graded silicon matrix composite materials by selective laser melting. *Compos. Struct.* 172, 251–258. <https://doi.org/10.1016/j.compositesstruct.2017.03.096>.
- Kao, A., Gan, T., Tonry, C., Krastins, I., Pericleous, K., 2020. Thermoelectric magnetohydrodynamic control of melt pool dynamics and microstructure evolution in additive manufacturing. *Philos. Trans. R. Soc. A: Math. Phys. Eng. Sci.* 378. <https://doi.org/10.1098/rsta.2019.0249>.
- Karakulak, E., 2019. A Review: Past, Present and Future of Grain Refining of Magnesium Castings. <https://doi.org/10.1016/j.jma.2019.05.001>.
- Kerschbaumer, M., Ernst, G., 2004. Hybrid manufacturing process for rapid high performance tooling combining high speed milling and laser cladding. *ICALEO 2004–23rd International Congress on Applications of Laser and Electro-Optics Congress Proceedings* 1710. <https://doi.org/10.2351/1.5060234>.
- Khairallah, S.A., Anderson, A.T., Rubenchik, A., King, W.E., 2016. Laser powder-bed fusion additive manufacturing: physics of complex melt flow and formation mechanisms of pores, spatter, and denudation zones. *Acta Mater.* 108, 36–45. <https://doi.org/10.1016/j.actamat.2016.02.014>.
- Kirk, M.M., Lee, Y., Greeley, D.A., Okello, A., Goin, M.J., Pearce, M.T., Dehoff, R.R., 2017. Strategy for texture management in metals additive manufacturing. *JOM* 69, 523–531. <https://doi.org/10.1007/s11837-017-2264-3>.
- Koike, R., Misawa, T., Aoyama, T., Kondo, M., 2018. Controlling metal structure with remelting process in direct energy deposition of Inconel 625. *CIRP Ann.* 67, 237–240. <https://doi.org/10.1016/j.cirp.2018.04.061>.
- Kou, S., 2002. Welding Metallurgy, vol. 4. John Wiley & Sons, Inc, Hoboken, NJ, USA. <https://doi.org/10.1002/0471434027>. <http://www.i-scholar.in/index.php/IWJ/article/view/150243>.
- Kulkarni, P., Dutta, D., 2000. On the integration of layered manufacturing and material removal processes. *J. Manuf. Sci. Eng., Trans. ASME* 122, 100–108. <https://doi.org/10.1115/1.538891>.

- Lamikiz, A., Sánchez, J.A., López de Lacalle, L.N., Arana, J.L., 2007. Laser polishing of parts built up by selective laser sintering. *Int. J. Mach. Tools Manuf.* 47, 2040–2050. <https://doi.org/10.1016/j.ijmachtools.2007.01.013>.
- Lauwers, B., Klocke, F., Klink, A., Tekkaya, A.E., Neugebauer, R., McIntosh, D., 2014. Hybrid processes in manufacturing. *CIRP Ann. – Manuf. Technol.* 63, 561–583. <https://doi.org/10.1016/j.cirp.2014.05.003>.
- Li, Z., Liu, C., Xu, T., Ji, L., Wang, D., Lu, J., Ma, S., Fan, H., 2019. Reducing arc heat input and obtaining equiaxed grains by hot-wire method during arc additive manufacturing titanium alloy. *Mater. Sci. Eng. A* 742, 287–294. <https://doi.org/10.1016/j.msea.2018.11.022>.
- Lin, D., Motlag, M., Saei, M., Jin, S., Rahimi, R.M., Bahr, D., Cheng, G.J., 2018. Shock engineering the additive manufactured graphene-metal nanocomposite with high density nanotwins and dislocations for ultra-stable mechanical properties. *Acta Mater.* 150, 360–372. <https://doi.org/10.1016/j.actamat.2018.03.013>.
- Liou, F., Slattery, K., Kinsella, M., Newkirk, J., Chou, H.N., Landers, R., 2007. Applications of a hybrid manufacturing process for fabrication of metallic structures. *Rapid Prototyp. J.* 13, 236–244. <https://doi.org/10.1108/13552540710776188>.
- Liu, B., Li, B.Q., Li, Z., 2019. Selective laser remelting of an additive layer manufacturing process on AlSi10Mg. *Results Phys.* 12, 982–988. <https://doi.org/10.1016/j.rinp.2018.12.018>.
- Liu, F., Cheng, H., Yu, X., Yang, G., Huang, C., Lin, X., Chen, J., 2018. Control of microstructure and mechanical properties of laser solid formed Inconel 718 superalloy by electromechanical stirring. *Optics Laser Technol.* 99, 342–350. <https://doi.org/10.1016/j.optlastec.2017.09.022>.
- Lu, Y., Sun, G., Wang, Z., Zhang, Y., Su, B., Feng, A., Ni, Z., 2019. Effects of electromagnetic field on the laser direct metal deposition of austenitic stainless steel. *Optics Laser Technol.* 119, 1–9. <https://doi.org/10.1016/j.optlastec.2019.105586>.
- Madireddy, G., Li, C., Liu, J., Sealy, M.P., 2019. Modeling thermal and mechanical cancellation of residual stress from hybrid additive manufacturing by laser peening. *Nanni Jishu yu Jingmi Gongcheng/Nanotechnol. Precis. Eng.* 2, 49–60. <https://doi.org/10.1016/j.npe.2019.07.001>.
- Manogharan, G., Wysk, R.A., Harrysson, O.L., 2016. Additive manufacturing-integrated hybrid manufacturing and subtractive processes: economic model and analysis. *Int. J. Comput. Integr. Manuf.* 29, 473–488. <https://doi.org/10.1080/0951192X.2015.1067920>.
- Martina, F., Colegrove, P.A., Williams, S.W., Meyer, J., 2015. Microstructure of interpass rolled wire + arc additive manufacturing Ti-6Al-4V components. *Metall. Mater. Trans. A: Phys. Metall. Mater. Sci.* 46, 6103–6118. <https://doi.org/10.1007/s11661-015-3172-1>.
- Martina, F., Colgrove, P., Roy, M., Williams, S., 2014. Residual stress reduction in high pressure interpass rolled wire+arc additive manufacturing Ti-6Al-4V components. *Solid Freeform Fabr. Proc.* 89–94.
- Martina, F., Roy, M.J., Szost, B.A., Terzi, S., Colegrove, P.A., Williams, S.W., Withers, P.J., Meyer, J., Hofmann, M., 2016. Residual stress of as-deposited and rolled wire+arc additive manufacturing Ti-6Al-4V components. *Mater. Sci. Technol. (U. K.)* 32, 1439–1448. <https://doi.org/10.1080/02670836.2016.1142704>.
- Martina, F., Williams, S.W., Colegrove, P., 2013. Improved microstructure and increased mechanical properties of additive manufacture produced Ti-6Al-4V by interpass cold rolling. *24th International SFF Symposium – An Additive Manufacturing Conference, SFF 2013* 490–496.
- Meiners, F., Ihne, J., Jürgens, P., Hemes, S., Mathes, M., Sizova, I., Bambach, M., Hamasaleh, R., Weisheit, A., 2020. New hybrid manufacturing routes combining forging and additive manufacturing to efficiently produce high performance components from Ti-6Al-4V. *Proc. Manuf.* 47, 261–267. <https://doi.org/10.1016/j.promfg.2020.04.215>.
- Merklein, M., Junker, D., Schaub, A., Neubauer, F., 2016. Hybrid additive manufacturing technologies – an analysis regarding potentials and applications. *Phys. Proc.* 83, 549–559. <https://doi.org/10.1016/j.phpro.2016.08.057>.
- Michl, D., Sydow, B., Bambach, M., 2020. Ring rolling of pre-forms made by wire-arc additive manufacturing. *Proc. Manuf.* 47, 342–348. <https://doi.org/10.1016/j.promfg.2020.04.275>.
- Moritz, J., Seidel, A., Kopper, M., Bretschneider, J., Gumpinger, J., Finaske, T., Riede, M., Schneeweiss, M., López, E., Brückner, F., Leyens, C., Rohr, T., Ghidini, T., 2020. Hybrid manufacturing of titanium Ti-6Al-4V combining laser metal deposition and cryogenic milling. *Int. J. Adv. Manuf. Technol.* 107, 2995–3009. <https://doi.org/10.1007/s00170-020-05212-1>.
- Näström, J., Brückner, F., Kaplan, A.F., 2019. Measuring the effects of a laser beam on melt pool fluctuation in arc additive manufacturing. *Rapid Prototyp. J.* 25, 488–495. <https://doi.org/10.1108/RPJ-01-2018-0033>.
- Ndi-Agbor, E., Cao, J., Ehmann, K., 2018. Towards smart manufacturing process selection in Cyber-Physical Systems. *Manuf. Lett.* 17, 1–5. <https://doi.org/10.1016/j.mflet.2018.03.002>.
- Nie, J., Chen, C., Shuai, S., Liu, X., Zhao, R., Wang, J., Liao, H., Ren, Z., 2020. Effect of static magnetic field on the evolution of residual stress and microstructure of laser remelted Inconel 718 superalloy. *J. Therm. Spray Technol.* <https://doi.org/10.1007/s11666-020-01039-0>.
- Nowotny, S., Brueckner, F., Thieme, S., Leyens, C., Beyer, E., 2015. High-performance laser cladding with combined energy sources. *J. Laser Appl.* 27, S17001. <https://doi.org/10.2351/1.4817455>.
- Olson, G., 1997. Computational design of hierarchically structured materials. *Science* 277, 1237–1242.
- Pantlejev, L., Koutný, D., Paloušek, D., Kaiser, J., 2017. Mechanical and microstructural properties of 2618 Al-alloy processed by SLM remelting strategy. *Mater. Sci. Forum* 891, 343–349. <https://doi.org/10.4028/www.scientific.net/MSF.891.343>.
- Parimi, L.L., Ravi, G., Clark, D., Attallah, M.M., 2014. Microstructural and texture development in direct laser fabricated IN718. *Mater. Charact.* 89, 102–111. <https://doi.org/10.1016/j.matchar.2013.12.012>.
- du Plessis, A., Sperling, P., Beerlink, A., Tshabalala, L., Hoosain, S., Mathe, N., le Roux, S.G., 2018. Standard method for microCT-based additive manufacturing quality control 1: porosity analysis. *MethodsX* 5, 1102–1110. <https://doi.org/10.1016/j.mex.2018.09.005>.
- Pragana, J.P., Cristina, V.A., Bragança, I.M., Silva, C.M., Martins, P.A., 2020. Integration of forming operations on hybrid additive manufacturing systems based on fusion welding. *Int. J. Precis. Eng. – Green Technol.* 7, 595–607. <https://doi.org/10.1007/s40684-019-00152-y>.
- Roehling, J.D., Smith, W.L., Roehling, T.T., Vrancken, B., Guss, G.M., McKeown, J.T., Hill, M.R., Matthews, M.J., 2019. Reducing residual stress by selective large-area diode surface heating during laser powder bed fusion additive manufacturing. *Addit. Manuf.* 28, 228–235. <https://doi.org/10.1016/j.addma.2019.05.009>.
- Safronov, V.A., Khmyrov, R.S., Kotoban, D.V., Gusarov, A.V., 2017. Distortions and residual stresses at layer-by-layer additive manufacturing by fusion. *J. Manuf. Sci. Eng. Trans. ASME* 139, 3–8. <https://doi.org/10.1115/1.4034714>.
- Schirra, J.J., Caless, R.H., Hatala, R.W., 2020. The Effect Of Laves Phase On The Mechanical Properties Of Wrought And Cast + Hip Inconel 718. Technical Report.
- Sealy, M.P., Madireddy, G., Li, C., Guo, Y.B., 2016. Finite element modeling of hybrid additive manufacturing by laser shock peening. *Solid Freeform Fabrication 2016: Proceedings of the 27th Annual International Solid Freeform Fabrication Symposium – An Additive Manufacturing Conference, SFF 2016* 306–316.
- Sealy, M.P., Madireddy, G., Williams, R.E., Rao, P., Toursangasarak, M., 2018. Hybrid processes in additive manufacturing. *J. Manuf. Sci. Eng., Trans. ASME* 140. <https://doi.org/10.1115/1.4038644>.
- Seidel, A., Finaske, T., Straubel, A., Wendrock, H., Maiwald, T., Riede, M., Lopez, E., Brueckner, F., Leyens, C., 2018. Additive manufacturing of powdery Ni-based superalloys Mar-M-247 and CM 247 LC in hybrid laser metal deposition. *Mater. Mater. Trans. A: Phys. Metall. Mater. Sci.* 49, 3812–3830. <https://doi.org/10.1007/s11661-018-4777-y>.
- Seow, C.E., Coules, H.E., Wu, G., Khan, R.H., Xu, X., Williams, S., 2019. Wire+?Arc additively manufactured Inconel 718: effect of post-deposition heat treatments on microstructure and tensile properties. *Mater. Des.* 183, 108157. <https://doi.org/10.1016/j.matdes.2019.108157>.
- Shchitsyn, Y.D., Krivonosova, E.A., Trushnikov, D.N., Ol'shanskaya, T.V., Kartashov, M.F., Neulybin, S.D., 2020. Use of CMT-surfacing for additive formation of Titanium alloy workpieces. *Metallurgist* 64, 63–68. <https://doi.org/10.1007/s11015-020-00967-0>.
- Song, Y., Park, S., Jee, H., 1999. 3D welding and milling-a direct approach for fabrication of injection molds. In: *Proceedings of the Solid Freeform Fabrication Symposium*. University of Texas at Austin, pp. 793–800. In: <http://utwired.engr.utexas.edu/lff/symposium/proceedingsArchive/pubs/Manuscripts/1999/1999-092-Song.pdf>.
- Strong, D., Kay, M., Conner, B., Wakefield, T., Manogharan, G., 2018. Hybrid manufacturing – integrating traditional manufacturers with additive manufacturing (AM) supply chain. *Addit. Manuf.* 21, 159–173. <https://doi.org/10.1016/j.addma.2018.03.010>.
- Strong, D., Kay, M., Conner, B., Wakefield, T., Manogharan, G., 2019. Hybrid manufacturing-Locating AM hubs using a two-stage facility location approach. *Addit. Manuf.* 25, 469–476. <https://doi.org/10.1016/j.addma.2018.11.027>.
- Strong, D., Sirichakwal, I., Manogharan, G.P., Wakefield, T., 2017. Current state and potential of additive – hybrid manufacturing for metal parts. *Rapid Prototyp. J.* 23, 577–588. <https://doi.org/10.1108/RPJ-04-2016-0065>.
- Todaro, C.J., Easton, M.A., Qiu, D., Zhang, D., Birmingham, M.J., Lui, E.W., Brandt, M., StJohn, D.H., Qian, M., 2020. Grain structure control during metal 3D printing by high-intensity ultrasound. *Nat. Commun.* 11, 1–9. <https://doi.org/10.1038/s41467-019-13874-z>.
- Vaithilingam, J., Goodridge, R.D., Hague, R.J., Christie, S.D., Edmondson, S., 2016. The effect of laser remelting on the surface chemistry of Ti6Al4V components fabricated by selective laser melting. *J. Mater. Process. Technol.* 232, 1–8. <https://doi.org/10.1016/j.matchar.2016.01.022>.
- Wang, Y., Shi, J., 2019. Texture control of Inconel 718 superalloy in laser additive manufacturing by an external magnetic field. *J. Mater. Sci.* 54, 9809–9823. <https://doi.org/10.1007/s10853-019-03569-7>.
- Wang, Y., Shi, J., 2020. Recrystallization behavior and tensile properties of laser metal deposited Inconel 718 upon in-situ ultrasonic impact peening and heat treatment. *Mater. Sci. Eng. A* 786, 139434. <https://doi.org/10.1016/j.msea.2020.139434>.
- Wang, Z., Liu, R., Sparks, T., Liu, H., Liou, F., 2015. Stereo vision based hybrid manufacturing process for precision metal parts. *Precis. Eng.* 42, 1–5. <https://doi.org/10.1016/j.precisioneng.2014.11.012>.
- Webster, S., Ehmann, K., Cao, J., 2020. Energy density comparison via highspeed, in-situ imaging of cirected energy deposition. *Proc. Manuf.* 48, 691–696. <https://doi.org/10.1016/j.promfg.2020.05.101>.
- Webster, S., Wolff, S., Bennett, J., Sun, T., Cao, J., Ehmann, K., 2019. Porosity formation and meltpool geometry analysis using high-speed, in situ imaging of directed energy deposition. *Microsc. Microanal.* 25, 2556–2557. <https://doi.org/10.1017/s1431927619013515>.
- Weertman, J., 1966. Rate of growth of fatigue cracks calculated from theory of infinitesimal dislocations distributed on a plane. *Int. J. Fract. Mech.* 2, 460–467.
- Wippermann, A., Gutowski, T.G., Denkena, B., Dittrich, M.A., Wessarges, Y., 2020. Electrical energy and material efficiency analysis of machining, additive and hybrid manufacturing. *J. Clean. Prod.* 251, 119731. <https://doi.org/10.1016/j.jclepro.2019.119731>.

- Woo, W.S., Kim, E.J., Jeong, H.I., Lee, C.M., 2020. Laser-assisted machining of Ti-6Al-4V fabricated by DED additive manufacturing. *Int. J. Precis. Eng. Manuf. – Green Technol.* 7, 559–572. <https://doi.org/10.1007/s40684-020-00221-7>.
- Wu, D., Liu, D., Niu, F., Miao, Q., Zhao, K., Tang, B., Bi, G., Ma, G., 2020. Al-Cu alloy fabricated by novel laser-tungsten inert gas hybrid additive manufacturing. *Addit. Manuf.* 32, 100954. <https://doi.org/10.1016/j.addma.2019.100954>.
- Xiao, Z., Chen, C., Hu, Z., Zhu, H., Zeng, X., 2020. Effect of rescanning cycles on the characteristics of selective laser melting of Ti6Al4V. *Optics Laser Technol.* 122, 105890. <https://doi.org/10.1016/j.optlastec.2019.105890>.
- Xie, Y., Zhang, H., Wang, G., Zhou, F., 2014. A novel metamorphic mechanism for efficient additive manufacturing of components with variable wall thickness. In: Solid Freeform Fabrication Symposium (SFF). Austin, TX, Aug, pp. 210–223. <http://sffsymposium.engr.utexas.edu/sites/default/files/2014-019-Xie.pdf>.
- Xie, Y., Zhang, H., Zhou, F., 2016. Improvement in geometrical accuracy and mechanical property for arc-based additive manufacturing using metamorphic rolling mechanism. *J. Manuf. Sci. Eng., Trans. ASME* 138, 1–8. <https://doi.org/10.1115/1.4032079>.
- Xiong, Z., Zhang, P., Tan, C., Dong, D., Ma, W., Yu, K., 2020. Selective laser melting and remelting of pure tungsten. *Adv. Eng. Mater.* 22. <https://doi.org/10.1002/adem.201901352>.
- Xue, L., 2007. Damage accumulation and fracture initiation in uncracked ductile solids subject to triaxial loading. *Int. J. Solids Struct.* 44, 5163–5181. <https://doi.org/10.1016/j.ijsolstr.2006.12.026>.
- Yamazaki, T., 2016. Development of a hybrid multi-tasking machine tool: integration of additive manufacturing technology with CNC machining. *Proc. CIRP* 42, 81–86. <https://doi.org/10.1016/j.procir.2016.02.193>.
- Yang, X., Liu, J., Cui, X., Jin, G., Liu, Z., Chen, Y., Feng, X., 2019. Effect of remelting on microstructure and magnetic properties of Fe-Co-based alloys produced by laser additive manufacturing. *J. Phys. Chem. Solids* 130, 210–216. <https://doi.org/10.1016/j.jpcs.2019.03.001>.
- Yang, Y., Gong, Y., Qu, S., Rong, Y., Sun, Y., Cai, M., 2018. Densification, surface morphology, microstructure and mechanical properties of 316L fabricated by hybrid manufacturing. *Int. J. Adv. Manuf. Technol.* 97, 2687–2696. <https://doi.org/10.1007/s00170-018-2144-1>.
- Yang, Y., Gong, Y., Qu, S., Xie, H., Cai, M., Xu, Y., 2020. Densification, Mechanical Behaviors, and Machining Characteristics of 316L Stainless Steel in Hybrid Additive /Subtractive Manufacturing. pp. 177–189.
- Yasa, E., Kruth, J.P., Deckers, J., 2011. Manufacturing by combining selective laser melting and selective laser erosion/laser re-melting. *CIRP Ann. – Manuf. Technol.* 60, 263–266. <https://doi.org/10.1016/j.cirp.2011.03.063>.
- Ye, Z.p., Zhang, Z.J., Jin, X., Xiao, M.Z., Su, J.Z., 2017. Study of hybrid additive manufacturing based on pulse laser wire depositing and milling. *Int. J. Adv. Manuf. Technol.* 88, 2237–2248. <https://doi.org/10.1007/s00170-016-8894-8>.
- Zhang, C., Gao, M., Zeng, X., 2019a. Workpiece vibration augmented wire arc additive manufacturing of high strength aluminum alloy. *J. Mater. Process. Technol.* 271, 85–92. <https://doi.org/10.1016/j.jmatprotec.2019.03.028>.
- Zhang, Q., Xie, J., Gao, Z., London, T., Griffiths, D., Oancea, V., 2019b. A metallurgical phase transformation framework applied to SLM additive manufacturing processes. *Mater. Des.* 166. <https://doi.org/10.1016/j.matdes.2019.107618>.
- Zhang, Z., Kong, F., Kovacevic, R., 2020. Laser hot-wire cladding of Co-Cr-W metal cored wire. *Optics Lasers Eng.* 128. <https://doi.org/10.1016/j.optlaseng.2019.105998>.
- Zhao, Y., Sun, J., Guo, K., Li, J., 2019. Investigation on the effect of laser remelting for laser cladding nickel based alloy. *J. Laser Appl.* 31, 022512. <https://doi.org/10.2351/1.5096126>.
- Zhou, C., Jiang, F., Xu, D., Guo, C., Zhao, C., Wang, Z., Wang, J., 2020. A calculation model to predict the impact stress field and depth of plastic deformation zone of additive manufactured parts in the process of ultrasonic impact treatment. *J. Mater. Process. Technol.* 280. <https://doi.org/10.1016/j.jmatprotec.2020.116599>.
- Zhou, X., Zhang, H., Wang, G., Bai, X., Fu, Y., Zhao, J., 2016. Simulation of microstructure evolution during hybrid deposition and micro-rolling process. *J. Mater. Sci.* 51, 6735–6749. <https://doi.org/10.1007/s10853-016-9961-0>.